Stefanie Schaunigg, BSc

Evaluation of rock mass scour using Block Theory and the Block Scour Spectrum

MASTER'S THESIS

to achieve the university degree of

Master of Science

Master's degree programme: Earth Sciences

submitted to

Graz University of Technology

Supervisor

Univ.-Prof. D. S. Kieffer, B.A, M.S., PhD.

Institute of Applied Geosciences

Graz, April 2016

AFFIDAVIT

I declare that I have authored this thesis independently, that I have not used other than the declared sources/resources, and that I have explicitly indicated all material which has been quoted either literally or by content from the sources used. The text document uploaded to TUGRAZonline is identical to the present master‘s thesis dissertation.

Date

Signature

Acknowledgement

Herby I would like to thank everyone who made it possible that this master thesis came off. I would not have been able to finish it without great people who kept on encouraging and supporting me.

First of all I would like to thank my family for their support and their patience. Thank you to my parents, without their help it would never have been possible for me to start studying.

I would also like to thank my husband Manuel for his support and useful ideas that sometimes really helped me through times where my motivation was not at its best.

One person that I would like to mention here as well, is my professor Univ.-Prof. D. S. Kieffer, B.A, M.S., PhD., who was helping me with his expert advice and suggestions. He helped me a lot with gaining all the information and kept me motivated through the long process of research.

This thesis would also not exist without great people from overseas. I would like to thank Richard E. Goodman, Professor Emeritus, from the University of California at Berkeley for his advice and his support. He helped me a lot to obtain relevant data for the Folsom dam auxiliary spillway, located in California.

Another big thank you goes to the team of Hydro Quebec that assisted me with the data for the spillway case study in Quebec, Canada. They never hesitated to help me out.

I would also like to thank Markus Kaspar MSc who helped me a lot with questions regarding block theory and who was so nice to let me use his data for the Ricobyo dam spillway located in Zamora, Spain.

Table of contents

Table of figures

List of tables

1 Abstract / Kurzfassung

Abstract

Three spillways of large dams are presented in this thesis and their susceptibility to rock mass scour is investigated. The evaluation is based on “Block Theory” (Goodman & Shi, 1985) and the “Block Scour Spectrum” (Kieffer & Goodman, 2012).

The three spillways are located in California, Quebec and Spain. The “Folsom dam auxiliary spillway” is located in the Northeast of the city of Sacramento. The aim of its creation is additional protection for the areas around the dam site, the spillway should guarantee a 200-year level of protection from floods during seasons of heavy rain (www.usbr.gov/USACE trifold, 2013). The second spillway is located in Quebec, Canada. Its construction was finished already in 1979. As a third example the spillway of Ricobayo dam in Spain is introduced. A spillway where already some scour events have taken place. About 1 Million m^3 of rock material had been eroded after only a few years of usage.

All three spillways are built on a hard, blocky, granitic bedrock but nevertheless all of those three examples show different design approaches regarding scour. While the spillway of Ricobayo dam experienced major and potentially catastrophic failure events, the spillway of the Quebec dam has performed well. For the Folsom dam auxiliary spillway major protective measures have been implemented at great cost to guard against rock mass scour. The main purpose of this thesis is to understand, on a rational basis, the different spillway performances and how the susceptibility to scour can be evaluated in both natural and engineered environments.

Kurzfassung

Diese Arbeit beschäftigt sich vornehmlich mit dem Thema der Auskolkung, eine Erosionsart die bisher noch nicht genug Aufmerksamkeit erhalten hat. Auskolkung stellt eine ernst zunehmende Bedrohung dar, die aber erst in einigen Fallstudien bearbeitet wird/wurde.

Auskolkung betrifft vor allem Bereiche in denen die Oberflächenabflussrate besonders hoch ist. Infrastruktur die in solchen Gebieten errichtet wird, läuft andauernd Gefahr von der Erosion des Untergrundes zerstört zu werden. Dabei wird das Fundament nicht nur vom Wasser selbst, aber auch vom Material das durch die Strömung transportiert wird, beeinflusst. Die Stabilität des Gesteins-

verbandes leidet demnach unter der zusätzlichen Belastung und die Festigkeit kann beträchtlich minimiert werden. Im Bereich der Entlastungsrinnen von Staudämmen ist dieses Phänomen der Erosion besonders interessant zu beobachten. Es ist wichtig diese Problematik im Auge zu behalten um Katastrophen, wie die des Ricobayo Staudammes in Spanien, zu verhindern.

In dieser Arbeit werden drei Entlastungsrinnen von großen Dämmen vorgestellt und auf die Stabilität ihres Untergrundes hin untersucht. Dafür wird die „Block Theorie“ verwendet die 1985 von Goodman und Shi vorgestellt wurde. Die Reaktion des Untergrundes auf das strömende Wasser wird zusätzlich mit dem sogenannten „Block Erodibility Spectrum“ (Kieffer & Goodman, 2012) untersucht, dieses gibt eine richtungsabhängige Evaluierung der Mobilisierung von Blöcken.

Die drei Entlastungsrinnen befinden sich in Kalifornien, Quebec und Spanien. Der „Folsom dam auxiliary spillway“ liegt nord-östlich von Sacramento und befindet sich noch in der Bauphase. Ziel der Errichtung ist zusätzlicher Schutz für die Gebiete rund um den Stausee, eine 200-jährige Sicherheit vor überlaufendem Wasser, in besonders Niederschlagsreichen Zeiten, soll somit möglich werden (www.usbr.gov/USACE trifold, 2013).

Die zweite Entlastungsanlage liegt in Quebec, Kanada. Es handelt sich hierbei um einen Kanal der bereits 1979 fertiggestellt wurde.

Als drittes Beispiel wird der Ricobayo Damm in Spanien vorgestellt. Dabei handelt es sich um eine Entlastungsrinne die schon von einigen Auskolkungsereignissen beeinflusst wurde. Es wurden bereits über 1 Million m^3 Gestein innerhalb weniger Jahre erodiert.

2 Introduction

The potential for spillways to erode is a complex topic that should not be underestimated. The spillways have the task to pass excess water in case of high water and are designed to withstand the forces of the flow. As for the removal of natural blocks, exposed in the spillways, the “Block Theory” (Goodman & Shi, 1985) combined with the “Block Scour Spectrum” (Kieffer & Goodman, 2012) give an indication of where and how removal can take place.

This potential of scour of the rock surface should therefore be investigated in this thesis. It deals with the stability of the underlying rock mass of three spillways of major dams located in California, Quebec and Spain. The general working steps for this thesis were:

- Gaining information on all three dam sites. This was achieved through internet study, email contacts, review of publications and personal communication
- Interpreting design drawings and information on spillway geometry and joint orientations
- Using Block Theory to identify removable blocks
- Usage of the Block Scour Spectrum
- Interpretation of the results

3 Background

3.1 Definition of scour

Generally one can say that scour is not an event that is governed by just one single process, but to more factors that work together. Rock mass scour is governed by the interaction of water and the rock mass itself. Air entrainment can also be an important factor, so generally scour is a process involving a liquid phase, a gaseous phase and a solid phase.

According to Bollaert the following three failure processes are mainly occurring in rock masses (Bollaert, 2002):

- Block removal
- Fracture of intact rock
- Abrasion

The occurrence of these failure modes depends on the turbulent flow of water, the shape of the blocks, and their exposure to flow (Bollaert, 2010).

3.1.1 Block removal

Very important for the removal of blocks are the orientations of the discontinuities that form the block (for example joint planes, faults or bedding planes). Through these discontinuities transient water pressure can act underneath the block and can cause removal. Different types of movements are possible, including uplift of a block (Figure 3-1), lateral displacement or even a combination of those mentioned (George & Sitar, 2012). Which failure type actually occurs depends on the size of the block, its kinematic removability, its stability characteristics and the protrusion of a block compared to the surrounding rock mass. These factors define the importance and relevance of the pressure forces mentioned in equation 3.1 that may cause the block to fail (Bollaert & Hofland, 2004):

Static uplift forces	f (density)
Quasi steady uplift forces	f (block protrusion, local flow velocity)
Turbulent uplift forces	f (turbulent pressure fluctuations)

$$F_{total} = F_{buoy} + F_{QSL} + F_{TUL} \quad \text{(Eq. 3.1)}$$

Total lift = buoyancy + quasi-steady lift + turbulent lift

$f(\rho_w)$ $f(V)$ $f(t,V)$

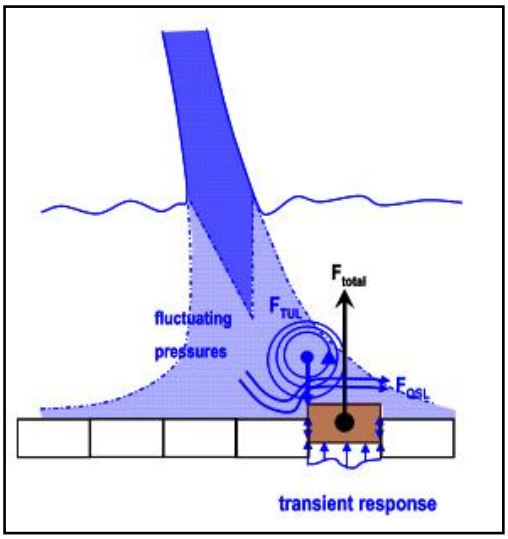

Fig. 3-1: Removal of a block through uplifting (Bollaert, 2010).

3.1.2 Fracture of intact rock

Another failure mode that can occur is fracture propagation through intact rock. Tip propagation along existing fractures is most common, but fracturing is also possible in massive rock. Fracturing is a mechanism that happens suddenly but also over a period of time, so generally there is a difference between sudden/brittle failure and fatigue failure.

Sudden fracturing takes place when the stress intensity of the rock mass is greater than the fracture toughness of the rock. The stress intensity increases, through the presence of fluctuating water pressures inside fissures, at the edges of closed-end fissures. The stresses inside the fissures are governed by the absolute value of the water pressure, the geometry of the fissure and the stabilizing support given by the surrounding rock mass. How much resistance a rock mass has against fracturing depends on the mineral composition of the mass, the in-situ stress fields, as well as the unconfined compressive strength and the tensile strength of the rock (Bollaert, 2002) (Bollaert, 2004).

Fatigue failure is generally happening when the stress intensities do not exceed the resistance of the rock mass against failure. But the continuous presence of pressure in fissures due to water causes the block to break in a long term.

A combination of quasi-steady forces and brittle/fatigue failure ends with the peeling off of the rock mass. This type of collapse is typical for rocks that are built in horizontal, thin layers (for example sedimentary rocks) (Bollaert, 2010).

Figure 3-2 shows the failure modes that are described by Bollaert (2010):

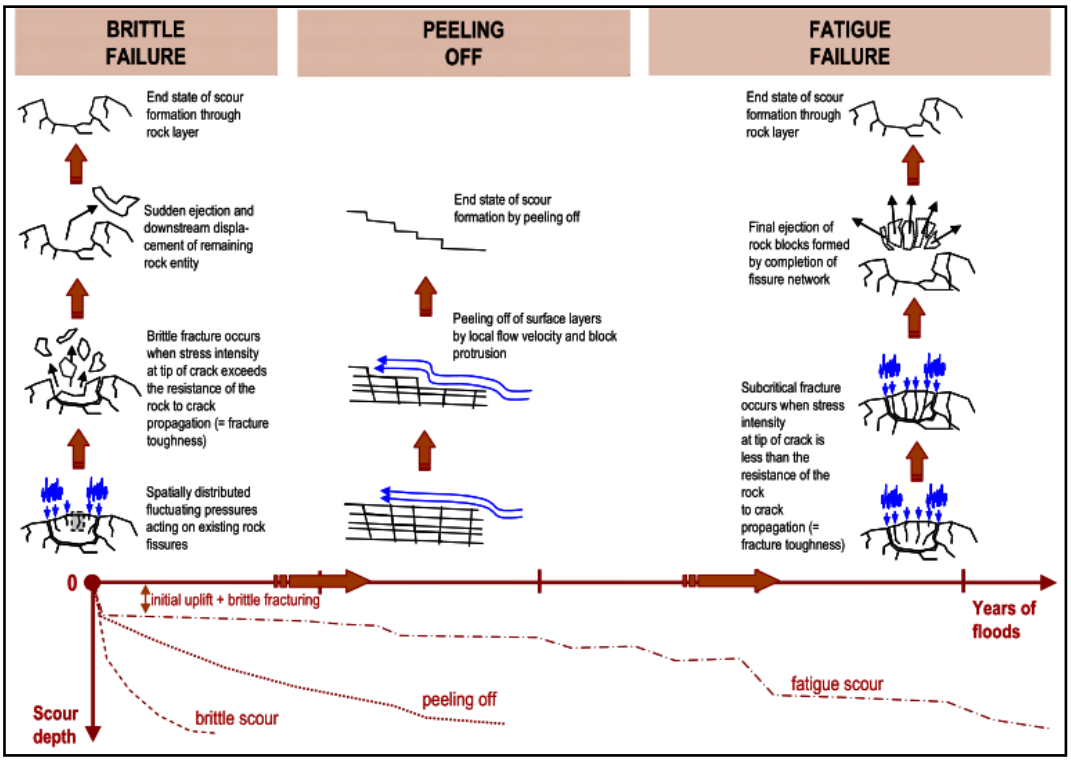

Fig. 3-2: Sequence of failure phenomena of rock (Bollaert, 2010).

3.2 Scour models

3.2.1 Comprehensive Scour Model

The “Comprehensive Scour Model” (CSM) was developed by Bollaert in 2001 and is an entirely physics-based model that uses the principles of linear elastic fracture mechanics to evaluate crack propagation, followed by the simulation of the dynamic uplift of the fractured medium due to net uplift forces and impulsions. For expressing the scour resistance of the fractured medium geomechanical characteristics, such as UCS (unconfined compressive strength) are used (Bollaert & ASCE, 2010). The corresponding computational modules, which are part of the CSM, for the aforementioned failure modes are:

1. *Dynamic Impulsion (DI) module*: expresses the dynamic uplift of blocks as a function of rock block density, shape, dimensions and time evolution of net uplift forces on the block (Bollaert, 2002).

2. *Comprehensive Fracture Mechanics (CFM) module*: expresses the hydrodynamic fracturing of closed-end joints as a function of water pressure fluctuations at the boundary, geometry and type of fissure, as their geomechanical characteristics (Bollaert, 2002).

3. *Quasi Steady Impulsion (QSI) module*: peeling off of thin layers of exposed rock (Bollaert et al., 2012).

The CSM model does not consider scour by abrasion (Bollaert & ASCE, 2010). While modules 1 and 3 are not time dependent, module 2 is. Module 2 accounts for the time that is needed to allow a fissure propagate until a distinct block is created (Bollaert, 2010). As hydraulic boundary conditions for each of the modules, the near-prototype pressure fluctuations recorded in an experimental facility are extrapolated. Plunge pool turbulent flow conditions are re-computed and the boundary conditions are automatically updated for the following layer after break-up and uplift of a layer of rock blocks (Bollaert, 2002). The model is generally applied for rock scour within spillways and plunge pools, concrete fracturing of spillway chutes and for uplift of stilling basin concrete linings.

The CSM (Bollaert, 2002) (Bollaert, 2004(1)) (Bollaert & Schleiss, 2005) is based on experimental and numerical investigations of dynamic water pressures in rock joints (Bollaert, 2002). The failure of the fractured rock is computed through the model following each of the aforementioned mechanisms. There are three modules to consider (Figure 3-3): the falling jet, the plunge pool and the rock mass. The latter applies the failure mechanisms (Bollaert & ASCE, 2010).

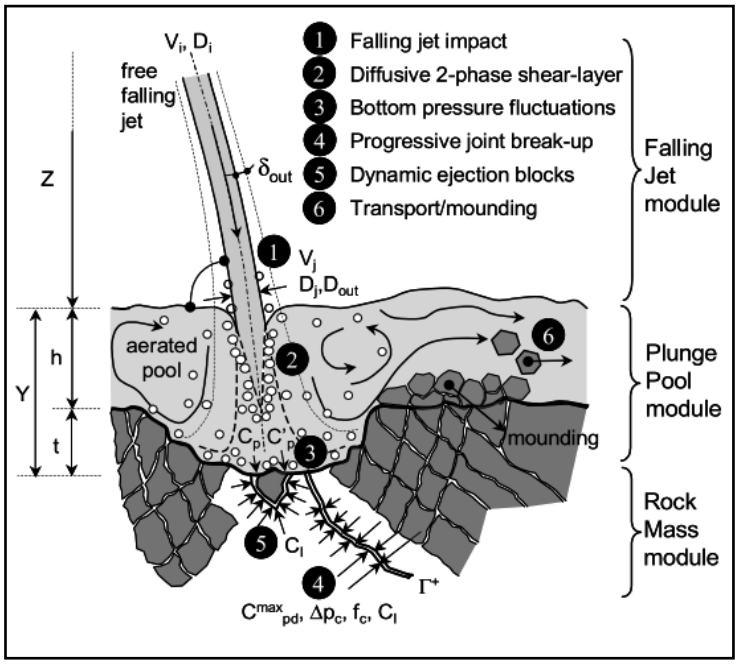

Fig. 3-3: Main events responsible for break-up of rock, (Bollaert, 2010).

Falling Jet Module: describes the transformation of the hydraulic and geometric characteristics of the jet from dam issuance down to the plunge pool.

Important factors are:

- V_i = velocity
- D_i = diameter
- T_u = initial turbulence intensity, defined as the ratio of velocity fluctuations to the mean velocity

The longitudinal location of impact, the total trajectory length (L), the velocity (V_j) and the diameter (D_j) at impact are computed by the module (Bollaert & ASCE, 2010).

Plunge Pool Module: the characteristics of the jet when traversing the plunge pool are described and the water pressure at the water-rock interface is defined.

Important factors are (Bollaert & ASCE, 2010):

- Y = plunge pool water depth
- D_j = jet diameter at impact
- Y/D_j = directly related to jet diffusion
- C_{pa} = mean dynamic pressure coefficient
- C'_{pa} = root-mean-square coefficient of fluctuating dynamic pressure

Rock Mass Module: for determining the pressures inside the rock joints, the pressures at the bottom are used (Bollaert & ASCE, 2010).

Important factors are:

- C^{max}_p = maximum dynamic pressure coefficient
- Δp_c = characteristic amplitude
- f_c = frequency of pressure cycles
- C^{max}_i = maximum dynamic impulsion coefficient

Further information and a detailed description of the CSM model can be found in (Bollaert, 2002), (Bollaert, 2004) and (Bollaert & Schleiss, 2005).

3.2.2 Erodibility Index (K_n)

Annandale introduced one of the most comprehensive scour models. It focuses on a number of factors that influence the scour process. Annandale's Erodibility Index is a semi-empirical, geomechanical approach based on about 150 field observations. The general idea was the observation of the behavior of rock under the influence of stream power.

Through the evaluation of whether or not erosion occurred in case studies, Annandale created this Erodibility Index (K_n) (Annandale, 1995). The index is dimensionless and incorporates many rock mass parameters. For the evaluation of scour susceptibility it also takes the geological structure into account. Generally rock erodibility is based on a rippability index developed by Kirsten (Kirsten, 1982). This index was modified from the Q-System introduced by Barton (Barton et al., 1974). The Q-System is used to classify rock masses for tunnel support, the equation is presented on page 24. Equation 3.2 shows Annandale's erodibility index (Annandale, 1995). With this approach it is possible to calculate the resistance of any earth material against erosion. The parameters that are used will be explained later on in this chapter:

$$K_n = M_s * K_b * K_d * J_s \quad \text{(Eq.3.2)}$$

K_n = Erodibility Index

M_s = Mass strength factor, based on UCS (unconfined compressive strength)

K_b = Particle/Block size factor, based on RQD (rock quality designation) and number of discontinuity sets

K_d = discontinuity shear strength number, based on joint roughness and alteration

J_s = Relative shape and orientation factor, based on strike and dip of discontinuities relative the flow direction

(Annandale, 1995)

The stream power, or also known as rate of energy dissipation, quantifies the relative magnitude of the erosive power of water. Turbulence can cause pressure fluctuations and energy loss. An increase in turbulence intensity results in increased rates of energy dissipation and a rise of the magnitude of fluctuating pressures (Sawadogo, 2010).

The estimation of the rate of energy dissipation represents therefore the relative magnitude of fluctuating pressure and therefore the erosive power of water

(Annandale, 1995). The rate of energy dissipation per unit area (kW/m^2) in an open channel is presented in equation 3.3.

$$\boldsymbol{P = \frac{\gamma q \Delta E}{A}} \quad \text{(Eq.3.3)}$$

P = stream power (kW/m^2)

γ = unit weight of water (9,81 KN/m^3)

q = unit discharge (m^3/s)

ΔE = energy loss in terms of head per unit length of flow (m/m)

A = flow area (m^2)

$$\boldsymbol{\Delta E = \frac{v^2}{2g}} \quad \text{(Eq.3.4)}$$

γ = unit weight of water (9,81 KN/m^3)

v = velocity

(Annandale, 1995)

The Erodibility Index (Annandale, 1995) is a method that helps predicting the formation of scour in rock masses. Equation 3.5 (Annandale, 1995) expresses the relation of the disturbing agent and the possible resistance that the material has against erosion. This is possible through the formation of a balance of the stream power "P", which was calculated through equation 3.3. and the resistance of the rock against erosion, which is indicated through the index "f(K_n)".

$$\boldsymbol{P = f(K_n)} \quad \text{(Eq.3.5)}$$

P = magnitude of the agitating agent

f(K_n) = functional possible resistance of material against erosion

K_n = Erodibility Index

(Annandale, 1995)

If the erodibility threshold has been exceeded (P > f(K_n)) the material will erode. If the erodibility threshold has not been exceeded (P < f(K_n)) no erosion will occur.

With Annandale's index the erosive capacity for a variety of flow conditions (for example open channels, knick-points, hydraulic jumps, head-cuts and plunge pools) is provided. Through the case studies of hydraulic testing, Annandale created a threshold (Annandale, 1995) relationship between the earth material

erodibility and the flow erosive capacity. This threshold is shown in figure 3-4. Scour is likely to occur when the stream power of water and the erodibility index plot above the threshold.

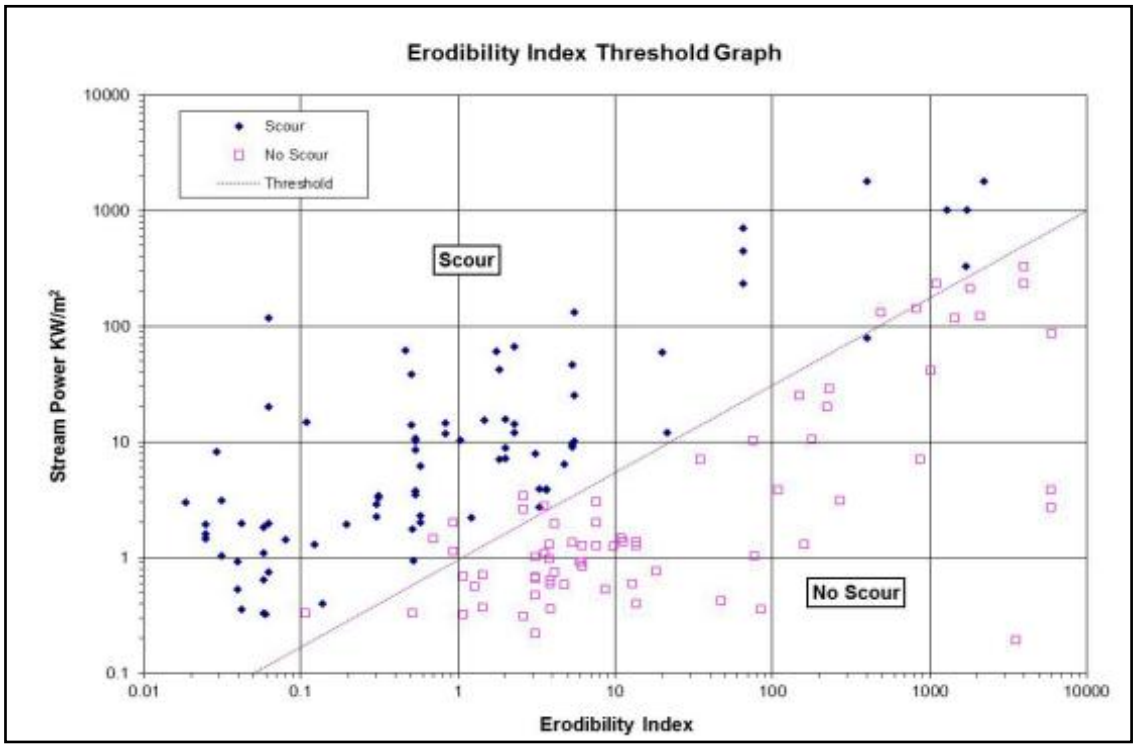

Fig. 3-4: Graphical representation of erosion threshold, after (Annandale, 1995).

3.2.2.1 Annandale`s Erodibility Index parameters

M_s: The mass strength factor is based on the unconfined compressive strength of the rock (UCS). For calculating the M_s the relevant parameters are therefore the UCS values in MPa and its coefficient of relative density (C_r) as shown in equation 3.6.

$$M_s = C_r * UCS \quad \text{(Eq. 3.6)}$$

C_r = coefficient of relative density (-)

UCS = unconfined compressive strength (MPa)

M_s = mass strength factor (MPa)

The coefficient of the relative density is a result of using formula 3.7.

$$C_r = \frac{g * \rho_r}{27 * 10^3} \quad \text{(Eq. 3.7)}$$

g = acceleration due to gravity (9,81 m/s^2)

ρr = density of material (kg/m^3)

27 * 10^3 = reference unit weight of block (N/m^3)

Table 3-1 shows mass strength values for different earth materials:

Material description	Uniaxial strength (MPa)	Mass strength number (M_s) (MPa)
Very soft cohesive soil	0-0.08	0.02
Soft cohesive soil	0.08-0.14	0.04
Firm cohesive soil	0.14-0.21	0.09
Stiff cohesive soil	0.21-0.35	0.19
Very stiff cohesive soil	0.35-0.75	0.41
Very soft rock	1-3	1-2
Soft rock	3-13	2-8
Hard rock	13-26	8-35
Very hard rock	26-106	35-70
Extremely hard rock	106-212	70-280

Tab. 3-1: Mass strength number of rock, (Annandale, 2006).

K_b: The particle size factor is based on the RQD (Rock Quality Designation) and the number of discontinuity sets. It is a factor characterized by the mean size of individual rock units, formed through the spacing of the discontinuities.

The basis for the identification of the RQD can be for example a drill core. The number of joints within a certain length (e.g. 10 cm) of the core can then be used to calculate the rock quality as shown in equation 3.8 (Deere, 1963).

$$RQD = \frac{\sum core\ pieces > 10\ cm}{Total\ core\ run\ length\ (cm)} * 100 \quad \text{(Eq. 3.8)}$$

For calculating the particle size factor the value J_n is also necessary. J_n represents the joint set number. This value depends on how many joints sets are appearing in the rock mass. After observation the correct number can then be used from table 3-2.

Intact; no or few joints	1,00
One joint set	1,22
One joint set plus random	1,50
Two joint sets	1,83
Two joint sets plus random	2,24
Three joint sets	2,73
Three joint sets plus random	3,34
Four joint sets	4,00
More than four joint sets	5,00

Tab. 3-2: Values for the J_n depending on the number of joint sets in the rock mass (Barton et al., 1974).

The particle size factor can then be calculated using equation 3.9:

$$K_b = \frac{RQD}{J_n} \quad \text{(Eq. 3.9)}$$

RQD = Rock quality designation (% of pieces longer than 0.1m)

J_n = Joint number

K_d: The discontinuity shear strength number is based on joint roughness and alteration. The joint roughness is proportional to the strength of the rock and the degree of alteration is inversely proportional to the strength. K_d can be evaluated using equation 3.10. Typical values for these factors are presented in table 3-3 and 3-4:

$$K_d = \frac{J_r}{J_a} \quad \text{(Eq. 3.10)}$$

J_r = joint roughness number

J_a = joint alteration number

Kirsten (1982, 1988) has developed a rippability index to evaluate the machine power required for excavating various earth materials on which rock erodibility is based. This index has been modified from Barton's Q-system which can be used for the classification of rock masses for tunnel support (Barton et al. 1974, Barton 1988). The aforementioned factors are practically a corollary to the Q-system, as Barton uses the same parameters to evaluate rock mass characteristics, which is expressed by equation 3.11:

$$\boldsymbol{Q = \frac{RQD}{J_n} \times \frac{J_r}{J_a} \times \frac{J_w}{SRF}} \qquad \text{(Eq. 3.11)}$$

RQD = Rock Quality Designation

$\mathbf{J_n}$ = joint set number

$\mathbf{J_r}$ = joint roughness number

$\mathbf{J_a}$ = joint alteration number

$\mathbf{J_w}$ = joint water reduction factor

SRF = stress reduction factor

Typical values for J_n are shown in table 3-3. Values for J_a are shown in table 3-4.

Joint separation	**Roughness condition**	**J_r**
Joints are tight or closed during hydraulic flow	Discontinuous joints; stepped	4.0
	Rough/irregular	3.0
	Smooth; undulating	2.0
	Slickensided; undulating	1.5
	Rough/irregular; planar	1.5
	Smooth; planar	1.0
	Slickensided; planar	0,5
Joints are open and remain open during hydraulic flow	Joints are either open or contain relatively soft gouge of sufficient thickness to prevent wall contact during hydraulic flow	1.0
	Joints contain swelling clays	1.0

Tab. 3-3: Typical values for the factor J_r., (Barton et al., 1974).

Field identification of joint alteration	J_a for aperture width		
	<1.0 mm	1.0-5.0 mm	≥ 5.0 mm
Joint tightly healed with hard, impermeable mineral filling	0.75	1.0	1.5
Clean, open joint with fresh or discolored walls only; no infilling	1.0	1.5	2.0
Discolored to disintegrated joint walls, infilling is sand or gravel with <15% cohesionless fines in matrix	2.0	4.0	6.0
Discolored to disintegrated joint walls, cohesionless, nonswellling	3.0	6.0	10.0
Disintegrated to decomposed joint walls, nonswelling, lean clay or clay matrix	4.0	8.0	13.0
Disintegrated to decomposed joint walls, fat clay matrix	5.0	10.0	18.0

Tab. 3-4: Typical values for the factor J_a (Barton et al., 1974).

J_s: The relative ground structure number represents the influence of the strike and dip directions of discontinuities relative to the flow direction and the least favorable situation. Joint sets oriented against the stream direction make it easier for blocks to move, as can be seen in figure 3-5.

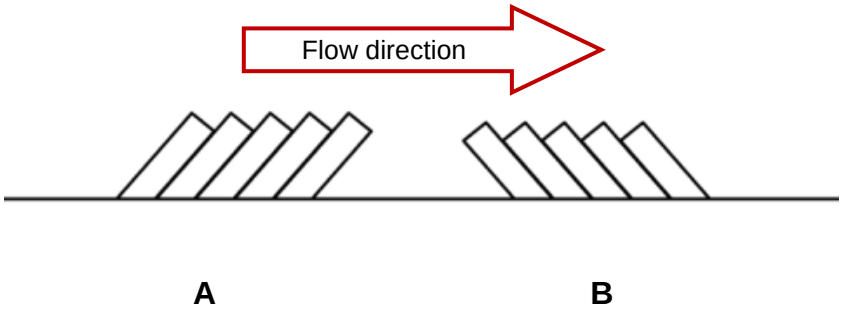

Fig. 3-5: Influence of the discontinuity orientation on the stability of the rock mass. A) Favorable Orientation, the discontinuities are dipping against the flow direction. B) Unfavorable orientation, dipping away from flow, modified after (Bureau of Reclamation, 2012).

Table 3-5 shows the values for the relative ground structure number. The ratio of joint spacing (r) is defined as the ratio of the shortest side of a rectangular block to the longest side (Figure 3-6).

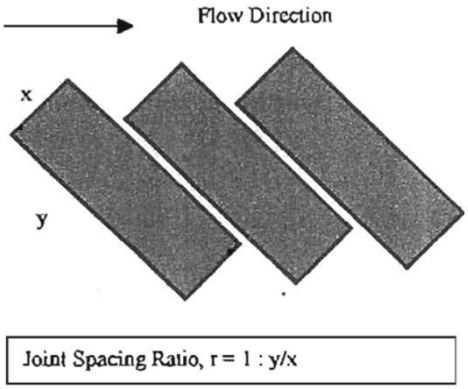

Fig. 3-6: Determination of the joint spacing ratio (r), (Annandale & Smith, 2001).

For calculating the dip of the least favorable discontinuity with respect to the flow direction the following variables are used: flow direction (FD), true dip (TD), dip direction (DD), ground slope (GS) and the strike. For a better understanding of these descriptions see figure 3-7 and 3-8.

- The FD (flow direction) is the dominant direction of flow projected on a horizontal plane and expressed as an azimuth angle (0° ≤ FD ≤ 360°).
- The GS (ground slope) is associated with the flow direction and is an angle measured from the horizontal in the vertical plane (0° ≤ GS ≤ 90°).
- The DD (dip direction) lies perpendicular to the strike of the least favorable joint set. It is expressed as an azimuth angle (0° ≤ DD ≤ 360°).
- The TD (true dip) of the least favorable joint set (0°≤ TD ≤ 90°) is measured in the vertical plane associated with the dip direction.
- The strike is perpendicular to the dip direction.

(Annandale & Smith, 2001)

First the apparent dip (AD) has to be calculated, using formula 3.12. It is the dip of the least favorable discontinuity with respect to the flow direction (FD).

$$\boldsymbol{tan(AD) = tan(TD) * [sin(strikeFD)]} \quad \text{(Eq. 3.12)}$$

AD = apparent dip

TD = true dip

FD = flow direction

The next step is to calculate the effective dip (ED) which is used in table 3-5. It is the difference between the apparent dip (AD) and the ground slope (GS), equation 3.13:

$$\boldsymbol{ED = AD - GS} \quad \text{(Eq. 3.13)}$$

ED= effective dip

AD = apparent dip

GS = ground slope

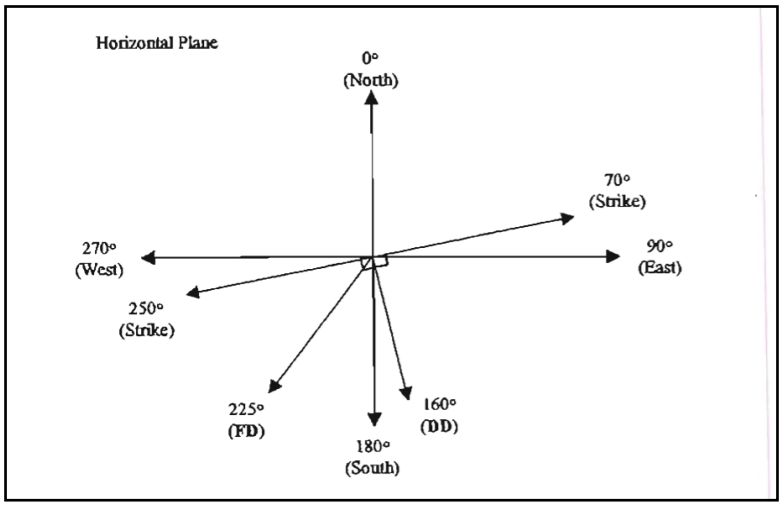

Fig. 3-7: Horizontal plane showing the relationships between the flow direction (FD, the dip direction (DD) and the strike, (Annandale & Smith, 2001).

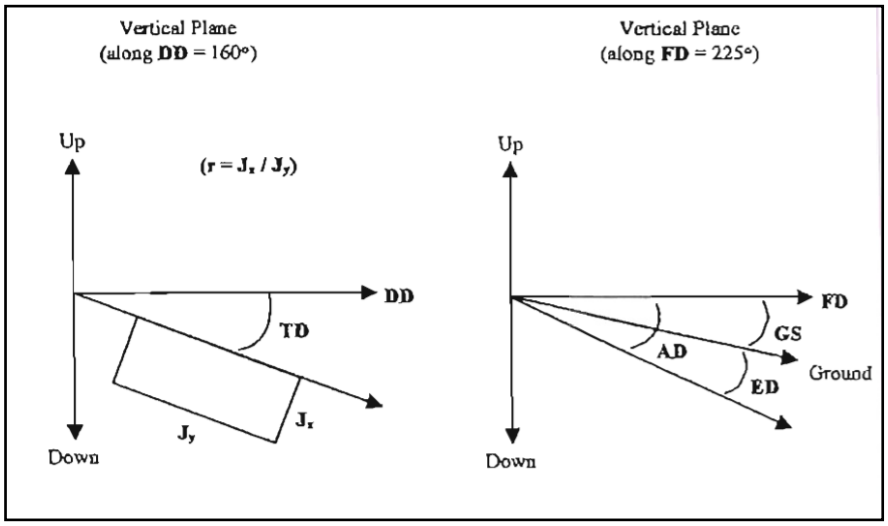

Fig. 3-8: Vertical plane showing the relationships between the dip direction (DD), the true dip (TD), the flow direction (FD), the ground slope (GS), the apparent dip (AD) and the effective dip (ED), (Annandale & Smith, 2001).

Dip Direction of Closer Spaced Joint Set (degrees)	Dip Angle of Closer Spaced Joint Set (degrees)	Ratio of Joint Spacing, r			
		1:1	1:2	1:4	1:8
180/0	90	1,14	1,20	1,24	1,26
In direction of stream flow	89	0,78	0,71	0,65	0,61
	85	0,73	0,66	0,61	0,57
	80	0,67	0,60	0,55	0,52
	70	0,56	0,50	0,46	0,43
	60	0,50	0,46	0,42	0,40
	50	0,49	0,46	0,43	0,41
	40	0,53	0,49	0,46	0,45
	30	0,63	0,59	0,55	0,53
	20	0,84	0,77	0,71	0,67
	10	1,25	1,10	0,98	0,90
	5	1,39	1,23	1,09	1,01
	1	1,50	1,33	1,19	1,10
0/180	0	1,14	1,09	1,05	1,02
Against direction of stream flow	-1	0,78	0,85	0,90	0,94
	-5	0,73	0,79	0,84	0,88
	-10	0,67	0,72	0,78	0,81
	-20	0,56	0,62	0,66	0,69
	-30	0,50	0,55	0,58	0,60
	-40	0,49	0,52	0,55	0,57
	-50	0,53	0,56	0,59	0,61
	-60	0,63	0,68	0,71	0,73
	-70	0,84	0,91	0,97	1,01
	-80	1,26	1,41	1,53	1,61
	-85	1,39	1,55	1,69	1,77
	-89	1,50	1,68	1,82	1,91
180/0	-90	1,14	1,20	1,24	1,26

Notes: 1. For intact material take $K_s = 1,0$
2. For values of r greater than 8 take K_s as for $r = 8$

Tab. 3-5: Values for the relative ground structure number (Annandale, 2006).

Annandale's semi-empirical, geo-mechanical index enables the erodibiliy of any earth material to be assessed. He defines the Erodibility Index (dimensionless) for material through using a range of values as already stated. Nevertheless a three dimensional solution and a perfect handle on the effect of joints are not given, for which the "Block Scour Spectrum" (Kieffer & Goodman, 2012), presented in this thesis has recently been developed. It seeks to improve Annandale's Erodibility Index through explicit consideration of the rock mass characteristics in three dimensions.

4 Methods

Block Theory (Goodman & Shi, 1985) is often used in Geotechnics to identify potentially dangerous blocks forming a jointed rock mass prior to their movement, and to assure stability of key blocks. Geometric information is the basis of the theory, which originates from structural geology and engineering mechanics. In this thesis Block Theory is used to consider the removability of 3D blocks, their corresponding failure modes, and their susceptibility to erosion by scour in an unlined spillway environment.

Several key assumptions are made in Block Theory (Goodman & Shi, 1985): 1) all joint surfaces are planar, 2) the joints extend completely through the volume of interest, 3) the blocks are rigid and 4) the input parameters are the discontinuities and the free faces.

4.1 Types of blocks

The concept of Block Theory is based on the allowance of many different combinations of discontinuities and the possibility to be depicted to directly identify kinematically removable blocks and evaluate their stability under arbitrary loading conditions (Goodman & Shi, 1985). For identifying these type of blocks, one distinguishes between finite and infinite blocks, a stereographic projection is used where the three dimensional space gets divided by the given joints into an upper and a lower hemisphere. The blocks are created through half spaces. The stability of blocks depends on their geometry, the direction of the resulting force and the magnitude of the friction angles on the block faces (Goodman & Shi, 1989).

The different block types that form are the following:

Finite blocks (Type I-IV and VI): this type of block is confined by joints on all four sides; finite blocks are subdivided into removable and non-removable blocks.

Infinite blocks (Type V): are not completely confined by joints, they will not cause any problems as they are not able to slide into the free space (Goodman & Shi, 1985).

Figure 4-1 shows the categories in which finite and infinite blocks can be subdivided:

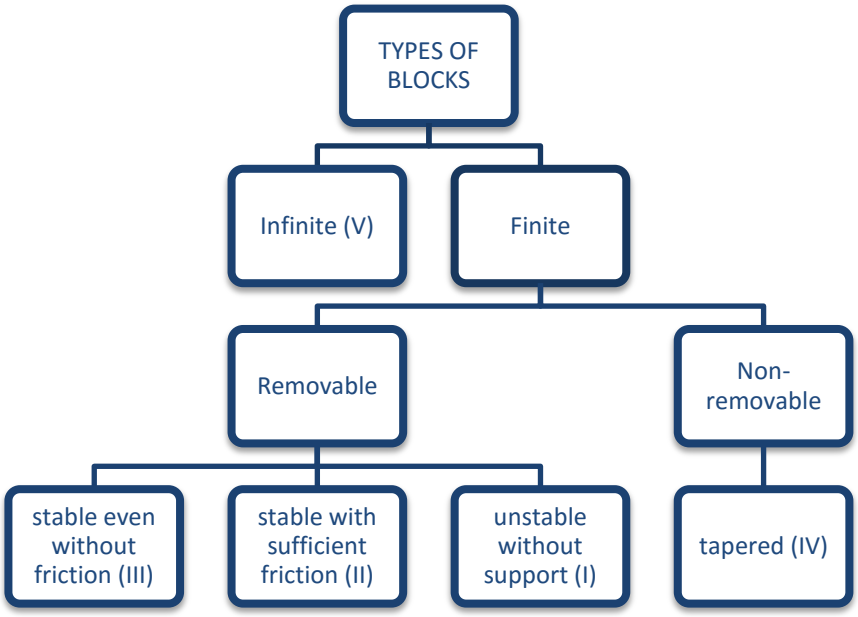

Fig. 4-1: Types of blocks, modified after Goodman and Shi (1985).

- *Type VI "Joint block":* is confined by joint planes from all sides but is not removable because no free plane is involved, the joint surfaces do not intersect the slope
- *Type V "infinite block"*: the block is not completely isolated by the joint planes, it does have infinite size and is non removable
- *Type IV "tapered block"*: this type of block is non-removable because of its shape, it is tapered
- *Type III "safe removable block"*: blocks of this type are stable even without friction, due to gravity. They can be unstable if the resultant force changes
- *Type II "potential key block"*: is safe due to sufficient friction, it can become unstable through water pressure or other kinds of forces
- *Type I "key block":* key blocks are removable and are located in a way that makes them unsafe, they will move unless support is provided

(Goodman & Shi, 1985)

Figure 4-2 illustrates the different types of blocks:

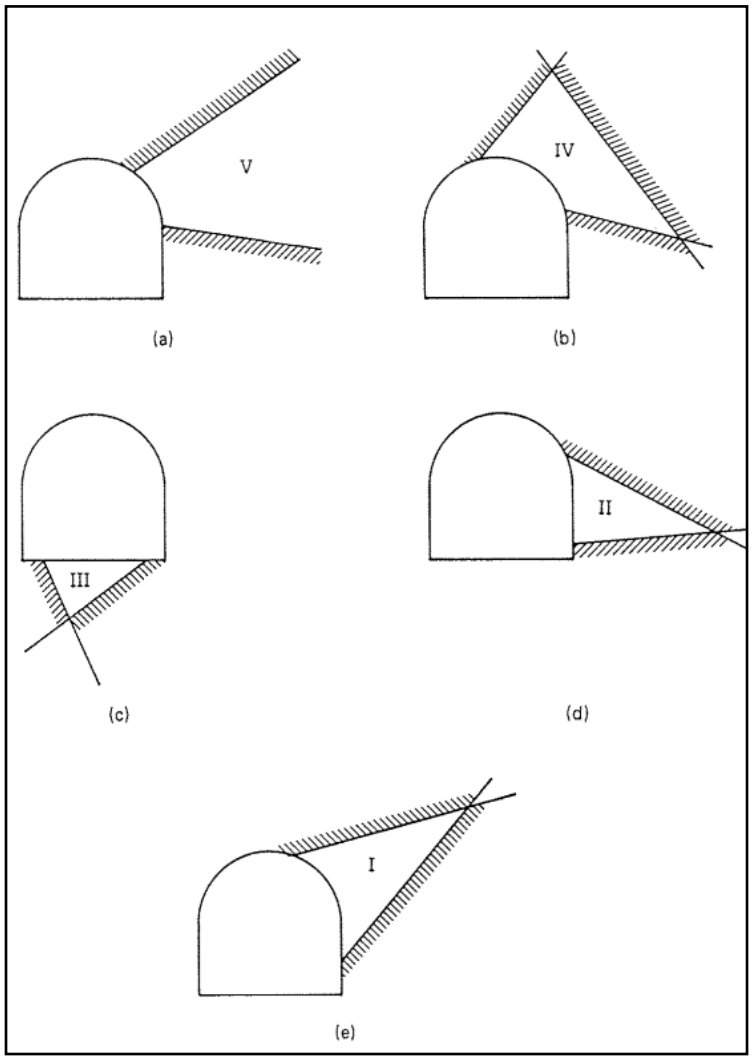

Fig. 4-2: Types of blocks: (a) infinite, (b) tapered, (c) stable, (d) potential key block, (e) key block (Goodman & Shi, 1985).

4.2 Removability

Block Theory says that for a given set of three non-repeating joints (J1, J2 and J3) and one free face, eight possible block shapes exist. How many joint pyramids (JP's), block shapes, are formed by the intersection of "n" joints is expressed by equation 4.1. JP's represent the block geometries and in a stereographic projection those JP's plot as a series of regions enclosed with portions of great circles (Goodman & Shi, 1985).

$$\mathbf{2}^{\boldsymbol{n}} \quad \text{(Eq.4.1)}$$

n = number of joints

Each block or JP is named by a number code which relates to which side of the joint plane the block exists in space. For identifying the space the number “0” and the number “1” are used. “0” or also titled “U” represents the upper half space, “1” or also titled “L” represents the lower half space. The Joint Pyramid code "100" for example indicates that joint 1 is formed in the lower half space, joint 2 and joint 3 in the upper half space (Goodman & Shi, 1985).

The stereonet can be subdivided into regions corresponding to each JP by plotting the great circle matching to each joint set (Goodman, 1976). A block is removable if its JP region plots completely within the “Space Pyramid” (SP) as defined by the free face. The SP is considered to be the upper half space of a slope, the airside of the slope. The free face is assumed to be planar over the region of interest and separates the SP from the EP (“Excavation Pyramid” – lower half space, rockside of the slope) (Goodman & Shi, 1985).

SP → airside of slope, upper half space

EP → rockside of slope, lower half space

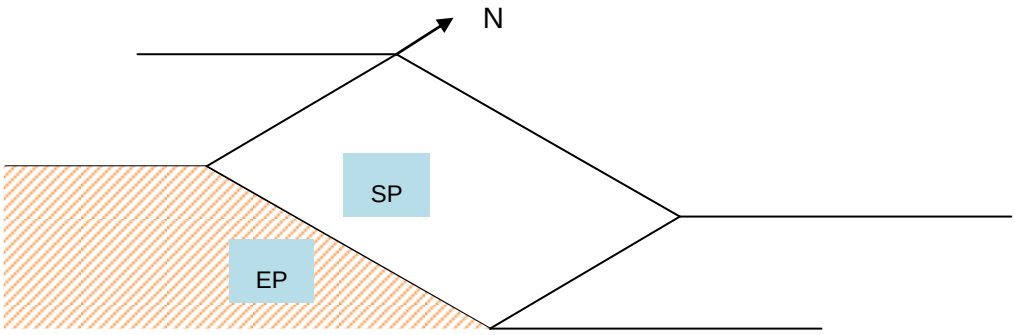

Fig. 4-3: Example for a Space Pyramid and an Excavation Pyramid, after (Goodman & Shi, 1985).

Blocks exposed to the free surface are called Block Pyramids. A JP is a joint plane subset of half-space that determine the BP (Block Pyramid). Through shifting the planes to pass through a common origin the BP (Fig. 4-4) is formed. (Goodman & Shi, 1985):

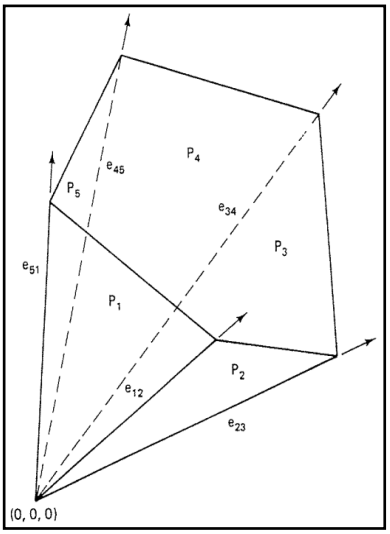

Fig. 4-4: The drawing represents a Block Pyramid (Goodman and Shi 1985).

The Block pyramids form through the intersection of the Space Pyramid and the Excavation Pyramid (Goodman & Shi, 1985):

$$\boldsymbol{BP} = \boldsymbol{EP} \cap \boldsymbol{JP} \quad \text{(Eq.4.2)}$$

4.2.1 Shi's theorem – Theorem of finiteness and Theorem of removability

To decide whether a block is finite or infinite (Fig. 4-5) Shi's theorem is used. According to the Theorem a block is finite if its Block Pyramid is empty (see equation 4.3):

$$\boldsymbol{EP} \cap \boldsymbol{JP} = \boldsymbol{empty} \quad \text{(Eq.4.3)}$$

Another way to distinguish a finite block from an infinite block is to observe the SP which is complimentary to the EP. A block is finite if its JP is a subset of the SP (equation 4.4):

$$\boldsymbol{JP} \subset \mathbf{SP} \quad \text{(Eq.4.4)}$$

(Goodman & Shi, 1985)

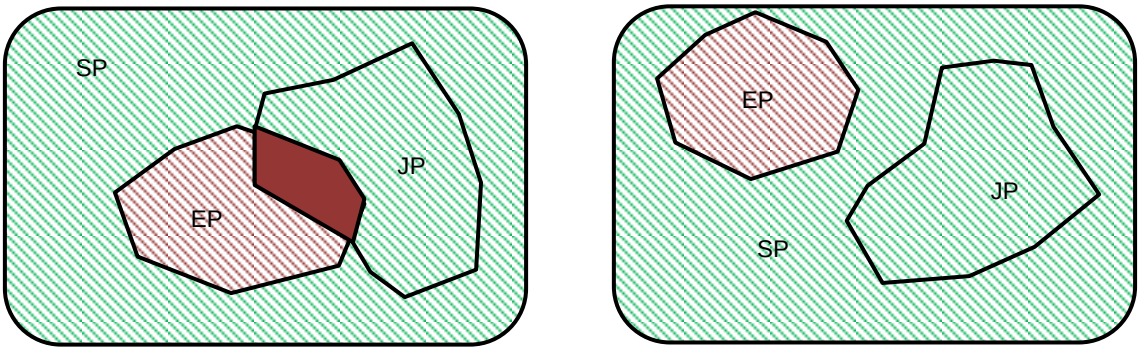

(a) (b)

Fig. 4-5: The drawings show the conditions for (a) an infinite, convex block and (b) a finite, convex block, modified after (Goodman & Shi, 1985).

The Theorem of removability helps to distinguish between a non-removable and a removable block, after identifying the finite ones. According to the Theorem of a block is removable if its Block Pyramid is empty and its Joint Pyramid is not empty. A block is tapered (not removable) if its Block Pyramid is empty and its Joint Pyramid is also empty (Goodman & Shi, 1985).

4.3 Examination of removable blocks

For Block Theory a “whole sphere projection” is used. In this case both hemispheres of a whole sphere are represented. For identifying removable blocks the dip magnitude and the dip direction of the free surface and the joints are plotted into this projection, the reference circle includes the lower hemisphere projection. The resulting number of JPs depends on the number of nonparallel joints. Figure 4-6 shows a result for a spillway surface. For this projection four joint sets were used and one free surface:

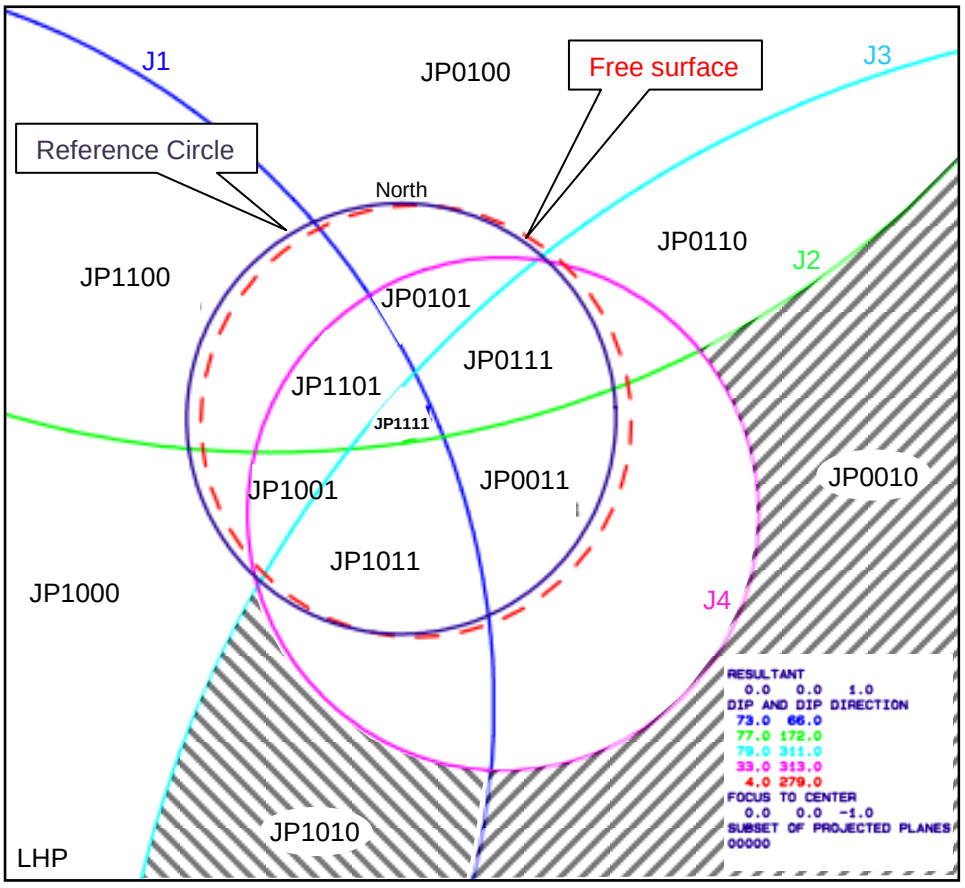

Fig. 4-6: Whole sphere stereographic projection of a spillway, LHP states that the reference circle includes the lower hemisphere projection.

The red dashed circle shows the free surface, everything that lies within this circle is inside the EP (excavation pyramid) and is therefore stable. JPs 1010 and 0010 lie completely outside of the EP or entirely within the SP (space pyramid) and are thus removable (Goodman & Shi, 1985).

4.3.1 Block failure mode analysis

After the removable blocks have been recognized the kinematic mode of failure needs to be identified using a three dimensional kinematic analysis. It is used to see if sliding is geometrically possible, does not confirm tough if sliding will occur. The possible modes of failure are based on the block geometry, the orientation of the active resultant force being applied to a block. In scour assessment the active resultant is comprised by the hydraulic forces and the self-weight of the block. Possible failure modes include lifting of a block, wedge or plane sliding (Goodman & Shi, 1985).

Through plotting the basic information with the Block Theory software, the failure modes for each JP are shown in the stereographic projection. Numbers indicate the type of failure:

- 0: lifting
- Single digit number: plane sliding
- Two digit number: wedge sliding
- No number shown: no failure mode identified

(Goodman & Shi, 1985)

4.4 Block Scour Spectrum (BSS)

The Block Scour Spectrum (Kieffer & Goodman, 2012) seeks to show the resistance of a block against removal by scour. The aforementioned leading techniques for assessing rock block removal considerate the influence of rock mass jointing on scour development but are not able to fulfill the three dimensional mechanics and kinematics of rock removal.

The “Erodibility Index Method (EIM)” by (Annandale, 1995) compares the resistive capacity of the rock mass to the erosive capacity of water, defined by stream power. The EIM does not consider the mechanisms of block removal, brittle fracture or fatigue failure in detail and does therefore only give a generalized evaluation for rock scour. Although the geometric influence of rock joint orientation is considered, an explicit consideration of block removal in a three dimensional fractured rock mass is not within the scope of the method.

The “Comprehensive Scour Model (CSM)” by (Bollaert, 2002) uses fracture mechanisms to estimate failure due to the action of dynamic water pressures, and also considers dynamic impulsion to describe rock block removal. The bounding fracture orientations are far more simplistic though than generally encountered in nature.

Both techniques are limited as they do not fulfill the three dimensional mechanics and kinematics of rock removal. The Block Scour Spectrum (Kieffer & Goodman, 2012) represents a three dimensional analytic approach for determining the resistance rock blocks offer to removal when subjected to hydraulic flow or jet impingement (Kieffer & Goodman, 2012). The Block Scour Spectrum offers the possibility to determine the resistance offered by different block types comprising the rock mass as a function of the resultant block loading direction. The block loading generally includes gravity and hydrodynamic forces. It is as-

sumed that block removal occurs by separation or translational sliding of blocks along existing discontinuity surfaces. Rotational failure modes can also be handled though. Other assumptions for the analysis are that the discontinuities possess frictional shear strength, that block fracturing does not occur and that the blocks are rigid. Input parameters that are required for the “BSS” are discontinuity orientations and friction angles, plus free surface orientations. The analysis includes three modules: kinematic, stability and spectrum (Kieffer & Goodman, 2012). These three modules are discussed and represented in chapter 5, shown on an example of Folsom dam spillway.

The results of the analysis can be used to optimize a spillway direction. The method also considers Type II (potential key blocks) and Type III (safe removable) blocks which are important in such environments, as there are no key blocks in fact, but the exposure of the surface to hydraulic flow can cause Type II and Type III blocks to move.

4.4.1 Friction cone concept

The BSS is based on the friction cone concept, it includes a more complex representation of compound friction cones of different joint planes. This is important for determining in which direction a block is more likely to slide. Important to understand is the factor of safety (or “uncertainty value”) which focuses on material conditions. Important values for the calculation are:

- $\varphi\ available$: actual friction angle that joint surfaces possess
- $\varphi\ required$: friction angle that provides stability under a given resultant force

The factor of safety can then be calculated with the following formula:

$$\boldsymbol{FS = \frac{\tan \varphi\ available}{\tan \varphi\ required}} \quad \text{(Eq. 4.5)}$$

Key blocks can then be recognized by removable blocks that have a FS value lower than 1. Figure 4-7 shows the concept of a friction cone.

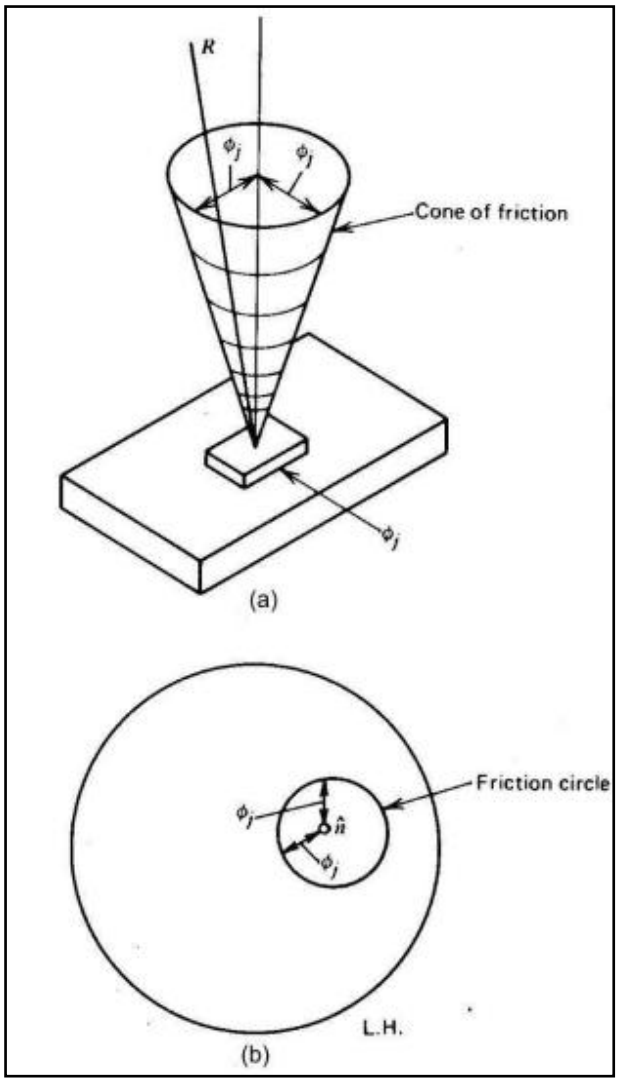

Fig. 4-7: Concept of the friction cone: a) apex of the friction angle (φj) around the normal to the plane. No movement of the block will occur when any resulting force plots within the friction cone. B) friction cone on a stereonet with the radius of the friction angle (φj) (Goodman, 1989).

The friction angle controls the shear strength for a planar discontinuity without filling. The size and the shape of the grains that are exposed on the surface of a discontinuity influence the friction angle of rocks. Fine grained rocks and rocks with a high mica content, such as phyllite have a low friction angle. Coarse grained rocks, like granite, have a high friction angle (Wyllie & Mah, 2004).

5 Observations and findings

5.1 Folsom dam auxiliary spillway, Folsom – USA

5.1.1 Location and general conditions

Folsom dam is a concrete gravity dam located in California in the North of the city of Folsom (Fig. 5-1). It lies about 41 km Northeast of Sacramento and impounds the American River forming Folsom Reservoir/Folsom Lake (Hall & Dressel).

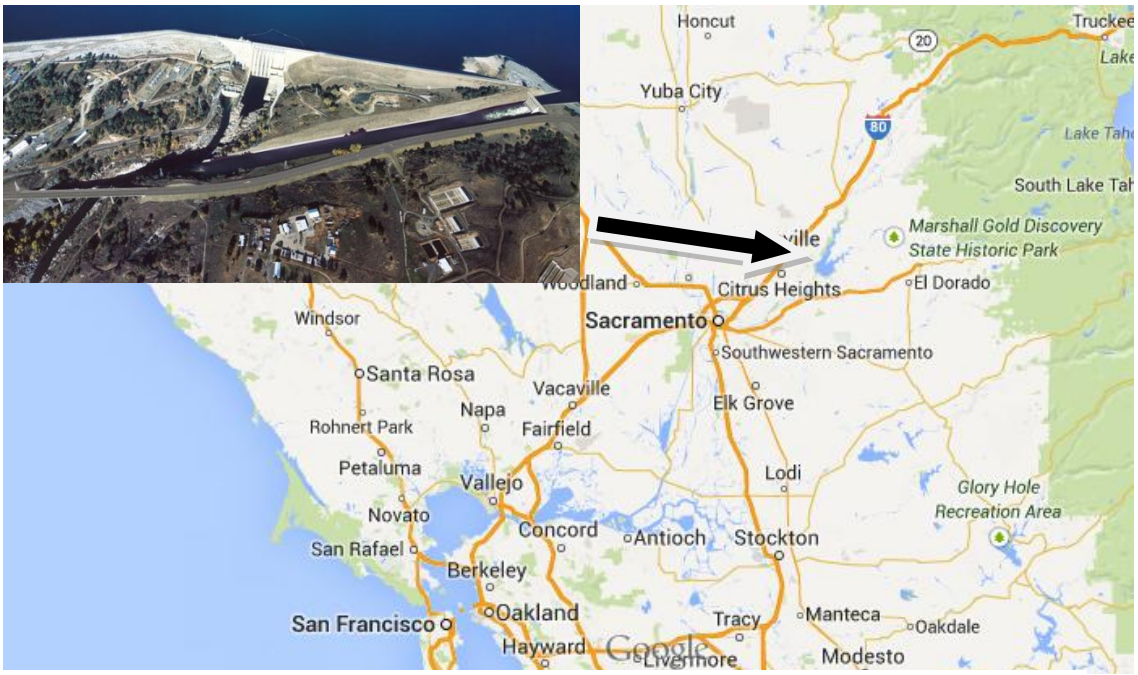

Fig. 5-1: Location of Folsom dam in California, USA (google maps, 2013).Small figure of the facility from (usbr.gov, 2013).

The dam crosses the American river and is flanked by earthfill wing dams. Folsom dam was constructed by the U.S. Army Corps of Engineers from 1948 - 1956 and is now operated by the U.S. Bureau of Reclamation. The main purpose of Folsom dam is flood control, hydroelectricity and water supply. The facility is part of the Central Valley Project of California.

To increase the safety regarding hydraulic (flood) and static (seepage) risks a new auxiliary spillway will be completed in 2017. It should improve Folsom dam's flood control and aims to release water during heavy storms together with the Folsom dam main section to reduce flooding risk. For this the Joint federal

project (JFP) was founded, including the Bureau of Reclamation and the U.S. Army Corps of Engineers (USACE). Together they aim to increase the safety of the Sacramento region. After all the work is completed, the area will look like shown in figures 5-2 and 5-3 (usbr.gov, 2013) (ussdams.com, 2013).

Fig. 5-2: Folsom dam auxiliary spillway (www.usbr.gov/USACE trifold, 2013).

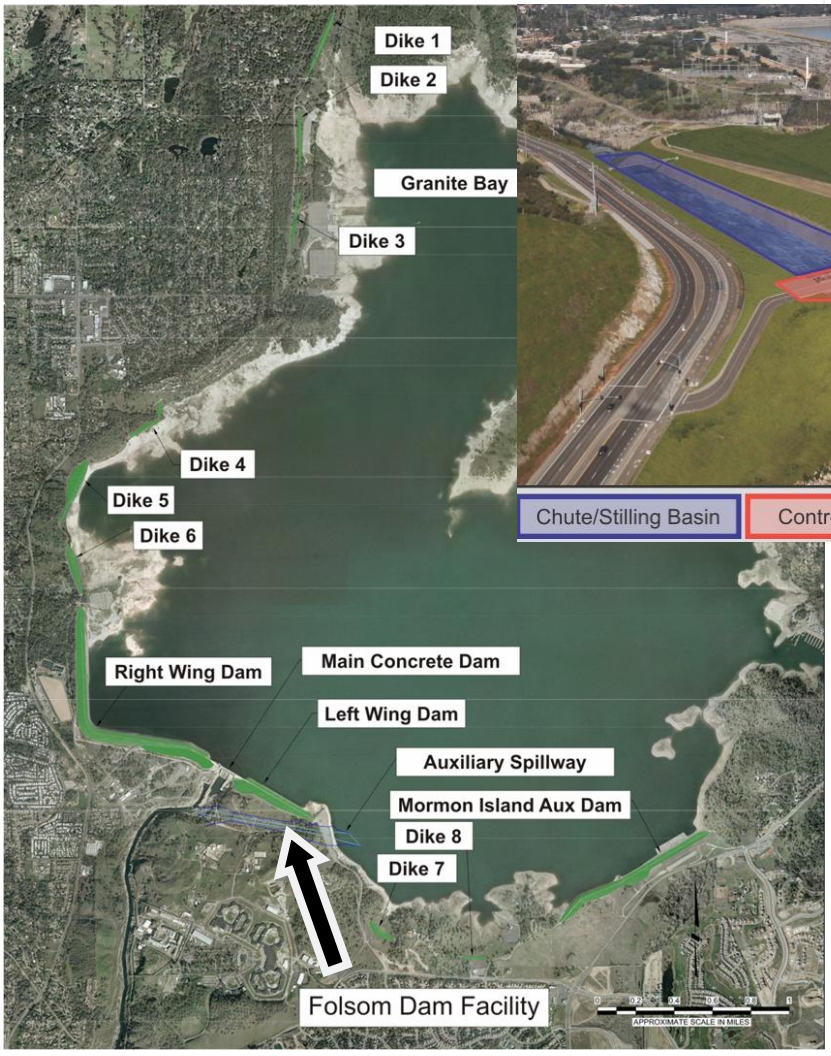

Fig. 5-3: Folsom dam facility (usbr.gov, 2013).

The new auxiliary spillway includes an approach channel, a control structure and a stilling basin. The control structure is designed to release up to 8,849 m^3/s of water (www.usbr.gov/USACE trifold, 2013). A stepped spillway at the end of the channel will help to reduce flow velocities. Figure 5-4 shows a cross section of Folsom dam auxiliary spillway:

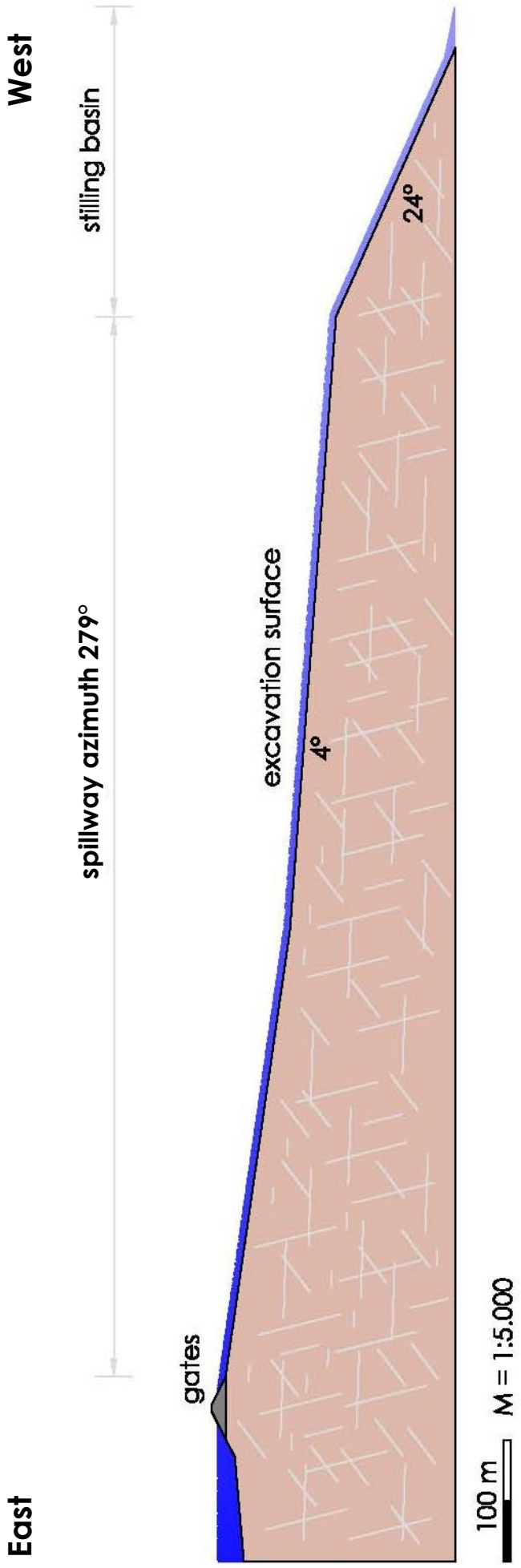

Fig. 5-4: Cross section of Folsom Dam auxiliary spillway, the scale is 1:5.000 in the horizontal and vertical direction, after (Hall & Dressel).

General facts about Folsom dam:

Dimensions:

Height	103.6 m
Normal operating depth at dam	83.9 m
Elevation	147.5 m
Crest elevation	146.5 m
Crest length	426.7 m
Crest width	11.0 m
Base width	82.3 m

Hydraulics and Hydrology

Storage capacity	111,013,366 m^3
Maximum water surface at elevation	146.3 m
Spillway capacity at elevation	16,055.6 m^3/s at 144.9 m
Drainage area	4,856.22 km^2
Hydrometeorological report (HMR)	HMR 58
Probable maximum flood (PMF) report	1996

Tab. 5-1: General information about Folsom dam (www.usbr.gov).

5.1.2 Geologic condition

The dam area is predominantly within the Mesozoic-age Foothills Metamorphic Belt, which is dominated by the North-Northwest trending Foothills Fault System, shown in Figure 5-5 (U.S. Army, Corps of Engineers, 2012). The Foothills Fault System has been considered to be inactive but recent studies show that some fault segments are indeed active, so minor sporadic earthquakes are possible. The closest of these fault segments is the Bear Mountain fault zone, the western part of which is situated along the east side of Folsom lake (U.S. Army, Corps of Engineers, 2012).

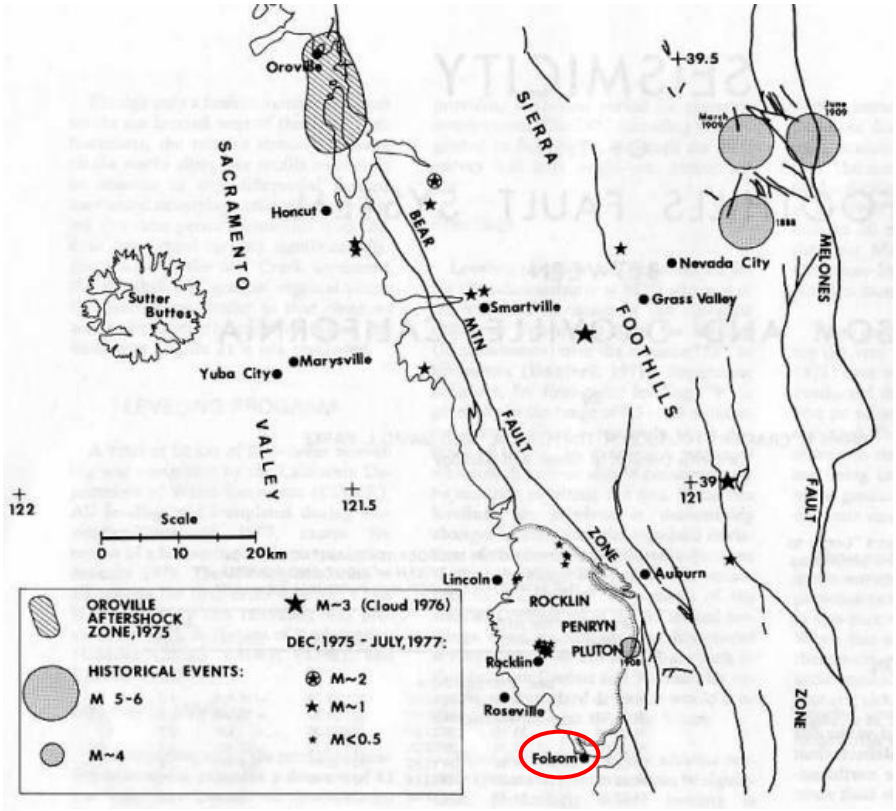

Fig. 5-5: Map of the Northern part of the Foothills Fault System, showing the possible seismic activity in the region of Folsom dam and Folsom dam auxiliary spillway through the „Bear Mountain Fault Zone“, the city of Folsom is indicated by the red circle, (Cramer et al., 1978).

The dam is generally situated in an area of weathered granitic and metamorphic rocks. The main part of Folsom dam is founded on quartz-diorite from the upper Jurassic. The quartz-diorite is extensively fractured and shows a complex joint system. A shear or fracture zone can be assumed through closely spaced joints. The basement of the JFP auxiliary spillway shows the same characteristics than the above mentioned. The excavated rock mass is part of the Rocklin Pluton, an intrusive which forms mostly through quartz-diorite and granodiorite of Mesozoic age. The rock material can be referred to as granite.

The main lithologic units in the area of Folsom dam and Folsom dam auxiliary spillay from youngest to oldest are:

- *Fill*: This kind of material is basically a leftover from the excavation of the main dam in the 1950s. The grain size varies from silty sand with gravel, over to cobbles and boulders.
- *Surficial deposits*: Cover the bedrock across most of the area.
- *Mehrten Formation*: This formation is of Tertiary age, volcanic tuff and breccias mudflow deposits limit the area.
- *Rocklin Pluton Quartz-Diorite*: The intrusive shows different stages of weathering and contains about 20% of mafic minerals.

(U.S. Army, Corps of Engineers, 2012)

Figure 5-6 shows a geologic map of the region around Folsom dam and figure 5-7 the corresponding geologic legend. In the South-East of the dam facility the Bear mountain fault zone is visible, which could affect the seismology of the area (U.S. Army, Corps of Engineers, 2012). Folsom dam and Folsom dam auxiliary spillway lie within the pink area (gr^{Mz}) which indicates Mesozoic, Plutonic rocks.

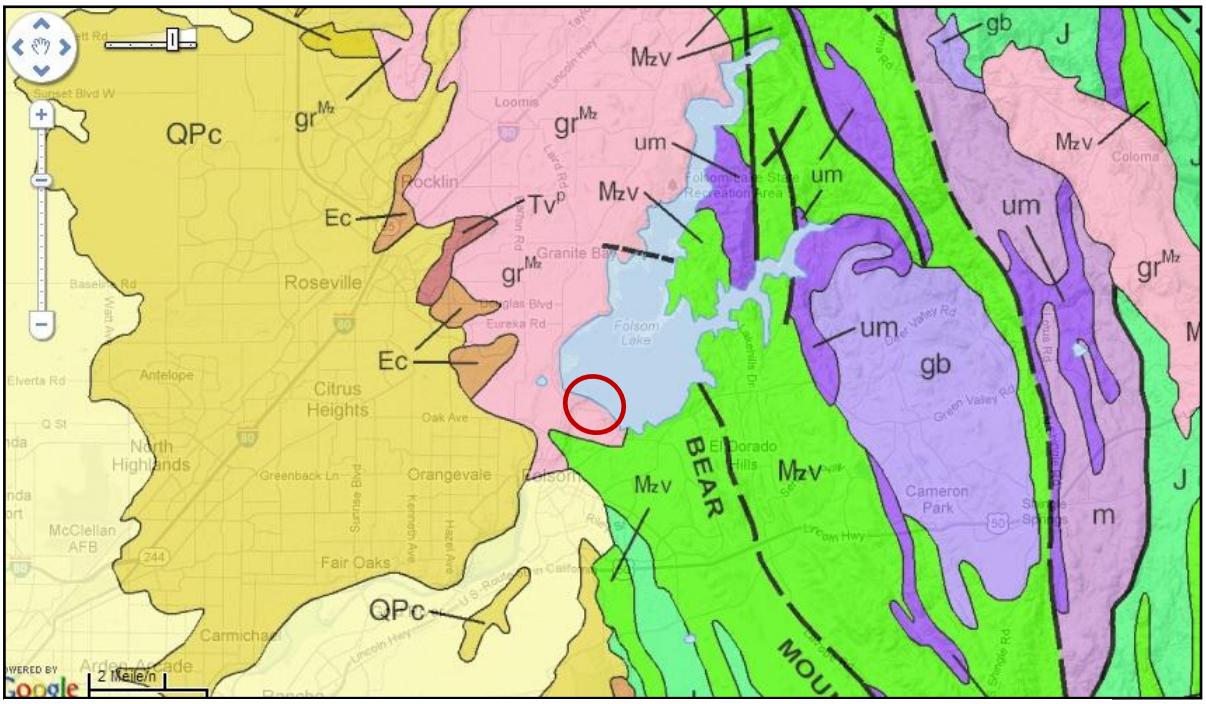

Fig. 5-6: Geologic map of the region around Folsom dam. The dam facility is indicated by the red circle (State of California, 2007).

Quaternary deposits	Q	Alluvium, lake, playa and terrace deposits						
	Qoa	Older alluvium, lake, playa and terrace deposits						
	QPc	Sandstone, shale and gravel deposits						
Tertiary sedimentary rocks	M	Sandstone, siltstone, shale, breccia and conglomerate, moderately to well consolidated	Tertiary volcanic rocks	Tv^{p}	Pyroclastic and volcanic mudflow deposit			
	Mc	Sandstone, shale, conglomerate and fanglomerate, moderately to well consolidated						
	Ec	Sandstone, shale, conglomerate. Moderately to well consolidated						
Mesozoic sedimentary rocks	J	Shale, sandstone, minor conglomerate, chert, slate, limestone; minor pyroclastic rocks	Mesozoic volcanic rocks	Mzv	Andesite and Rhyolite flow rocks, greenstone, volcanic breccias and other pyroclastic rocks	Mesozoic plutonic rocks	gr^{Mz}	Granite, quartz monzonite, granodiorite and quartz diorite
	m	Metasedimentary and metavolcanic rocks; mostly slate, quartzite, hornfels, chert					um	Ultramafic rocks, mostly serpentine
							gb	Gabbro and dark dioritic rocks

Fig. 5-7: Geologic legend of the region (State of California, 2007).

5.1.2.1 Bedrock weathering

The strength and deformability of the quartz diorite bedrock is affected by the degree of weathering, fracturing and alteration. The quartz diorite at the site shows a variable weathering profile that grades downward, from more weathered through less weathered to unweathered rock. The depth of the weathering is affected by the spacing and the permeability of joints, fractures and shear zones (U.S. Army, Corps of Engineers, 2012). Through core mapping and a surface mapping the Corps divided the degree of weathering of the quartz diorite into 5 zones, from surface to depth:

- *Decomposed*: The material can be crumbled by hand, the quartz diorite is weathered to a sandy silty soil with traces of clay
- *Highly weathered:* the rock mass is discolored, minerals such as biotite and hornblende are leached out
- *Moderately weathered*: 10 to 50 percent of the rock is weathered, discoloration is still evident
- *Slightly weathered*: slight weathering along discontinuities and slight discoloration, < 10% of the rock volume is weathered
- *Unweathered*: No evidence of chemical or mechanical weathering

(U.S. Army, Corps of Engineers, 2012)

5.1.2.2 Shear zone (S1) and main joints

Shear zone 1 (S1) strikes approximately East-West and lies to the North of the auxiliary centerline in the control structure area. S1 shows intervals of intense fracturing and shearing, gouge seams, variable weathering and variable degrees of clay and other alteration. Signs for hydrothermal alteration and the strike length of about 457.2 m propose that S1 is a major fault with probably a great depth extent. Figure 5-8 shows the S1 in the headwall and floor of the spillway of the Phase II excavation (U.S. Army, Corps of Engineers, 2012).

Fig. 5-8: Photograph, looking North from the left cut slope, showing S1 in the headwall and the floor of the spillway during phase II excavation. The red circle indicates two cars for scale, (U.S. Army, Corps of Engineers, 2012).

The Bureau of Reclamation names the four principal joint sets as A, B, C and D. This data was received after getting results from acoustic and optic televiewer surveys of drill holes and surface mapping. 2.567 joints were linked to the four major joint sets, Reclamation`s stereogram in figure 5-9 shows the result. For each of the joint sets the average orientation is indicated through a pole and a great circle.

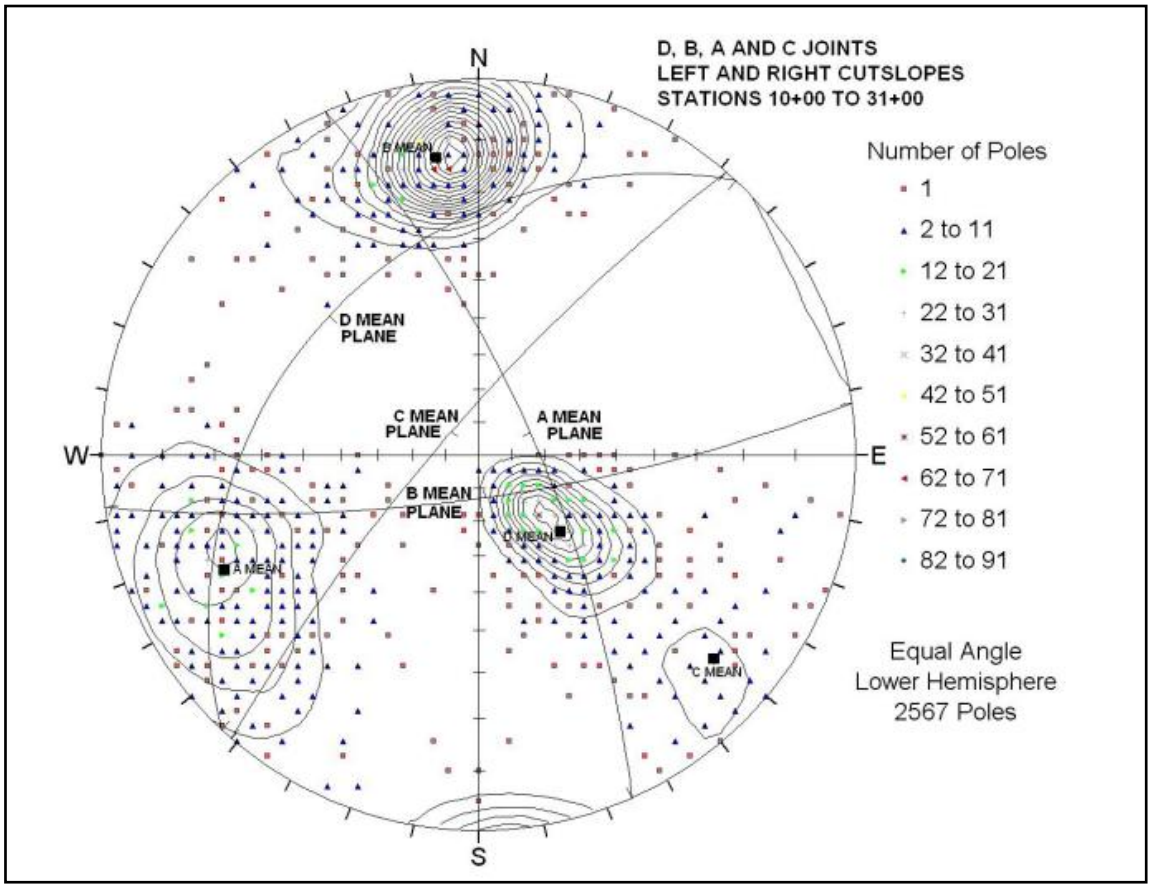

Fig. 5-9: The stereogram shows the average orientation of the four different joint sets (A, B, C, D), data and plot from the Bureau of Reclamation (U.S. Army, Corps of Engineers, 2012).

Through this plot it was possible for Reclamation to identify four major joint sets (U.S. Army, Corps of Engineers, 2012):

Joint set	Average orientation	
	Dip direction (degrees)	Dip (degrees)
A	066	73NE
B	172	77SE
C	311	79NW
D	313	33NW

Tab. 5-2: Average orientation of the four major joint sets identified by Reclamation, (U.S. Army, Corps of Engineers, 2012).

These dip and dip directions were used in this thesis to work with Block Theory.

For the D-joints there are two different kinds, some show a shallower dipping then others. For this thesis only the value of 33/313 was used as an average value from the measurements.

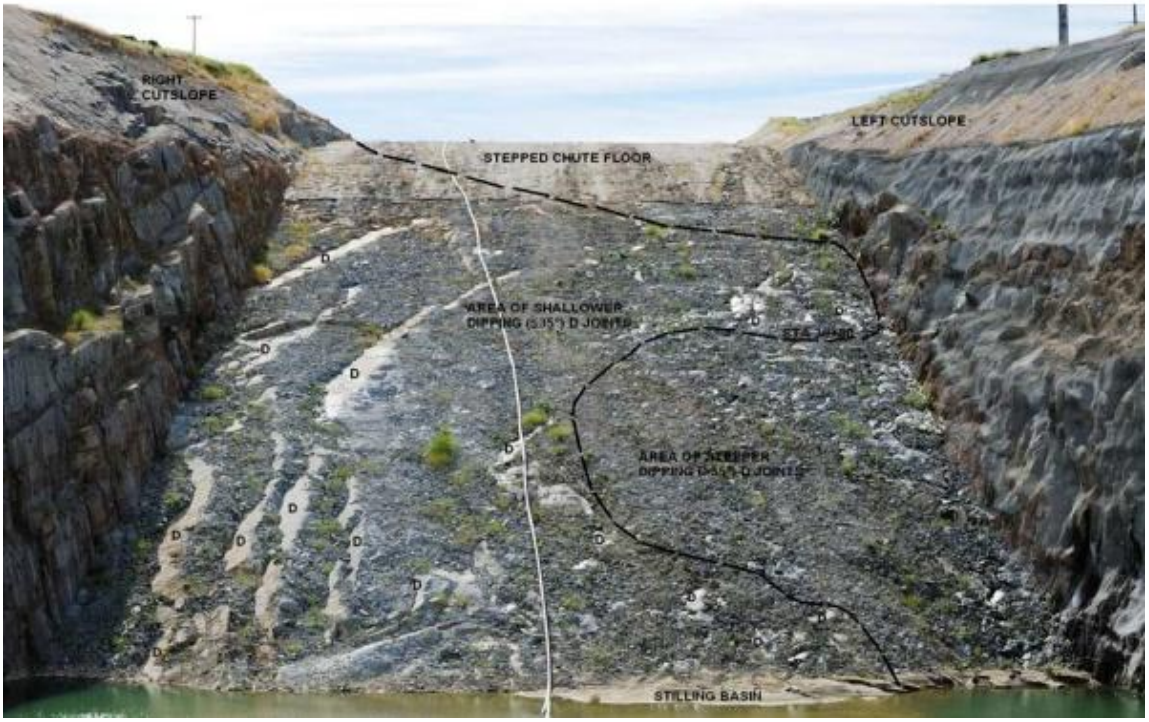

Fig. 5-10: The photograph shows the two different kind of D-joints, on the left side of the picture the D-joints are dipping shallower than at the right side of the picture (U.S. Army, Corps of Engineers, 2012).

5.1.3 Construction stages for the spillway chute and the stilling basin excavation

The most important construction stages for Folsom dam auxiliary spillway are Phase I and Phase II of the excavation. Phase I included excavation of approximately 240,834.78 m^3 of common material (no rock) and 137,619.87 m^3 of rock (U.S. Army, Corps of Engineers, 2012). The excavated section was partly cut out of soil-like, decomposed granite and partly out of competent rock material (Hall & Dressel).

In Phase II approximately another 626,934.98 m^3 of common material and 680,453.82 m^3 of rock were excavated. Phase II also included to have as steep of a cut slope as possible. A 3.6 m wide bench was planned and decided to be build in this phase of the excavation. It is situated about 1.2 m below the top of the JFP spillway walls (U.S. Army, Corps of Engineers, 2012).

Both project parts were undertaken in slightly to unweathered rock. Also some support and erosion protection was necessary in the region of the cut slopes.

For instance another 12-foot wide bench was build to reduce erosion and add stability. Also slope drains were established to ensure safety, which is necessary as the spillway will be subjected to very large hydrodynamic loads, the design discharge capacity is about 4,530.69 m^3/s (U.S. Army, Corps of Engineers, 2012).

Both of the phases have been finished. The whole Folsom dam auxiliary spillway program is scheduled to be completed in October 2017 (www.usbr.gov/USACE trifold, 2013).

5.1.4 BSS Analysis

For the new auxiliary spillway of Folsom dam a block erodibility spectrum ("BSS") was made for the flat spillway surface and for the front slope where the spillway enters the stilling basin. The results are presented in this chapter.

For using this application the necessary information of the Folsom dam auxiliary spillway were gathered. As main joints the values presented in section 5.1.2.2 were taken (U.S. Army, Corps of Engineers, 2012). The average inclination of the upper spillway surface is 4° and the inclination of the stepped chute slope that enters the stilling basin has an average inclination of 24°. The auxiliary spillway runs in azimuth of 279 (U.S. Army, Corps of Engineers, 2012). All these details together with the rock joint orientations formed the basis of the Block Theory analyses. The removable blocks were identified, a failure mode analysis was performed and the Block Scour Spectrum was created.

5.1.4.1 Analysis of the upper spillway surface

For the analysis of the upper spillway surface an inclination of 4° was used (U.S. Army, Corps of Engineers, 2012). Figure 5-11 shows a schematic drawing of the upper spillway part and the surrounding topography (Hall & Dressel).

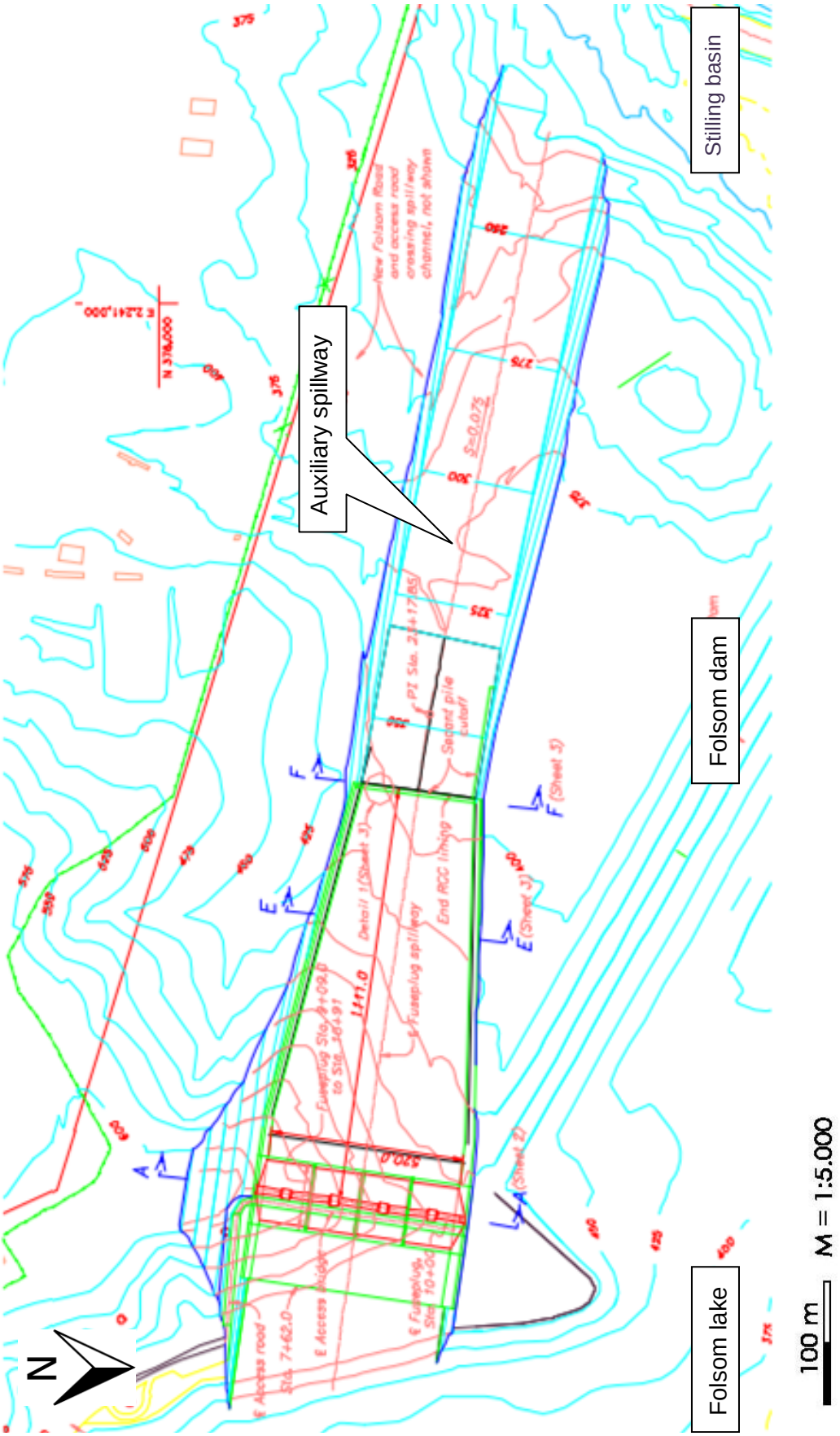

Fig. 5-11: Schematic sketch of the upper spillway surface and surrounding topography (Hall & Dressel).

5.1.4.2 Kinematic analysis

First the kinematic analysis was made. By plotting the orientation of the main joints and the free surface into a stereographic projection it was possible to identify the removable blocks for the upper part of the spillway. Figure 5-12 shows the result of the plot, the table in the left, lower corner shows the joint sets of the region which were used to create the following plots. Table 5-3 shows the enlarged table from the plot.

joint number	dip (degrees)	dip direction (degrees)	color
J1 (A)	73	66	dark blue
J2 (B)	77	172	green
J3 (C)	79	311	light blue
J4 (D)	33	313	purple
Free surface for the spillway surface	4	279	red
Free surface for the approach to stilling basin	24	279	red

Tab. 5-3: Orientations used for the kinematic analysis of Folsom dam auxiliary spillway, (U.S. Army, Corps of Engineers, 2012).

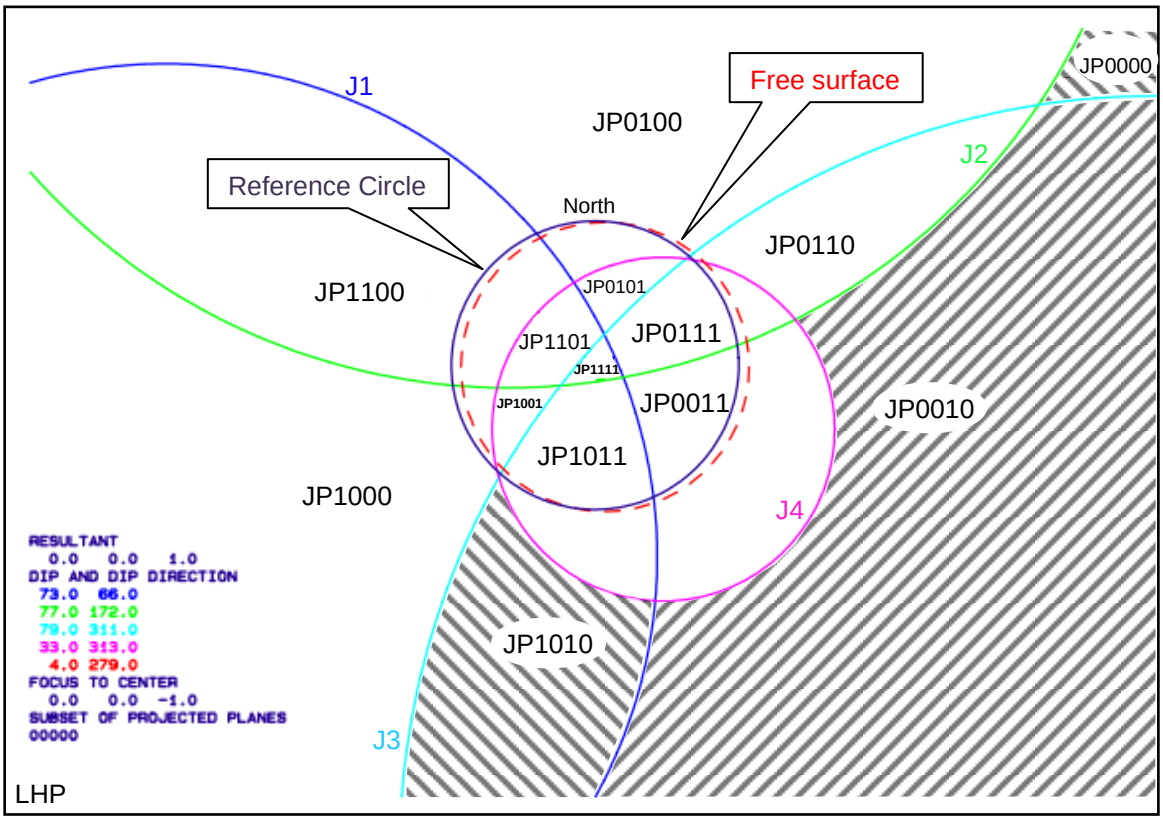

Fig. 5-12: Whole sphere stereographic projection of the upper spillway surface and the 5 joint sets comprising the rock mass. The shaded areas show the removable blocks. LHP = lower hemispherical projection

The red dashed circle shows the upper spillway surface, the blue circle represents the reference circle. The values on the right are the orientations of the joints and the free surface, triangles that lie completely outside the red circle show the removable blocks. Three blocks were identified and named with their Joint Pyramid codes, block 0010, block 1010 and block 0000. JP0000 is not shown in the stereographic projection.

Figure 5-13 shows the result of the kinematic analysis of the spillway when it approaches the stilling basin. The grey circle shows the reference circle and the red dashed circle represents the lower spillway surface. Three removable blocks were identified JP1000, JP1010 and JP0000.

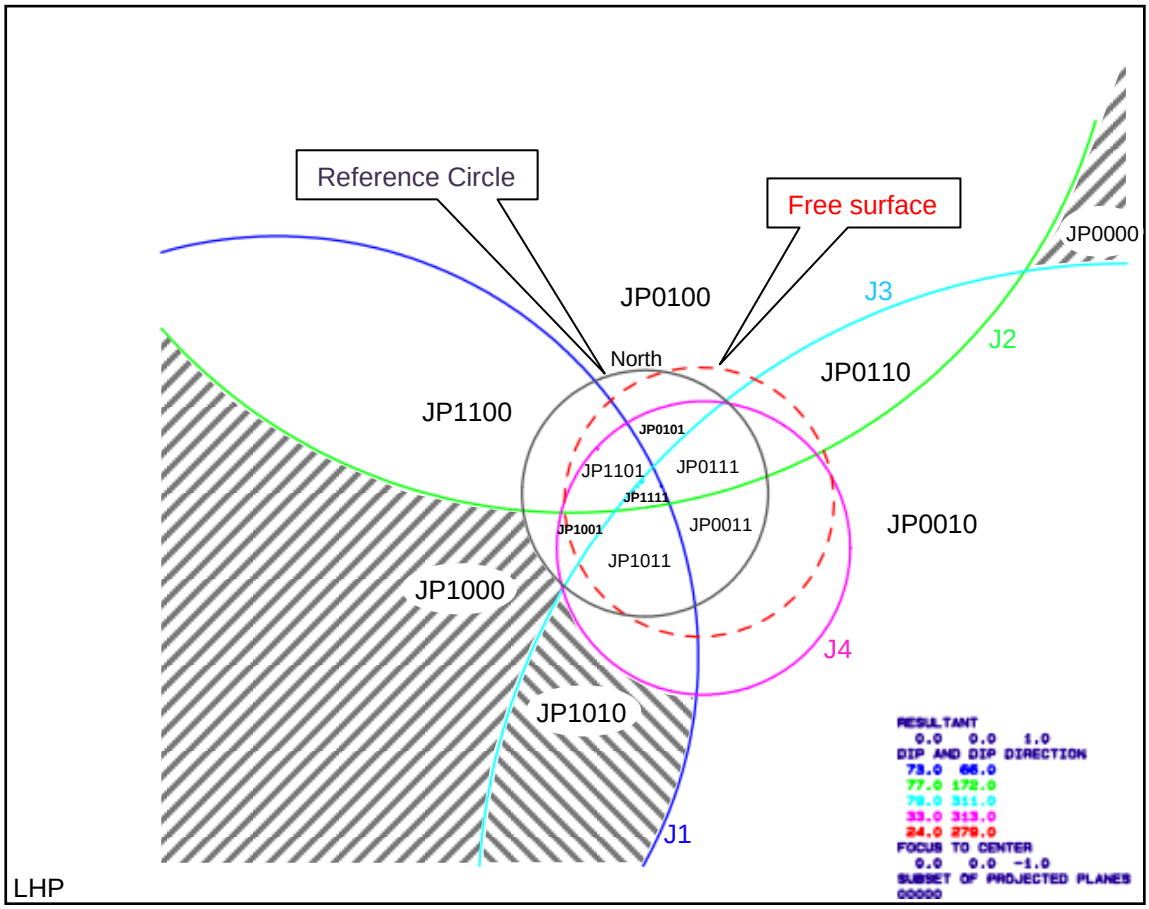

Fig. 5-13: Whole sphere stereographic projection of the spillway section where it approaches the stilling basin and the 5 joint sets comprising the rock mass. The shaded areas show the removable blocks. LHP = lower hemispherical projection

Position	Removable blocks	Block type
Spillway surface	0000	III
	1010	III
	0010	III
Spillway approaching stilling basin	0000	III
	1010	III
	1000	II

Tab. 5-4: List of the identified removable JP's for Folsom dam auxiliary spillway.

Table 5-4 shows the identified removable JP's for the spillway. The combination of the two results will be called the compound slope and is made up of the JP's 0000, 0010, 1000 and 1010.

5.1.4.3 Block Scour spectrum

In this section the results of the Block Scour Spectrum for the Folsom dam auxiliary spillway is presented. The analysis is performed with a discontinuity friction angle of 30° and 40° as these values cover the most expected friction angles for granite, after Barton (1973):

Rock class	Friction angle range	Rock types
Low friction	20-27°	schists with high mica content, shale, marl
Medium friction	27-34°	sandstone, siltstone, chalk, gneiss, slate
High friction	34-40°	basalt, **granite**, limestone, conglomerate

Tab. 5-5: Typical friction angle ranges for a variety of rock types. For granite a high friction of a range from 34° to 40° is expected, (Barton, 1973).

The limit equilibrium analysis is performed for all of the removable blocks, of the upper spillway and of the spillway section where it approaches the stilling basin. Figure 5-14 shows the friction cone for 30° for JP0010 from the upper spillway part. As a step degree of the friction angle 5° were used. The dashed lines show the mobilized friction angle along the block surface. The red digits represent different block failure modes, table 5-6 shows the failure possibilities.

Block 0010 is a type III block, it is stable under gravity, this means that no lifting under gravity will occur, but the water force will eventually take the block to a failure mode. Figure 5-14 shows the friction cone for 40° for JP0010.

Number on projection	Failure mode	Block type
0	I	Lifting or falling
1, 2, … (single-digit number)	II	Plane sliding
12, 24 (two-digit number)	II	Wedge sliding
No number	III	No failure mode

Tab. 5-6: Types of failure modes for identified removable JP‘s.

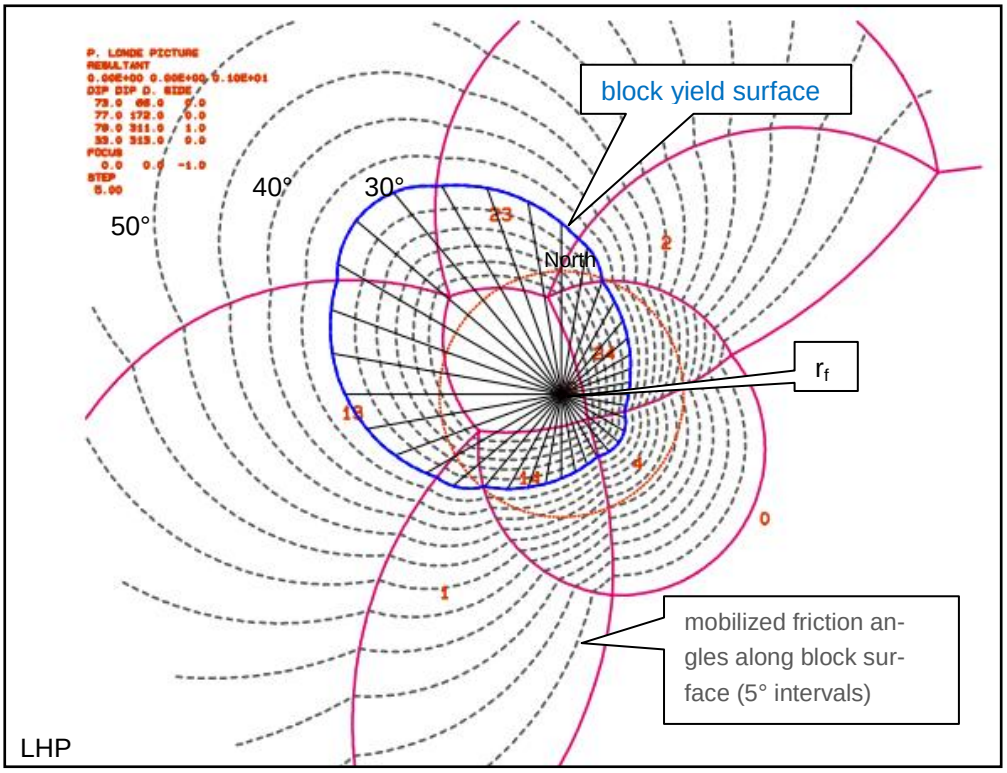

Fig. 5-14: Stability plot for JP0010 with an assumed friction angle of 30°.

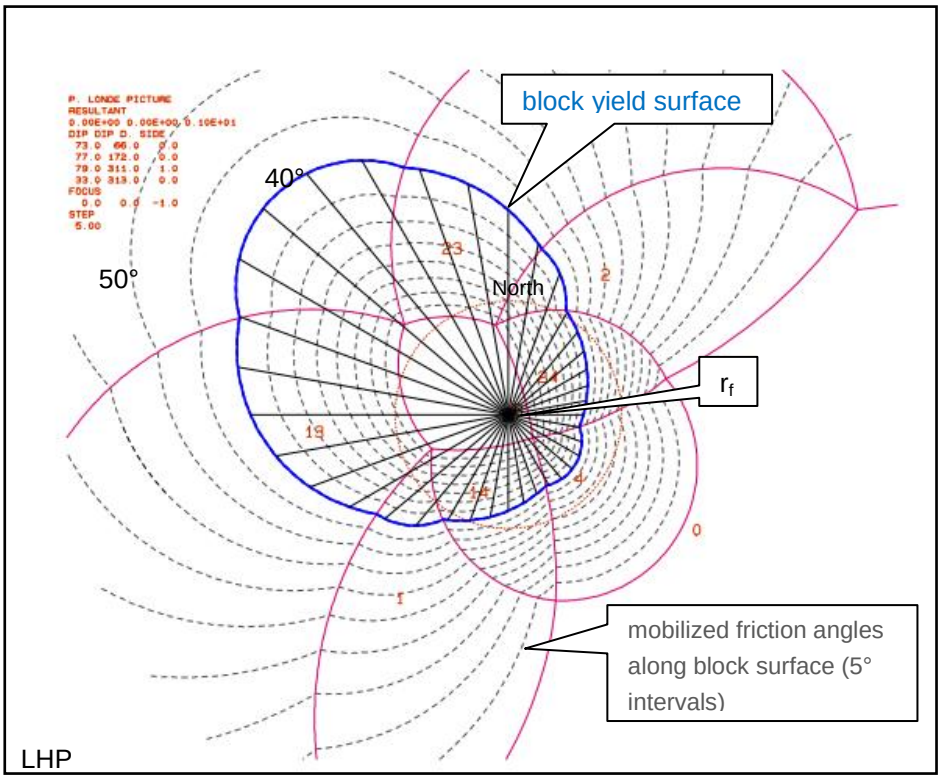

Fig. 5-15: Stability plot for JP0010 with an assumed friction angle of 40°.

Important to observe is the line of limit equilibrium and the distance to "r_f" (resultant force). The distance varies throughout the circle, as it can be seen in Figure 5-14 and 5-15 the distance is in the direction E-SE the smallest which indicates that the resistance in this direction is much smaller than to for example North-West. Also into the direction of the spillway flow (azimuth 279) the line of limit equilibrium is short compared to other directions. Nevertheless for an actual angle of rotation (θ) from these plots it is necessary to use equation 5.2. It uses the distances from "R" (radius of the reference circle) to the line of limit equilibrium:

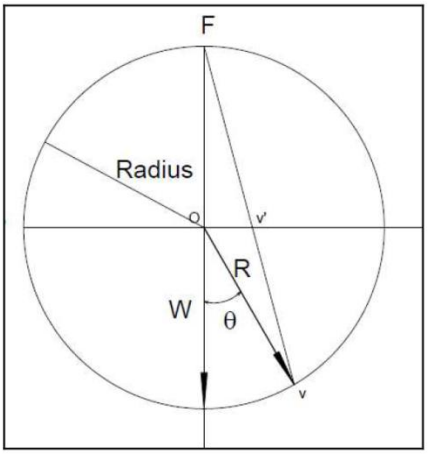

$$\boldsymbol{\theta = 2 * \arctan\left(\frac{ov'}{R}\right)} \text{ (Eq.5.2)}$$

R = radius of the reference circle

ov‘ = measured distance

Fig. 5-16: Drawing showing the transformation of the measured distances (ov') to the angle of rotation, see equation 5.2.

5.1.5 Results of the BSS analysis for Folsom dam auxiliary spillway, upper part and spillway when it approaches the stilling basin

For Folsom dam auxiliary spillway the analysis was made for the flat spillway surface and the spillway slope when entering the stilling basin. Both of the results can be seen in the Figures 5-17 – 5-22. In both cases 3 blocks are removable. The blocks with the JP codes 1010 and 0010 are removable for both parts of the spillway. The stability plots that lead to the results can be seen in the appendix.

5.1.5.1 Folsom dam auxiliary spillway, spillway surface

After analyzing the stereo-plots three blocks were identified to be removable: 0010, 1010 and 0000. The BSS analysis shows the following result with discontinuity friction angles of 30° and 40°:

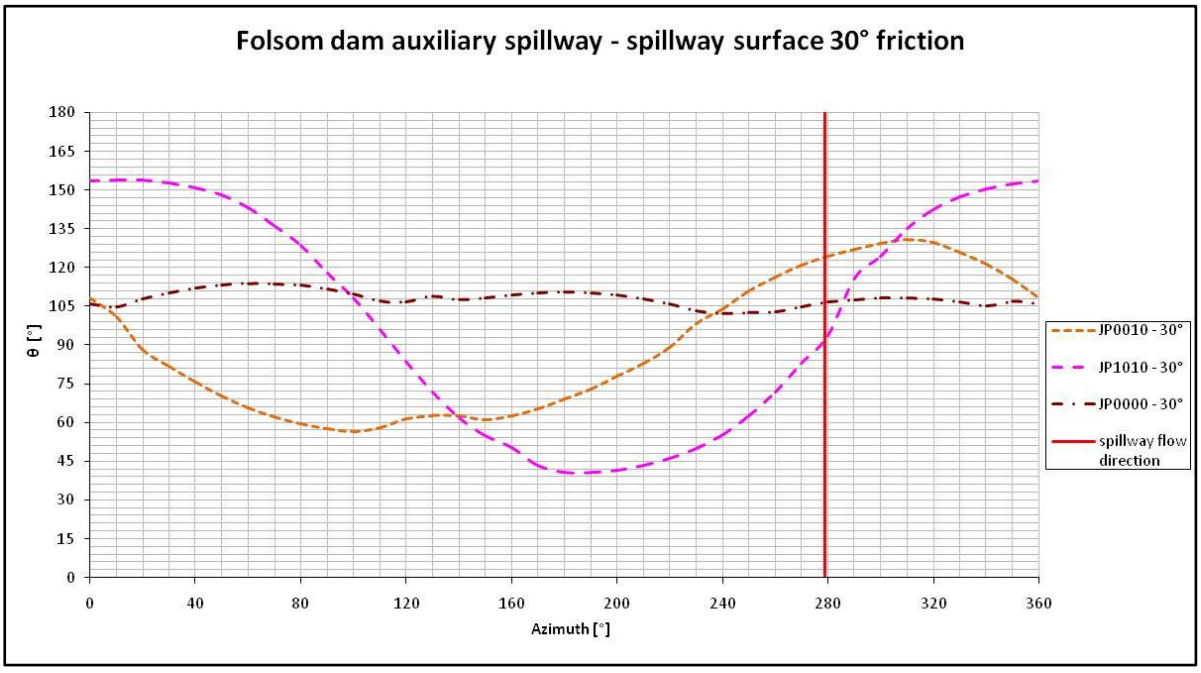

Fig. 5-17: Block Scour Spectrum for JP's 0010, 1010 and 0000 with φ = 30°.The diagram shows the azimuth versus the angle of rotation. The spillway flow (279°) is indicated by the red, vertical line.

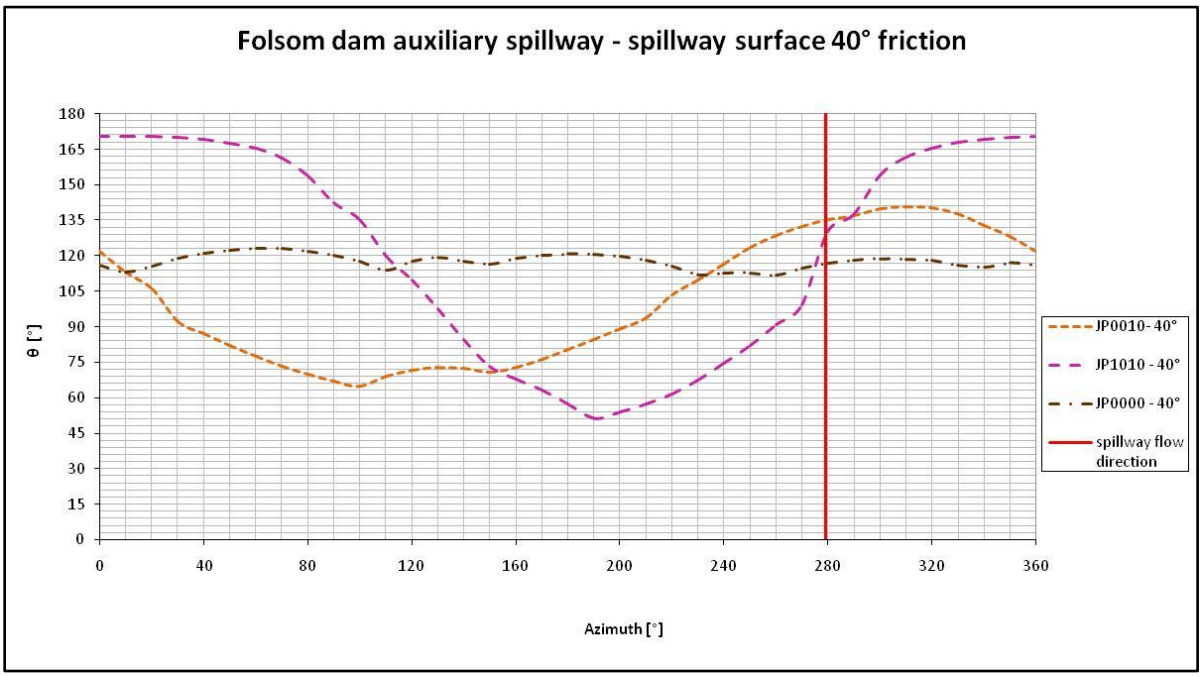

Fig. 5-18: Block Scour Spectrum for JP's 0010, 1010 and 0000 with φ= 40°. It shows similar results to figure 5-17 (φ = 30°), but the values are slightly shifted.

To show the minimum composite requirements for the removal of any block type, the Block Scour Spectrum Envelope (Kieffer & Goodman, 2012) is created, it shows where the most unfavorable direction of resultant hydraulic loading acts (Figure 5-19).

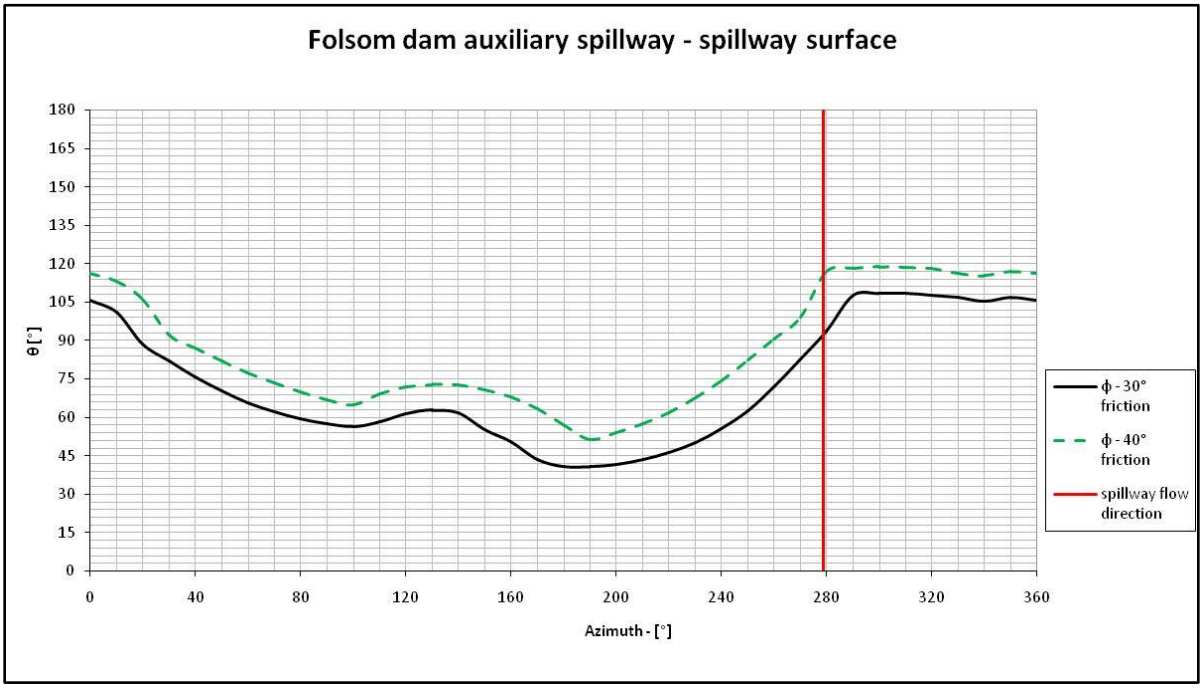

Fig. 5-19: Block Scour Spectrum Envelope for Folsom dam auxiliary spillway – spillway surface for the friction angles 30° and 40° (dashed line). The orientation of the spillway is indicated by the vertical, red line.

5.1.5.2 Folsom dam auxiliary spillway, approach stilling basin

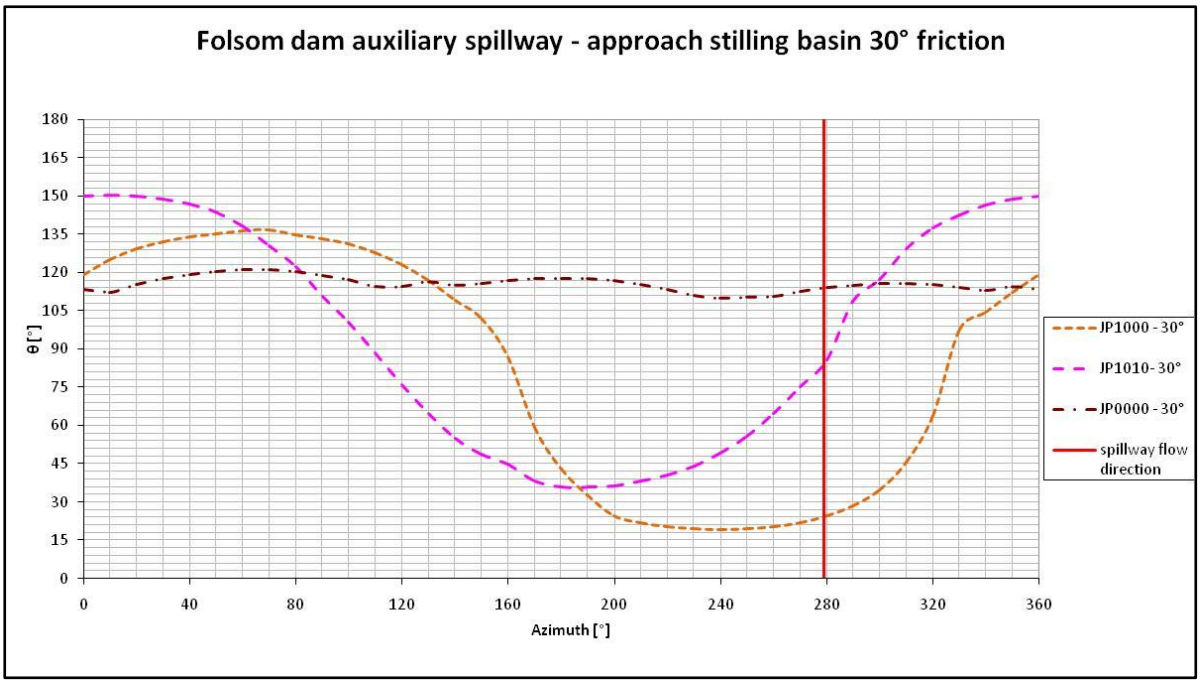

Fig. 5-20: Block Scour Spectrum for JP's 1000, 1010 and 0000 with φ = 30°.The diagram shows the azimuth versus the angle of rotation. The spillway flow (279°) is indicated by the red, vertical line. The angle of rotation is close to its minimum for JP1000 in the direction of 240°.

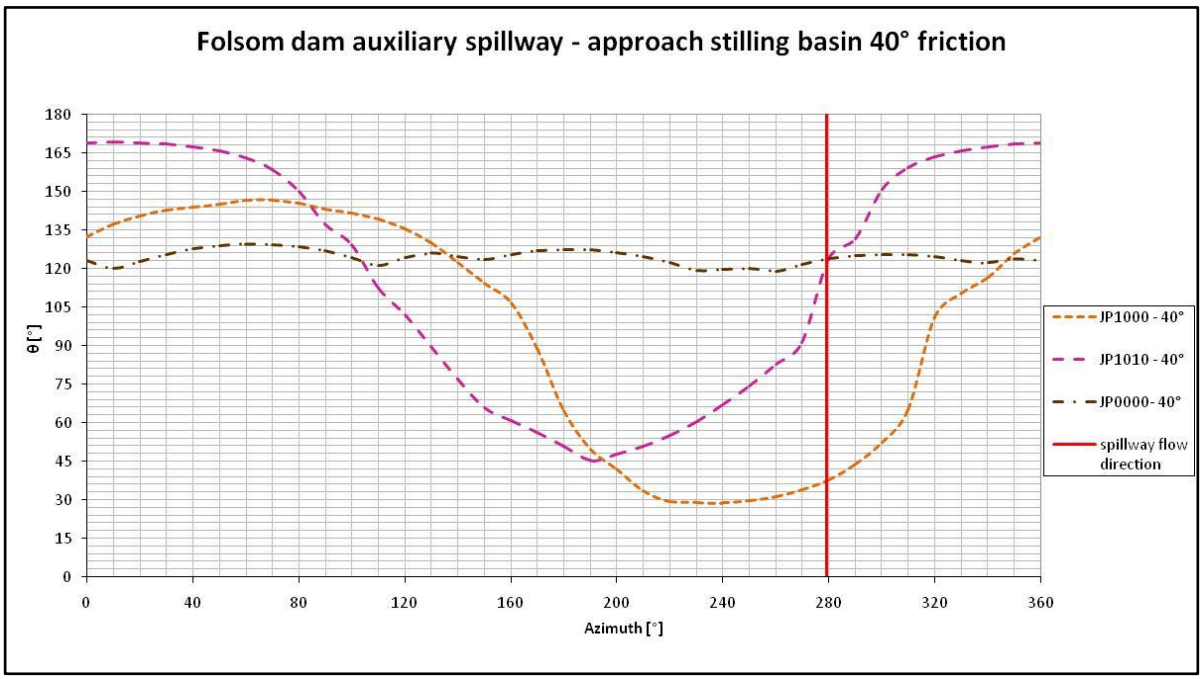

Fig. 5-21: Block Scour Spectrum for JP's 1000, 1010 and 0000 with φ= 40°. It shows similar results to figure 5-20 (φ = 30°), but the values are slightly shifted.

Figure 5-22 shows the Block Scour Spectrum Envelope for Folsom dam auxiliary spillway when approaching the stilling basin.

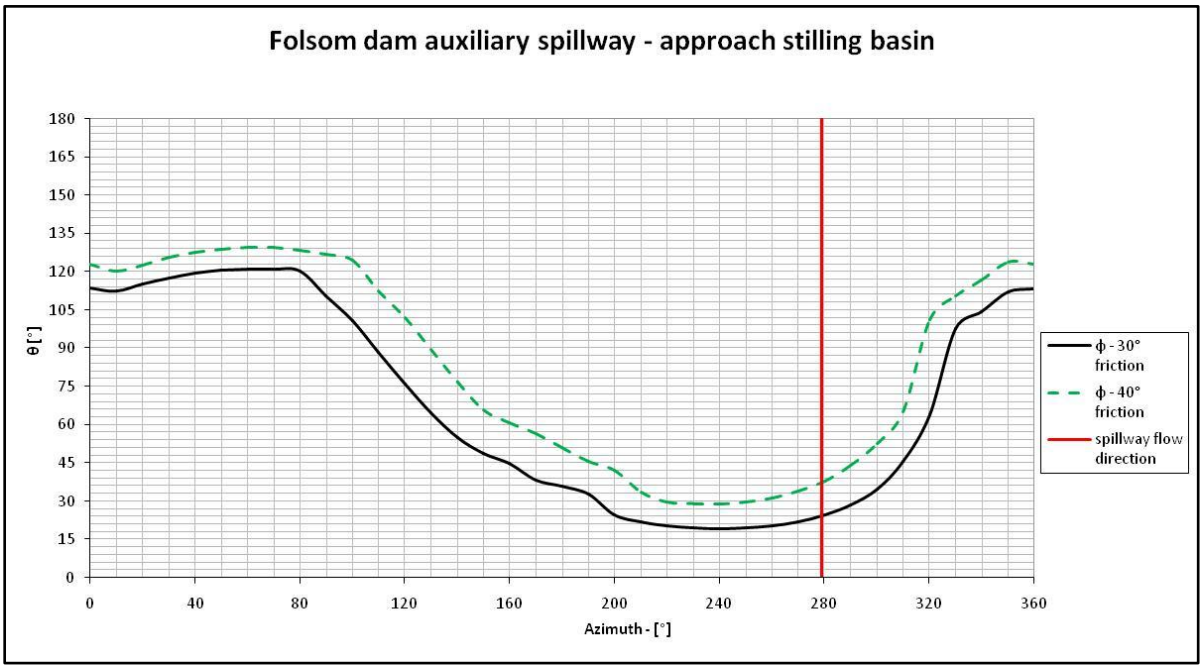

Fig. 5-22: Block Scour Spectrum Envelope for Folsom dam auxiliary spillway when approaching the stilling basin for friction angles 30° and 40°. The angle of rotation drops to minimum values in the direction of 240°.

5.2 Quebec dam spillway, Quebec – Canada

5.2.1 Location and general conditions

The Canadian spillway that is featured in this thesis is located in the Northern part of Quebec and it was completed in 1979. As it was not permitted to discuss sensitive details about the dam and the spillway, or to give an exact location of the facility, the spillway will therefore be called “Quebec dam spillway” and the focus lies on the BSS analysis of the granitic basement. Figure 5-23 shows the location of Quebec in North-America.

Fig. 5-23: Location of Quebec in North-America, (google maps, 2013)

Table 5-7 shows general information about the spillway and the dam facility:

Dimensions of the dam	
Type of dam	Embankment dam
Height	162 m
Length	2.835 m
Crest width	9 m
Dimensions of the spillway and the reservoir	
Maximum hydraulic head at crest	19,70 m
Maximum hydraulic head at the bottom of the stilling basin	38,1 m
Active volume of the reservoir	19.431 hm^3

Reservoir surface area	2.835 km^2
Mean depth of the reservoir	20 m
Spillway discharge capacity	16.280 m^3/s

Tab. 5-7: General information about the Quebec dam, (Nzakimuena & Zulfiquar, 2009) (Hydro-Québec, 2004) (Hydro Quebec, 2003).

5.2.2 Geologic condition

The complex geology of Quebec is influenced by early geological events and the last glaciations which lasted till about 10.000 years ago. Quebec consists of three main regions from a geological point of view (Figure 5-24):

- *The Canadian Shield* or also known as the Precambrian Shield or Laurentian Plateau formed about 1500-900 million years ago (covers about 95% of Quebec).
- *The St. Lawrence platform*, formed about 600 million years ago
- *The Appalachian orogen* (thrust sheets), formed between 460-380 million years ago

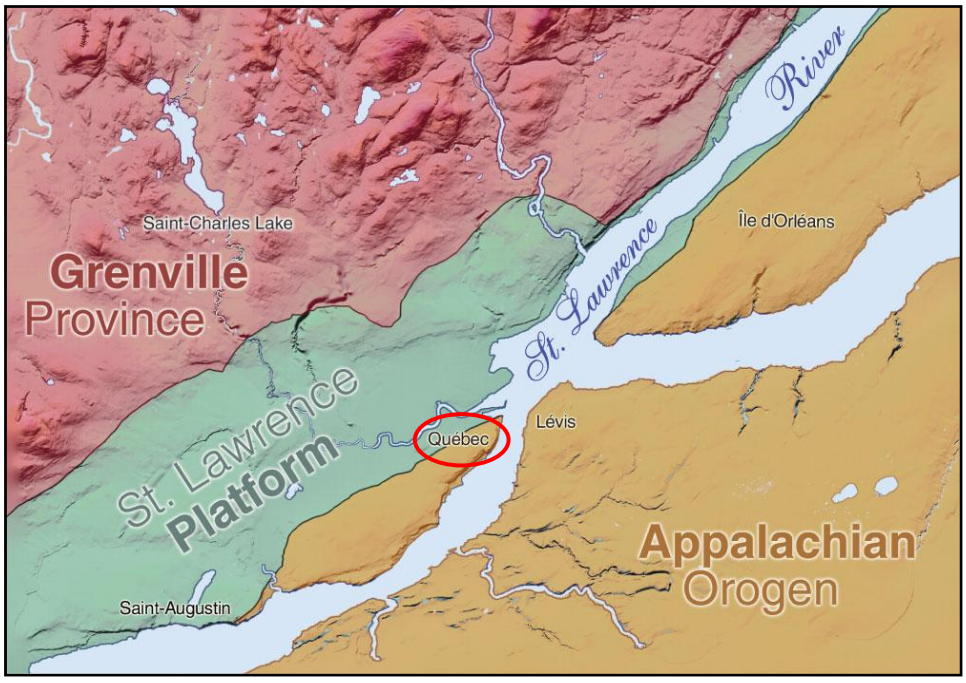

Fig. 5-24: Quebec's three main geologic regions: Grenville Province (part of the Canadian Shield), the St. Lawrence platform and the Appalachian Orogen. The figure shows a region in the South-Eastern part of Quebec, the city of Quebec is indicated by the red circle. The actual study area is situated to the North-West of Quebec and is part of the Canadian Shield (Natural Resources Canada, 2008).

5.2.2.1 The Canadian Shield

The spillway is located in an area of Quebec that belongs to the geological unit of the Canadian Shield which features some of the oldest igneous rocks in the world, some of them formed over 1 billion years ago (Quebec Biodiversity, 2013).The shield covers about 4.4 million square kilometers (see Figure 5-25) and represents the oldest part of the North American crustal plate (Canadian Shield Foundation, 2013). The main component is granite, but even though it is formed through ancient crystalline rocks, the complex was also influenced by the movement of ice sheets. Through invasion and withdrawal of mighty glaciers the topography of the Shield was formed, the weathered rock was scraped off, and some of it deposited on the shield.

Glacial deposits of boulders, gravel and sand are typical for this region. Also thick clay deposits are present, which deposited through postglacial seawater and lakes. (Quebec Biodiversity, 2013).

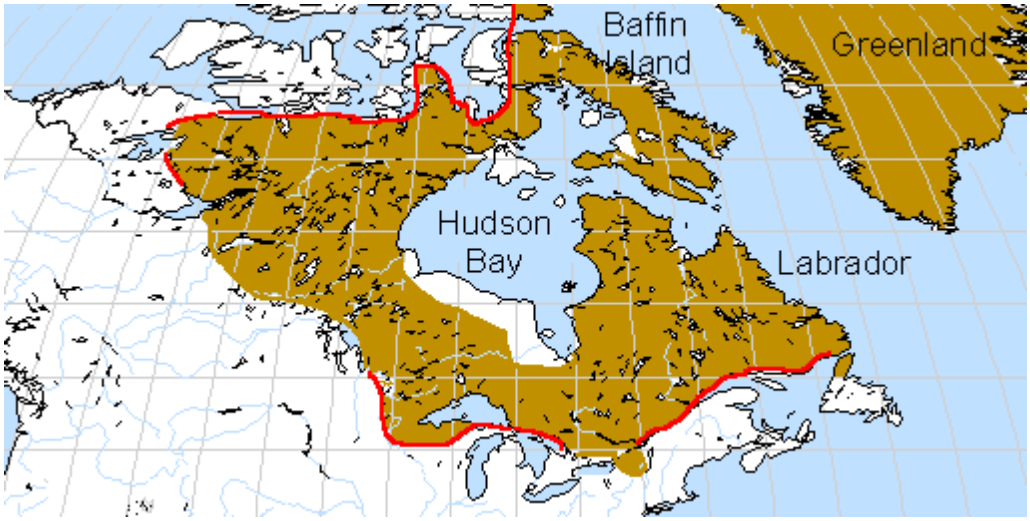

Fig. 5-25: Extent of the Canadian Shield, (Cox, 1999).

5.2.3 Data used for analysis with Block Theory

The data that was used for the analysis of the Quebec spillway is based on design drawings of the spillway provided by Hydro Quebec. One of the drawings represents a result of a geologic mapping. In total 42 joint orientations were given through the map. The main joint directions used for the BSS analysis were identified using the stereoplot program “Dips 6.0” from the company “Roc Science Inc.” (Roc Science Inc., 2013). Figure 5-26 and figure 5-27 show the results of the plots.

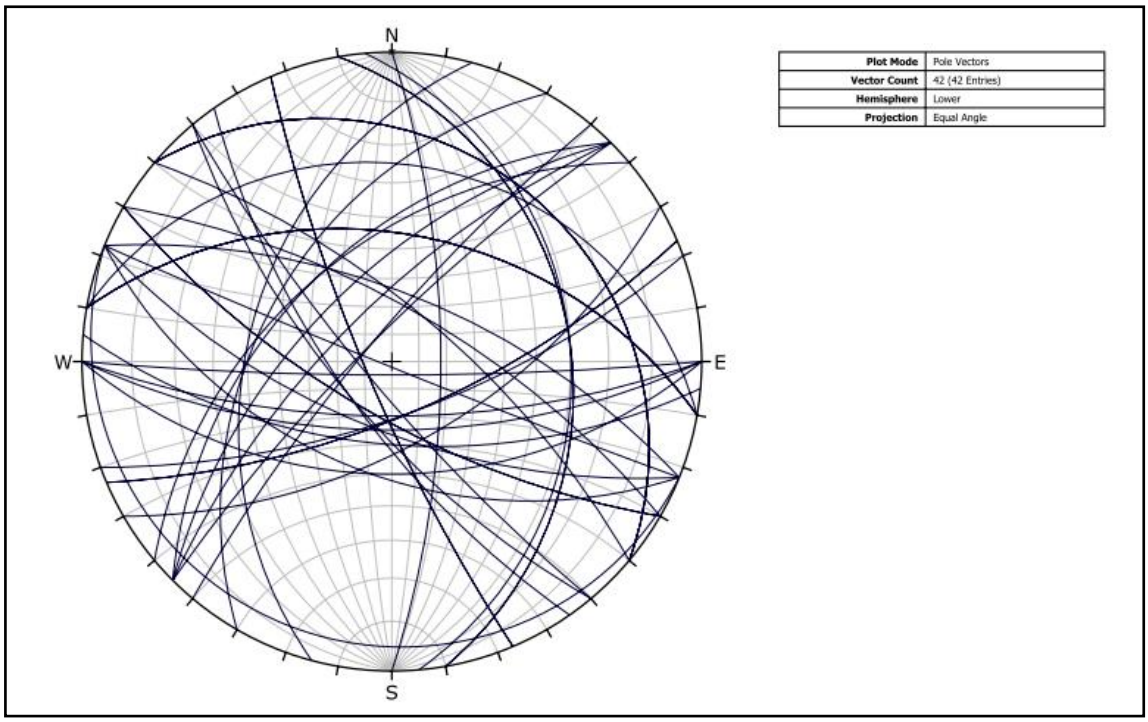

Fig. 5-26: Stereoplot showing the dips and dip directions of the 42 joint sets in an equal angle projection.

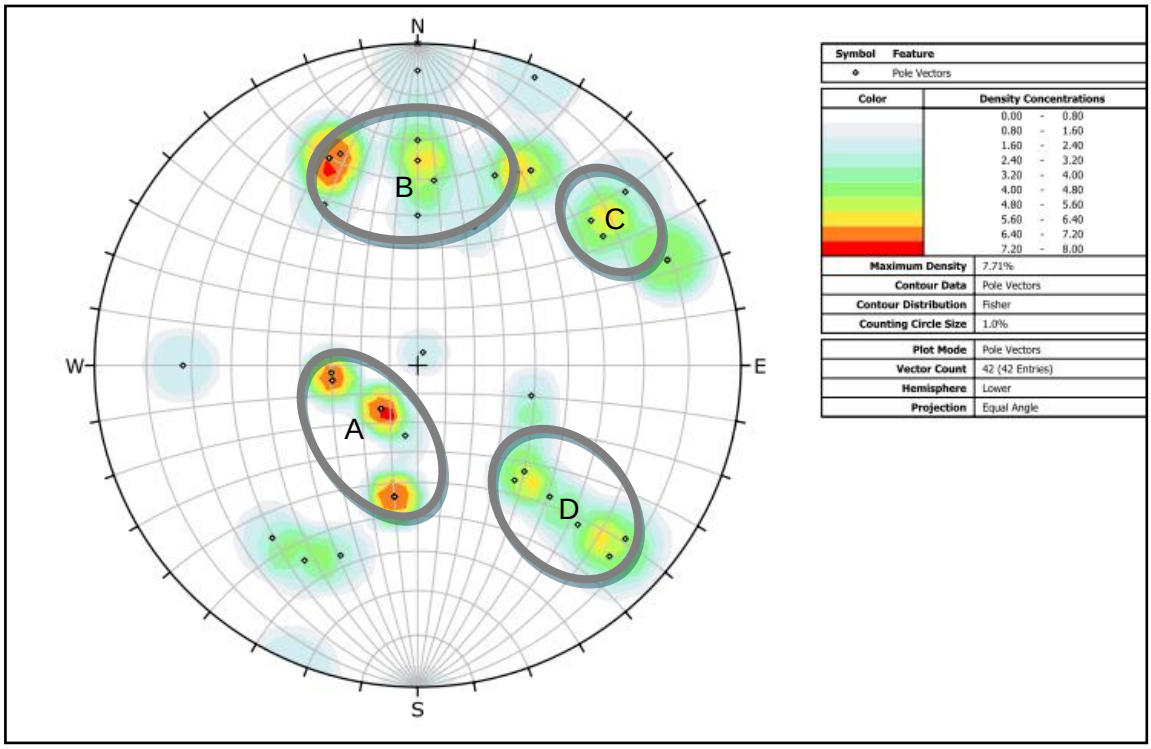

Fig. 5-27: Pole density of the 42 joint sets of the Quebec spillway, the letters mark the different joint sets (A,B,C,D).

For the analysis the joint orientations shown in table 5-8 are used, the spillway runs in azimuth 245° and the inclination of the spillway is 3.2° for the upper part of the chute and 5.7° for the lower part:

Joint set	Average orientation	
	Dip direction (degrees)	Dip (degrees)
A	040	20
B	185	60
C	235	70
D	315	60

Tab. 5-8: Joint sets used for the BSS analysis.

5.2.4 Kinematic analysis

Figure 5-28 shows the identified removable blocks for the upper part of the Quebec spillway, Figure 5-29 for the lower part.

joint number	dip (degrees)	dip direction (degrees)	color
J1 (A)	20	040	dark blue
J2 (B)	60	185	green
J3 (C)	70	235	light blue
J4 (D)	60	315	purple
Free surface	3	245	red

Tab. 5-9: Orientations used for the kinematic analysis of Folsom dam auxiliary spillway.

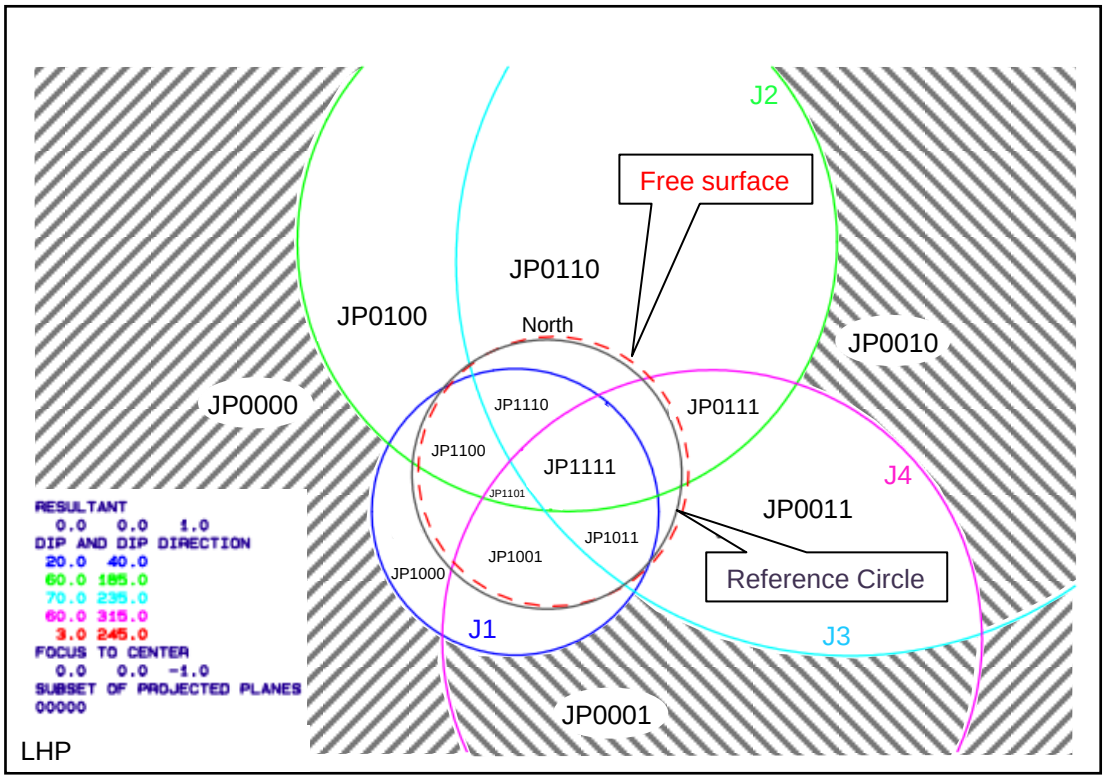

Fig. 5-28: Whole sphere stereographic projection of the upper spillway and the 5 joint sets comprising the rock mass. The shaded areas show the removable blocks. LHP = lower hemispherical projection.

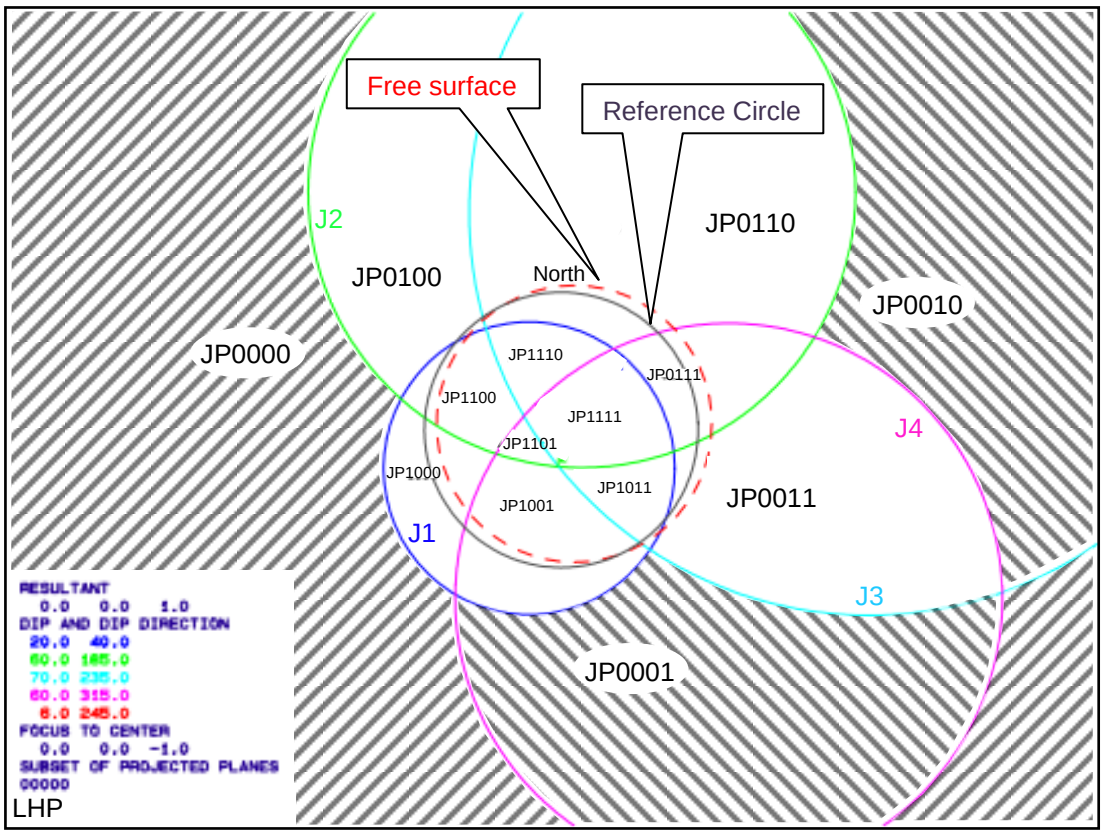

Fig.5-29: Whole sphere stereographic projection of the lower spillway.

Table 5-10 shows the result of the kinematic analysis for the Quebec dam spillway. Three blocks were identified to be removable; all of them are type III blocks.

Position	Removable blocks	Block Type
Spillway, upper and lower part	0010	III
	0000	III
	0001	III

Tab. 5-10: Identified removable blocks of the Quebec dam spillway.

5.2.5 Results of the BSS analysis for the Quebec spillway

Figure 5-30 and Figure 5-31 show the result for the BSS analysis. The stability plots that lead to the results can be found in the appendix.

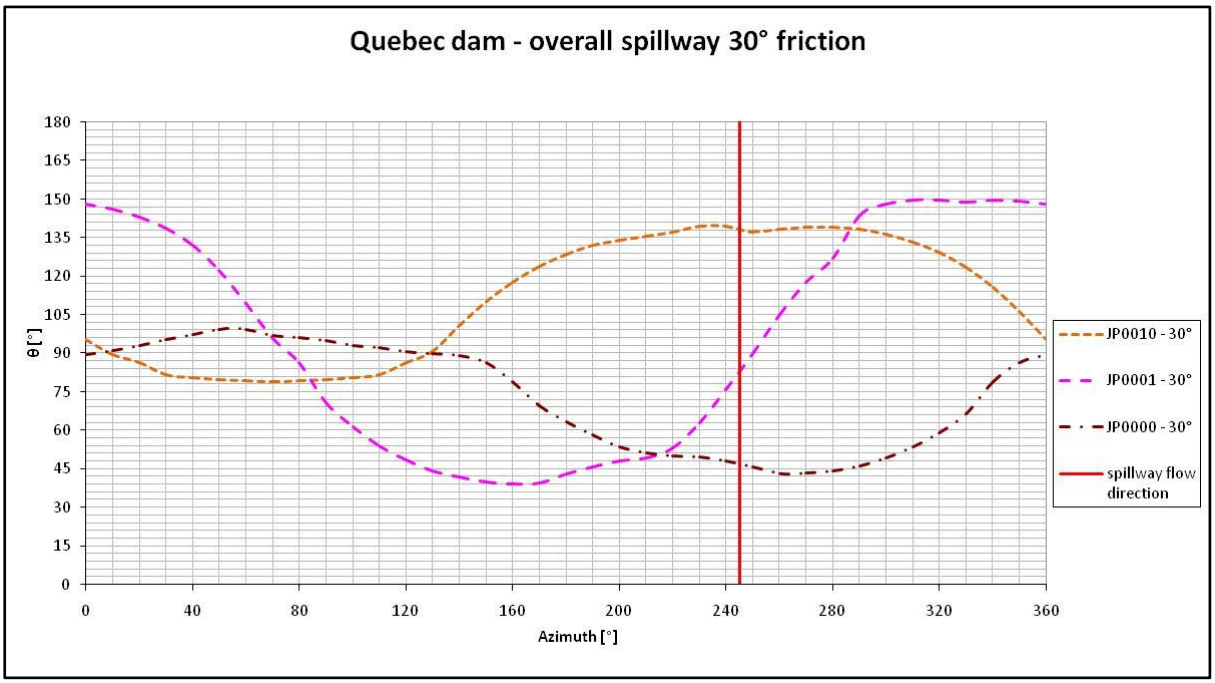

Fig. 5-30: Block Scour Spectrum for JP's 0010, 0001 and 0000 with φ = 30°. The diagram shows the azimuth versus the angle of rotation. The spillway flow (245°) is indicated by the red, vertical line.

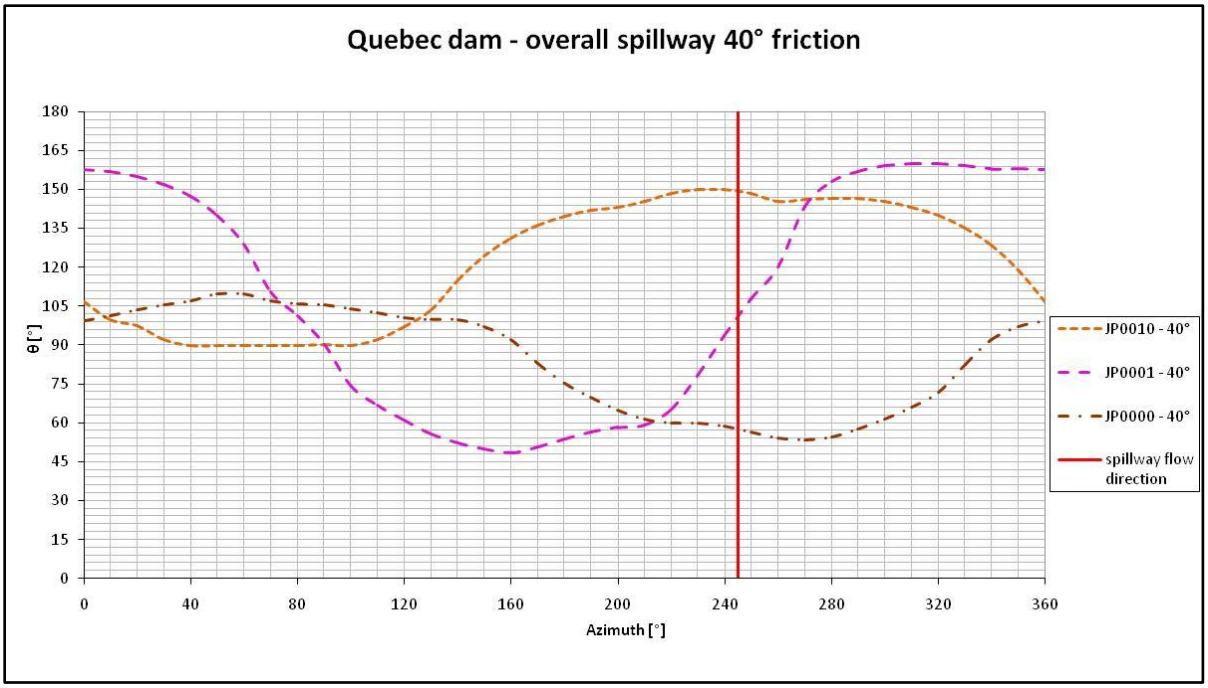

Fig. 5-31: Block Scour Spectrum for JP's 0010, 1010 and 0000 with φ= 40°. It shows similar results to figure 5-30 (φ = 30°), but the values are slightly shifted.

Also for the Quebec spillway a Block Scour Spectrum Envelope (Kieffer & Goodman, 2012) has been created (Figure 5-32).

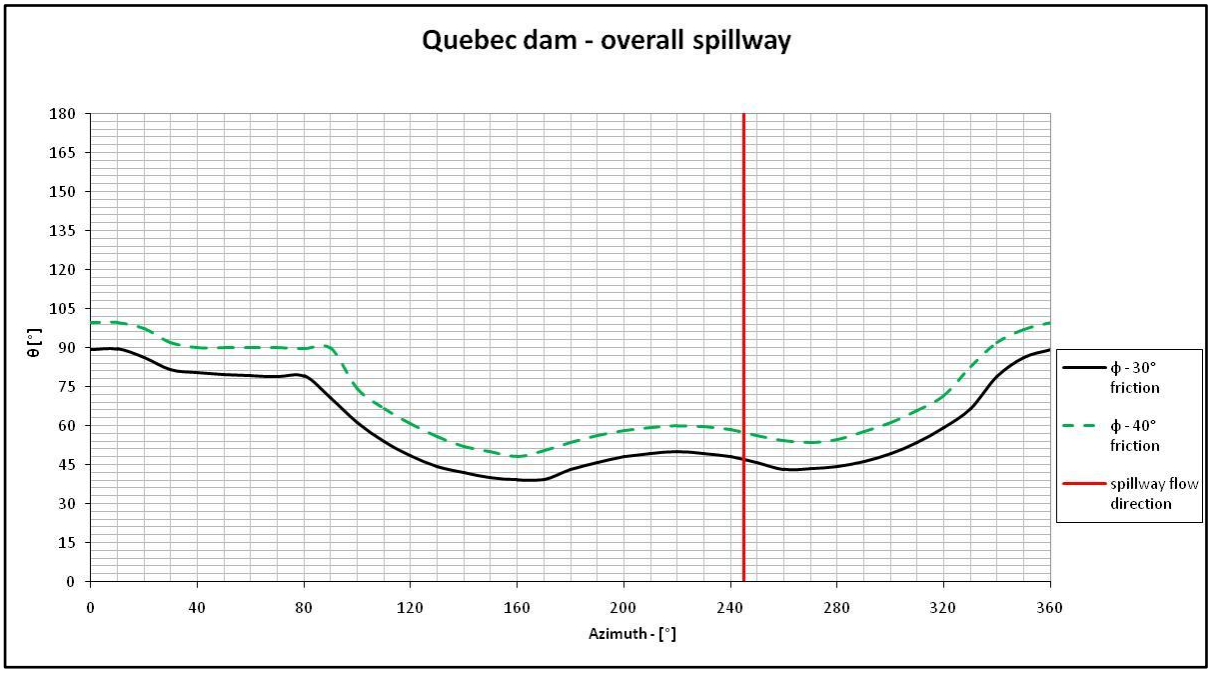

Fig. 5-32: Block Scour Spectrum Envelope for the Quebec spillway for friction angles of 30° and 40°. The spillway flow (245°) is indicated by the red line. The point of first mobilization is quite consistent for the entire spectrum.

5.3 Ricobayo dam spillway, Zamora – Spain

5.3.1 Location and general conditions

The Ricobayo Dam is located in the North-Western part of Spain, 10 km West of the city of Zamora. The dam is installed at the Rio Esla, which is a part of the Duero River system (Kaspar, 2012).

Fig. 5-33: Location of the Ricobayo dam and spillway (google maps, 2013).

The construction of the dam started in 1920 and ended in 1933. Table 5-11 shows general information about the dam facility.

General information	
Location	Muelas del Pan
River	Esla
Catchment area	17.020 km^2
Average annual flow	4.639 hm^3
Reservoir	
Storage capacity	1.178.88 hm^3
Active storage	1.078.40 hm^3
Maximum normal level	684,00 m
Dam	
Type	Gravity
Height above foundation	99,57 m
Crest length	270,00 m
Crest level	685,00 m
Dam volume	398.000 m^3
Foundation rock	Granite
Spillway	
Discharge capacity at max. normal level	4,743 m^3/s
Energy dissipation	Stilling basin

Tab. 5-11: General information about the Ricobayo dam and its spillway (Kaspar, 2012).

5.3.2 Geologic condition

The Ricobayo dam site is part of a granite massif that is known as the Ricobayo Batholith (Bureau of Reclamation, 2012). The batholith is Variscan age and is build up of two granite types:

- The carbajosa leucogranite
- Ricobayo two-mica granite

The Ricobayo granite covers an area of about 150 km^2. The granitic intrusive mostly consists of granodiorite, which is composed of plagioclase, feldspar, quartz, biotite and muscovite. Also other types of minerals can be found like

Apatite, Tourmaline and Zircon. The rock type can be described as holocrystalline with hypidiomorphic crystals. Its grain size is not uniformly distributed, the size varies from medium (1-5 mm) to coarse (>5 mm). The fabric of the rock is is massive with no major recognizable foliation. The granodiorite in this area is intensively jointed, this strong interaction of joints results in the formation of joint bound blocks with a volume of a few cubic meters (Iberduero S.A., 1986) (Kaspar, 2012).

Two major joint sets are characteristic for this region, one that is horizontally dipping, and one that is vertically dipping. The joints in the region of the spillway foundation are filled with rock flour and the general joint separation is less than 5 mm (maximum separation of 10 mm) (Bureau of Reclamation, 2012). A fault can be observed that trends perpendicular to the spillway, it shows intense shearing. The geology in the spillway chute contributed to the extensive scour events that took place over the years of 1934-1939 (Bureau of Reclamation, 2012).

5.3.3 Scour events at Ricobayo spillway

For the construction of the spillway at the Ricobayo dam it was necessary to excavate up to 20 m of overburden to receive an even surface with an inclination of about 0,5 degrees over the total distance, that was left unlined as it was thought that the hard rock was safe enough to resist erosion. The low inclination of the spillway should provide extra safety through keeping the spillway flow at a moderate velocity. The granodioritic bedrock needed to be excavated over a total length of approximately 400m (Kaspar, 2012).

The construction was designed for flood control and hydropower, and it was considered to sustain the irregular flow conditions of the Esla River. Throughout the year the flow rate of the river changes from about 6.800 m^3/s (500 years maximum) to only 5 m^3/s during the dry season (Guia Tecnica de Securidad de Presas, 1997) (Diego, 2007).

The construction of Ricobayo dam was finished in 1933. During the first years extraordinary intense rainfalls occurred and it was necessary to release a huge amount of water. The spillway was in permanent use from December 1933 to June 1934 (Guia Tecnica de Securidad de Presas, 1997). Therefore scour started to influence the spillway already in 1933. In the next 6 years, five major scour events occurred that eroded about $1.1x10^6$ m^3 of rock (Iberduero S.A. , year unknown). Figure 5-34 shows how these events influenced the appearance of the unlined spillway:

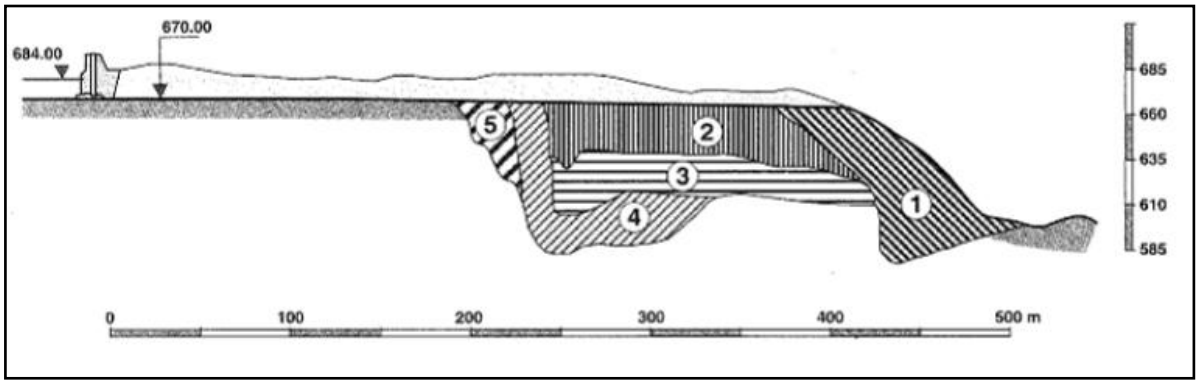

Fig. 5-34: Drawing of the influence on the spillway of the 5 major scour events. Illustration of the steepening of the slope and progressive upward erosion towards the reservoir, (Guia Tecnica de Securidad de Presas, 1997).

The major events that influenced the spillway happened 1) January 1934, 2) March 1934, 3) March 1935, 4) March 1936 and 5) January 1939. During those events the amount of discharge did not exceed the designed maximum capacity for the spillway.

- **Scour stage 1:** Through heavy rainfall that occurred in the first year after the completion of the dam and the spillway, the release of water was necessary. In December 1933 the spillway was used for the first time, a discharge of 100 m^3/s lead to the first damage in January. After that first landslide-like occurrence the spillway was used without a break until June 1934 (Iberduero S.A. , year unknown). Further scour happenings lead to the creation of a small plunge pool at the toe of the slope. The length of the spillway was reduced through progressive upstream erosion, which lead to a steepening of the slope angle. By the end the water flow resembled a waterfall (Kaspar, 2012).

- **Scour stage 2:** The second erosion event lead to an erosion of rock material over a length of approximately 200 m (Guia Tecnica de Securidad de Presas, 1997). A gorge was created and deepened through vertical erosion. These events ended in creating a new river bed in front of the spillway channel. The first repair works took place in summer 1934 (Kaspar, 2012).

- **Scour stage 3:** Spillway discharge of up to 1000 m^3/s resulted in the collapsing of the wall at the exit of the gorge. Erosion of the bottom of the channel and the right wall of the plunge pool was triggered (Kaspar, 2012).

- **Scour stage 4:** The plunge pool grew but no upstream regression occurred. A front wall that had been build after the second big scour stage collapsed, which activated the upstream erosion once again (Kaspar, 2012).

- **Scour stage 5:** In this last stage the spillway was affected at its edge, but there are no detailed documentations for this (Kaspar, 2012).

Figure 5-35 shows the topography of the unlined plunge pool:

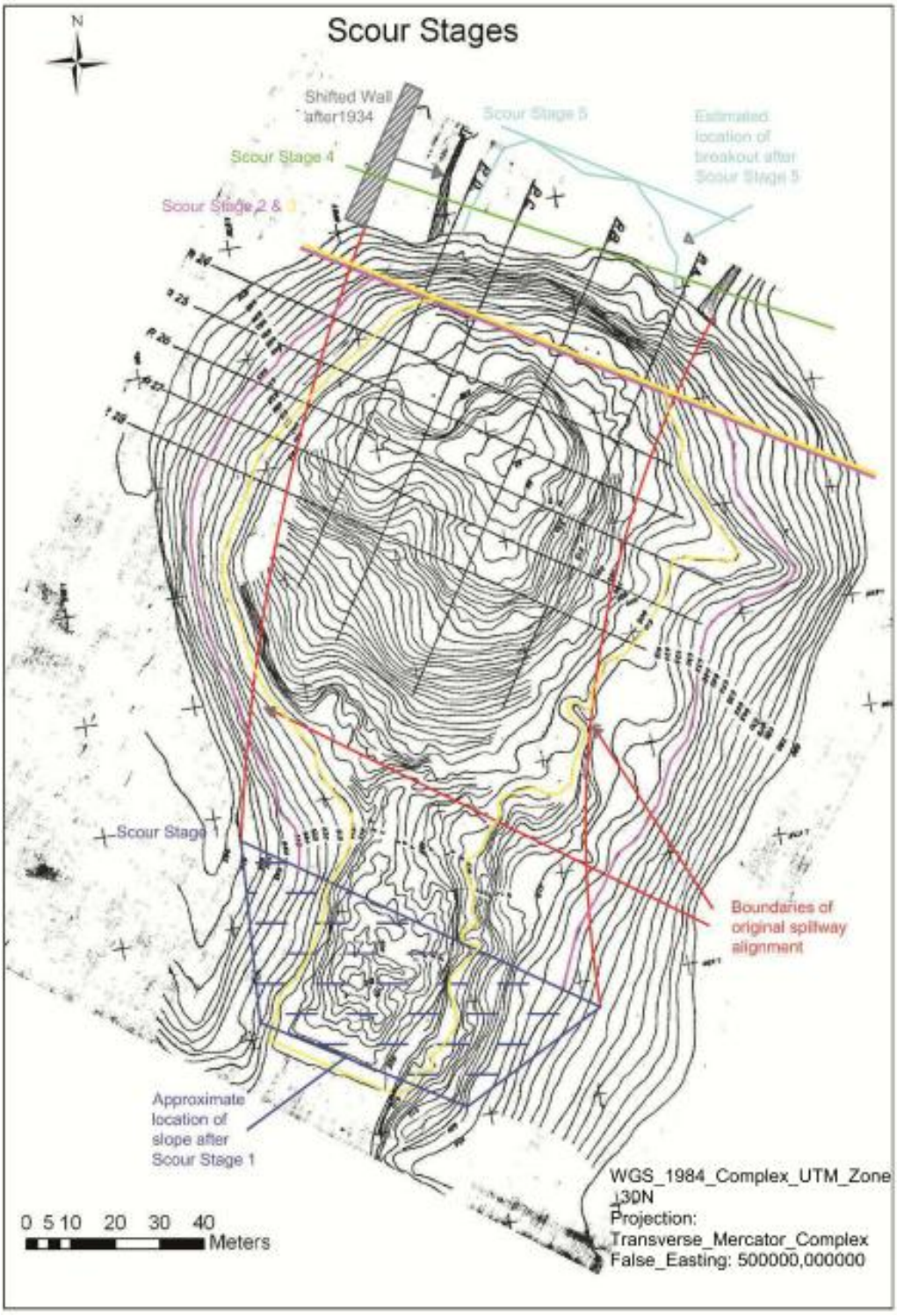

Fig. 5-35: Topography of the unlined plunge pool, modified after (Iberduero S.A., 1937).

5.3.4 Kinematic analysis

The results for the kinematic analysis and the BSS analysis are based on field observations by Markus Kaspar MSc (2012). Table 5-12 shows the joint orientations:

Joint set	Average orientation		
	Dip direction (degrees)	Dip (degrees)	Color
A (J2)	132	85	green
B (J5)	155	19	yellow
C (J4)	192	85	Purple
D (J3)	248	88	Light blue
E (J1)	340	31	Dark blue
Free surface for the spillway surface	216	1	Red
Free surface for the front slope	216	39	Red

Tab. 5-12: Joint orientations used by Kaspar (2012) for the kinematic analysis and the BSS analysis.

The spillway flow azimuth is 216° and the spillway inclination 1° at the flat spillway surface and 39° at the front slope (Kaspar, 2012). Figure 5-36 shows the result for the kinematic analysis of the flat spillway and Figure 5-37 represents the removable blocks for the front slope (Kaspar, 2012).

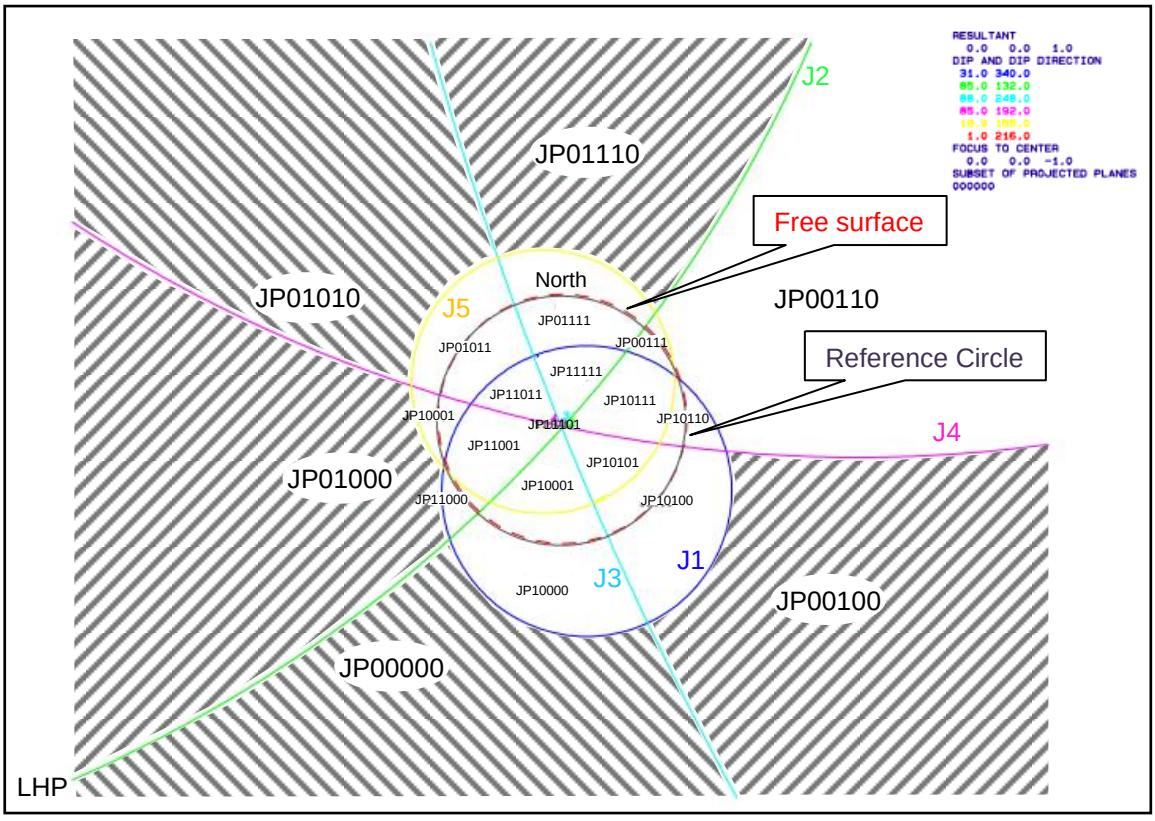

Fig. 5-36: Whole sphere stereographic projection of the flat spillway and the 6 joint sets comprising the rock mass. The shaded areas show the removable blocks. LHP = lower hemispherical projection (Kaspar, 2012).

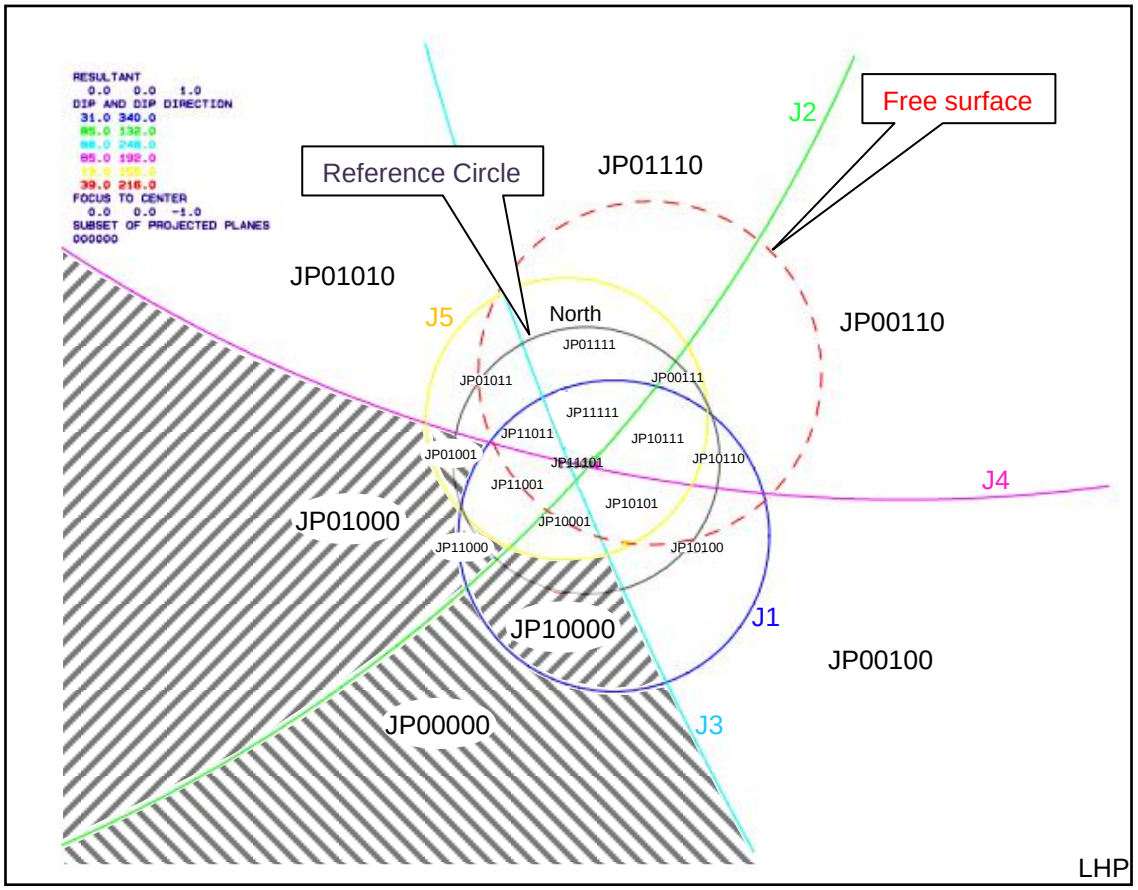

Fig. 5-37: Whole sphere stereographic projection of the front slope, (Kaspar, 2012). The shaded areas show the removable blocks.

Table 5-13 shows the result of the kinematic analysis for the Ricobayo dam spillway. Six removable blocks were identified for the flat spillway surface in the upper part and for the front slope as well.

Position	Removable blocks	Block type
Spillway surface	00000	III
	01010	III
	00010	III
	01000	III
	01110	III
	00100	III
Front slope	01001	II
	01000	III
	11000	II
	10000	II
	00000	III
	00010	III

Tab. 5-13: Summary of the removable blocks for Ricobayo Dam in the area of the spillway surface and the front slope, (Kaspar, 2012).

5.3.5 Results of the BSS analysis for the Ricobayo dam spillway, spillway surface and the front slope

5.3.5.1 Ricobayo dam spillway, spillway surface

Figure 5-38 till Figure 5-40 show the results of the BSS analysis for the flat spillway surface with an inclination of 1°. The stability plots that lead to the results can be found in the appendix. Six removable blocks were identified through using the kinematic analysis.

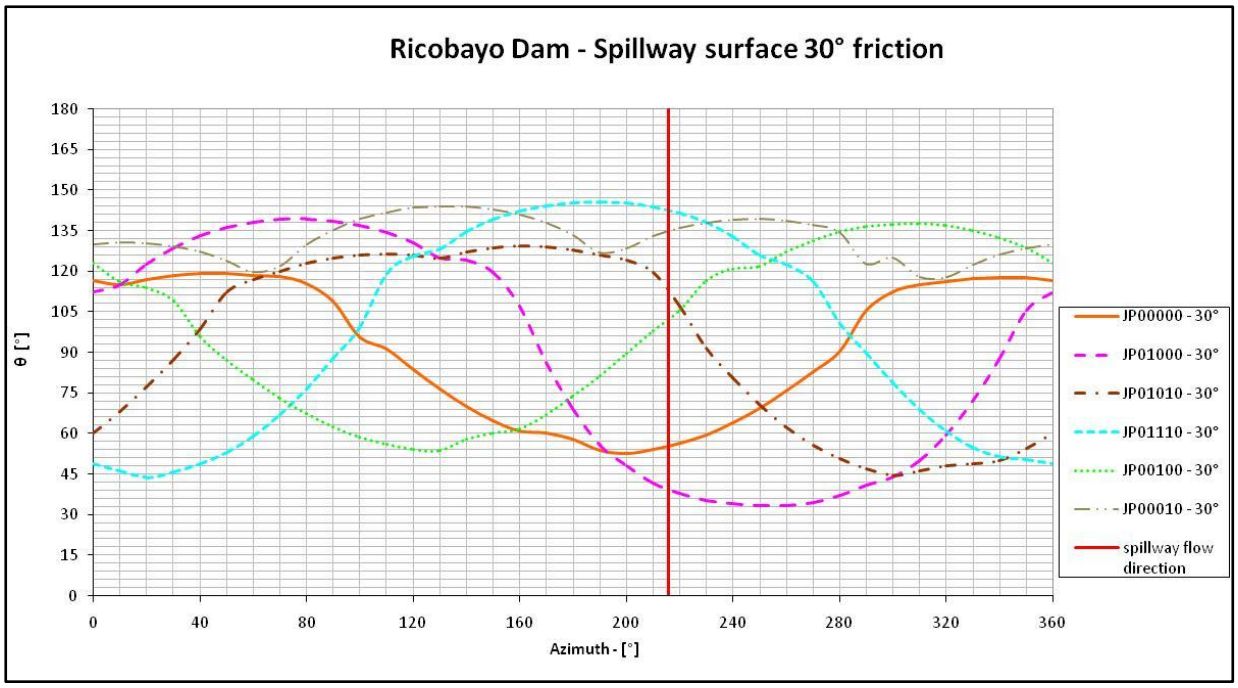

Fig. 5-38: Block Scour Spectrum for JP's 00000, 01000, 01010, 01110, 00100 and 00010 with φ = 30°.The diagram shows the azimuth versus the angle of rotation. The spillway flow (216°) is indicated by the red, vertical line (Kaspar, 2012).

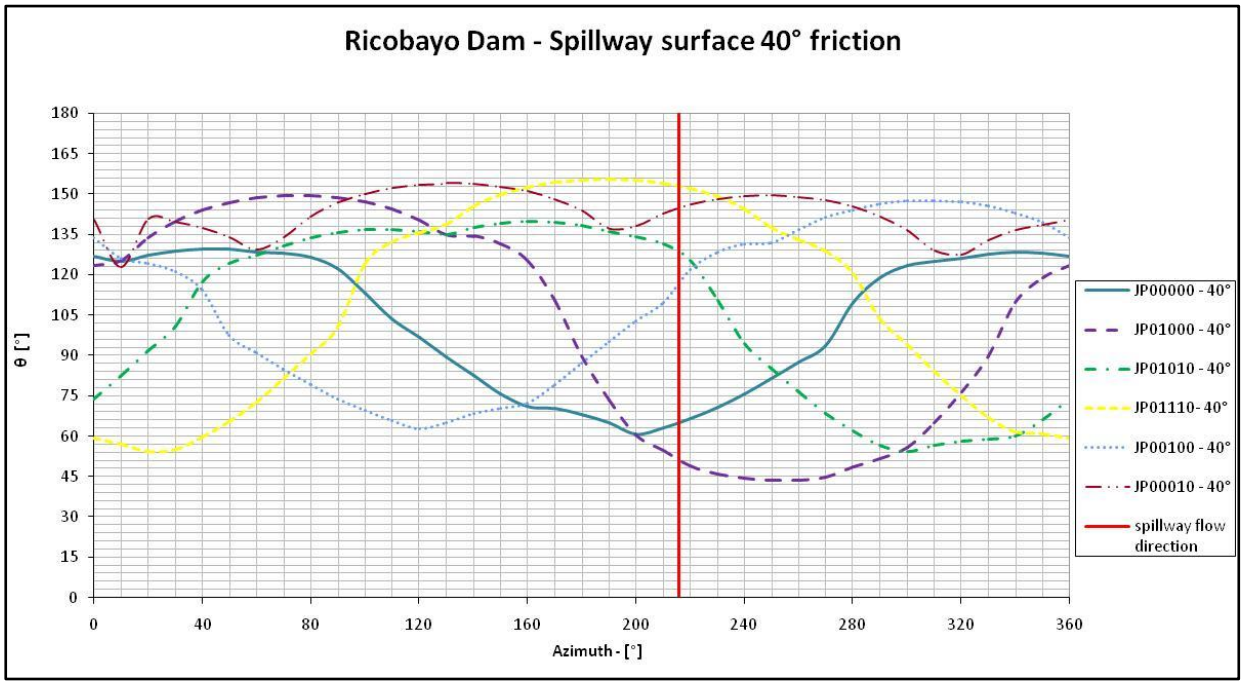

Fig. 5-39: Block Scour Spectrum for JP's 00000, 01000, 01010, 01110, 00100 and 00010 with φ= 40°. It shows similar results to figure 5-38 (φ = 30°), but the values are slightly shifted (Kaspar, 2012).

Figure 5-45 shows the related stability envelope diagram.

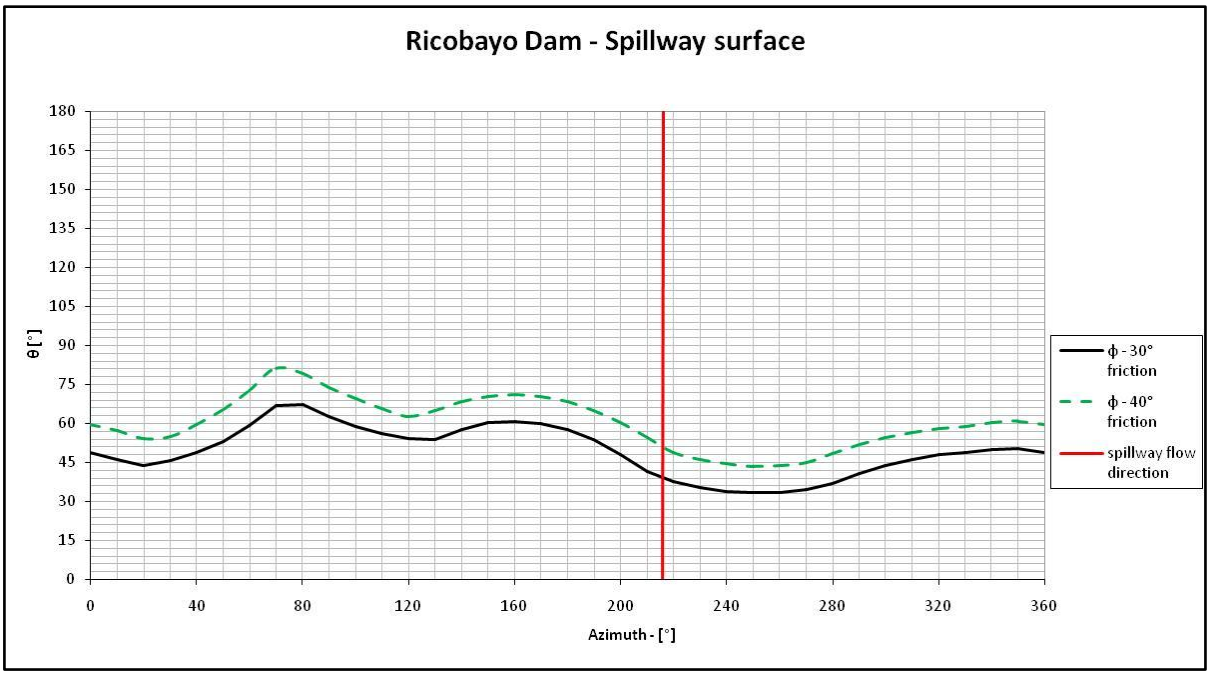

Fig. 5-40: Block Scour Spectrum Envelope of the angle of rotation for Ricobayo dam spillway surface (friction angle 30° and 40°), (Kaspar, 2012).

5.3.5.2 Ricobayo dam spillway, front slope

Figure 5-41 and 5-42 show the results of the BSS analysis for the front slope of the Ricobayo dam spillway.

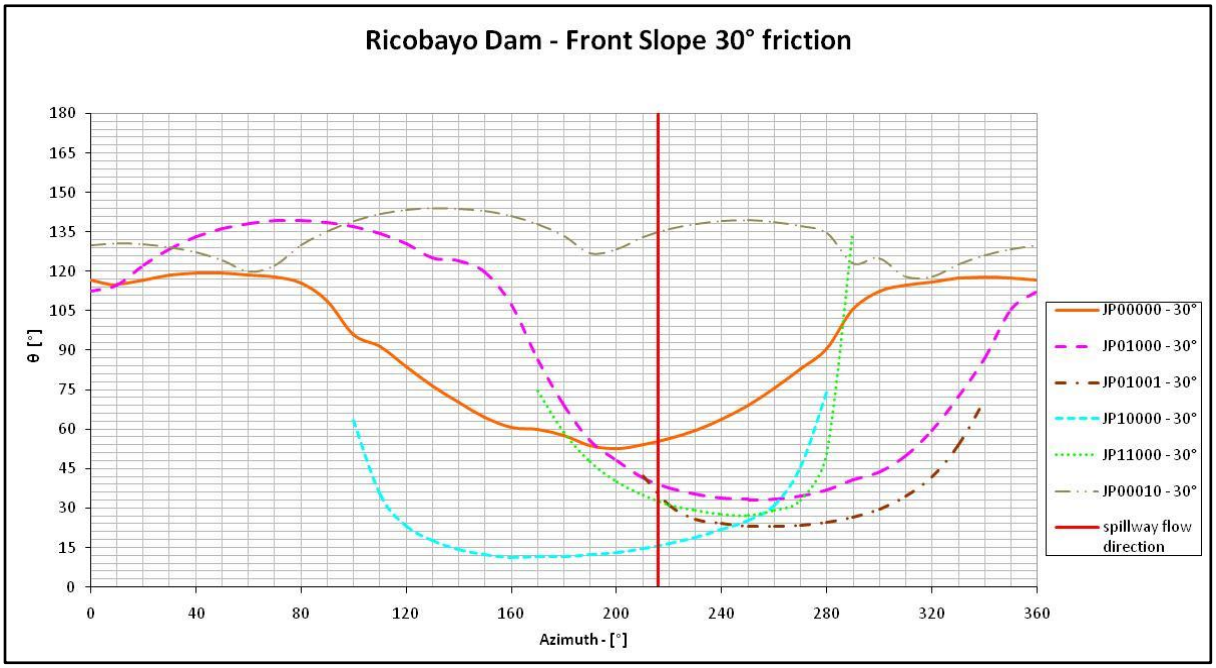

Fig. 5-41: Block Scour Spectrum for JP's 00000, 01000, 01001, 10000, 11000 and 00010 with φ = 30°.The angle of rotation is at its minimum for most of the blocks. The spillway flow (216°) is indicated by the red, vertical line (Kaspar, 2012).

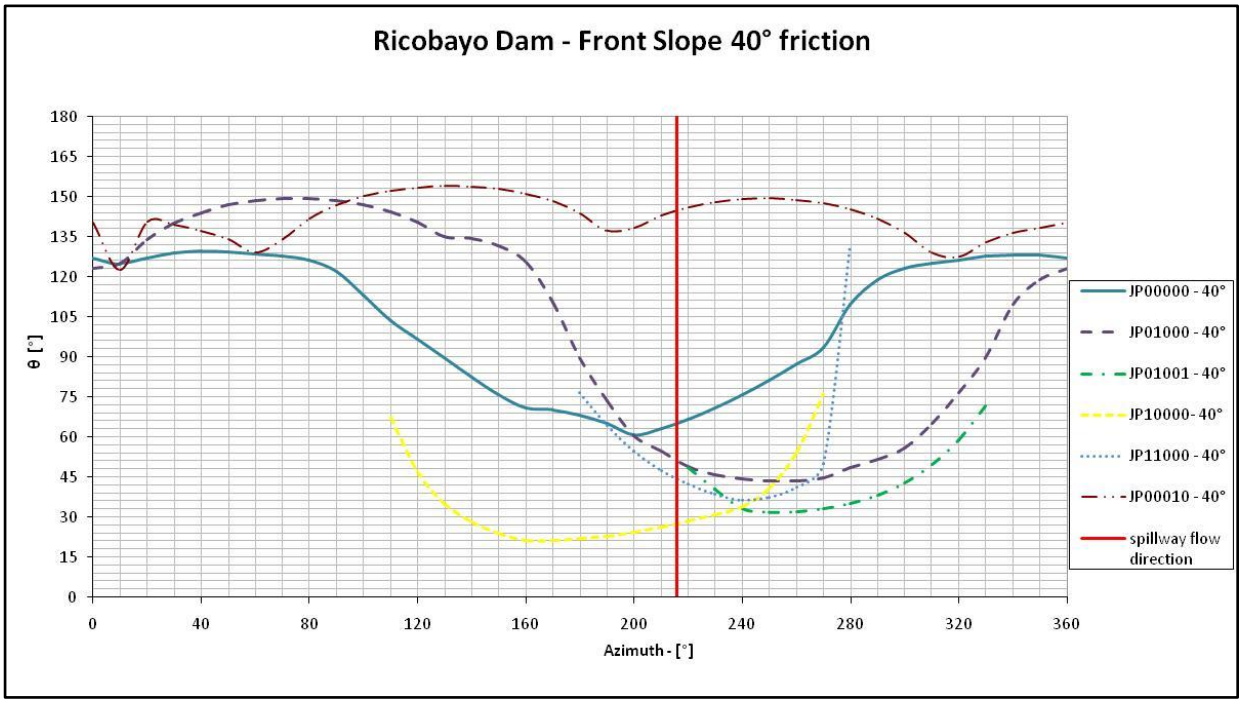

Fig. 5-42: Block Scour Spectrum for JP's 00000, 01000, 01001, 10000, 11000 and 00010 with φ= 40°. It shows similar results to figure 5-41 (φ = 30°), but the values are slightly shifted (Kaspar, 2012).

The Block Scour Spectrum Envelope for the Ricobayo dam spillway, front slope, is shown in Figure 5-43.

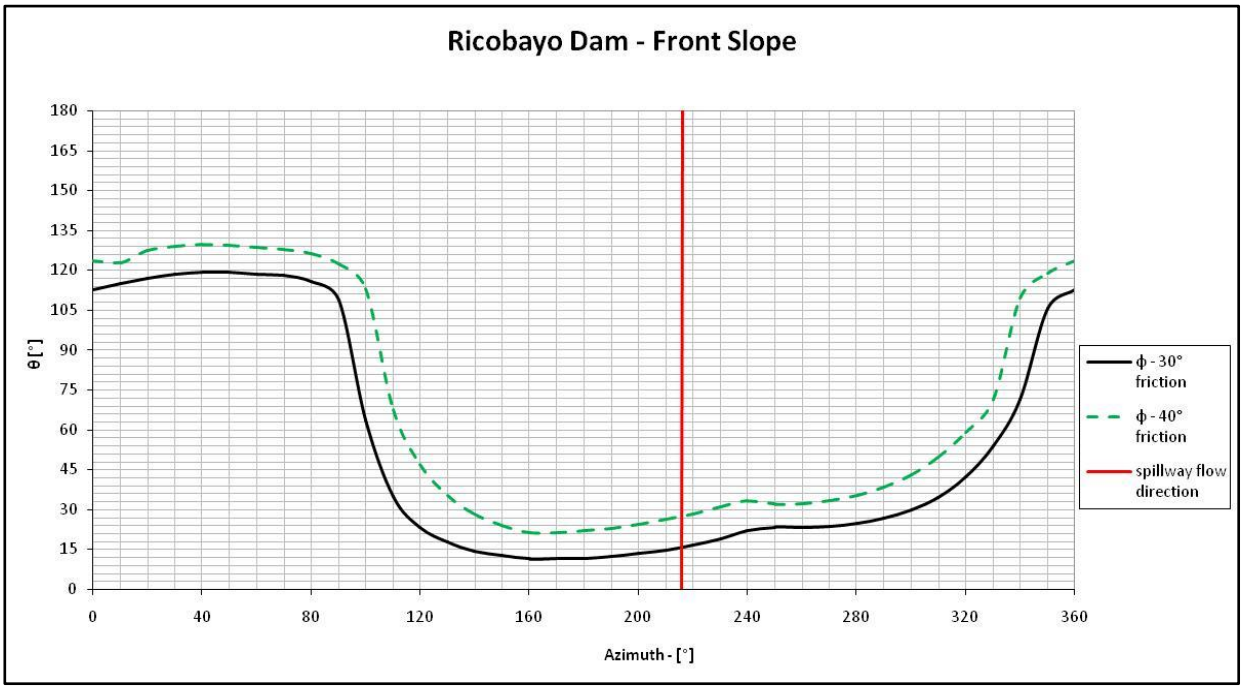

Fig. 5-43: Block Scour Spectrum Envelope for Ricobayo dam spillway front slope. Note that the angle of rotation shows low values in the orientation of the spillway (216°, vertical, red line) (Kaspar, 2012).

6 Interpretations

Through comparing the results one can say that the BSS is a promising index for assessing the effects of rock structure on scour potential. Figure 6-1 shows the Block Scour Spectrum envelopes for the Folsom dam auxiliary spillway - spillway surface, for the overall Quebec spillway and for the Ricobayo spillway - spillway surface. Figure 6-2 shows the Block Scour Spectrum envelopes for the Folsom dam auxiliary spillway - approaching stilling basin, for the overall Quebec spillway and for the Ricobayo spillway - front slope. The envelopes in both figures are shown with a friction angle of 30° and 40°. The vertical lines mark the orientation of the respective spillway flow.

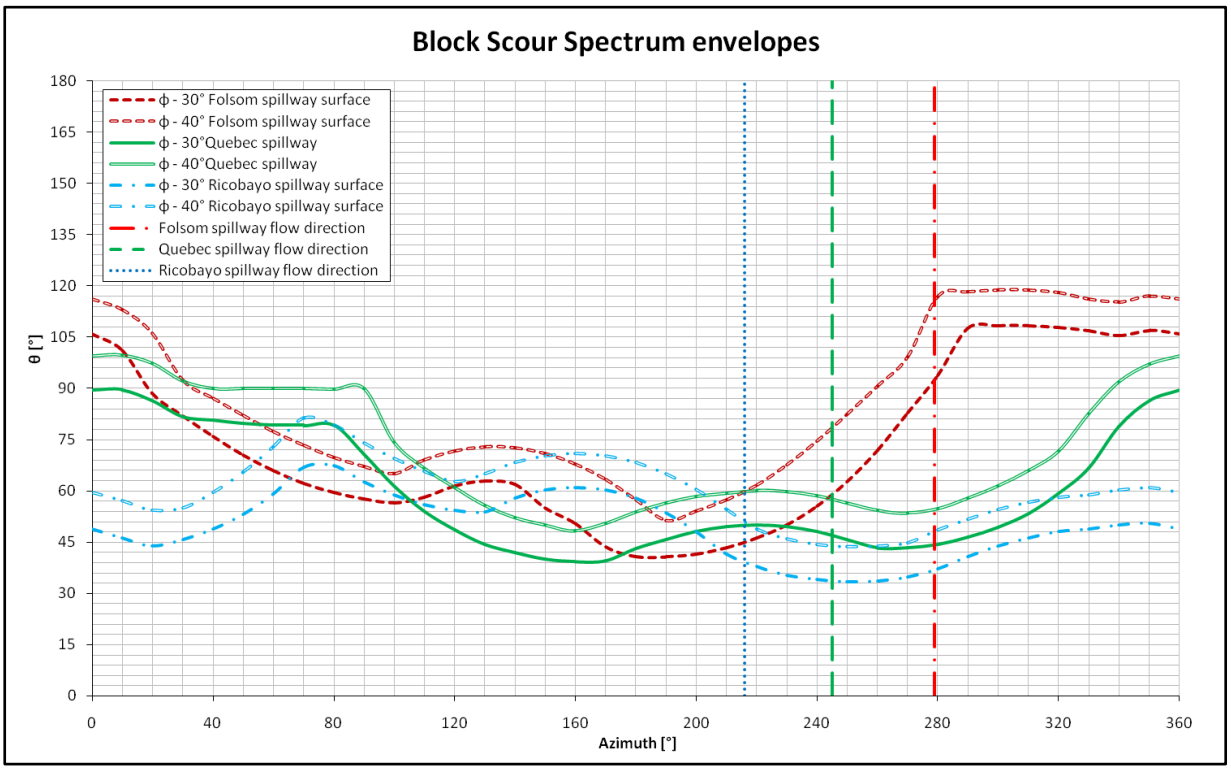

Fig. 6-1: 30° and 40° envelopes of the Folsom dam auxiliary spillway surface, the Quebec spillway and the Ricobayo spillway surface. The vertical lines mark the orientations of the different spillways.

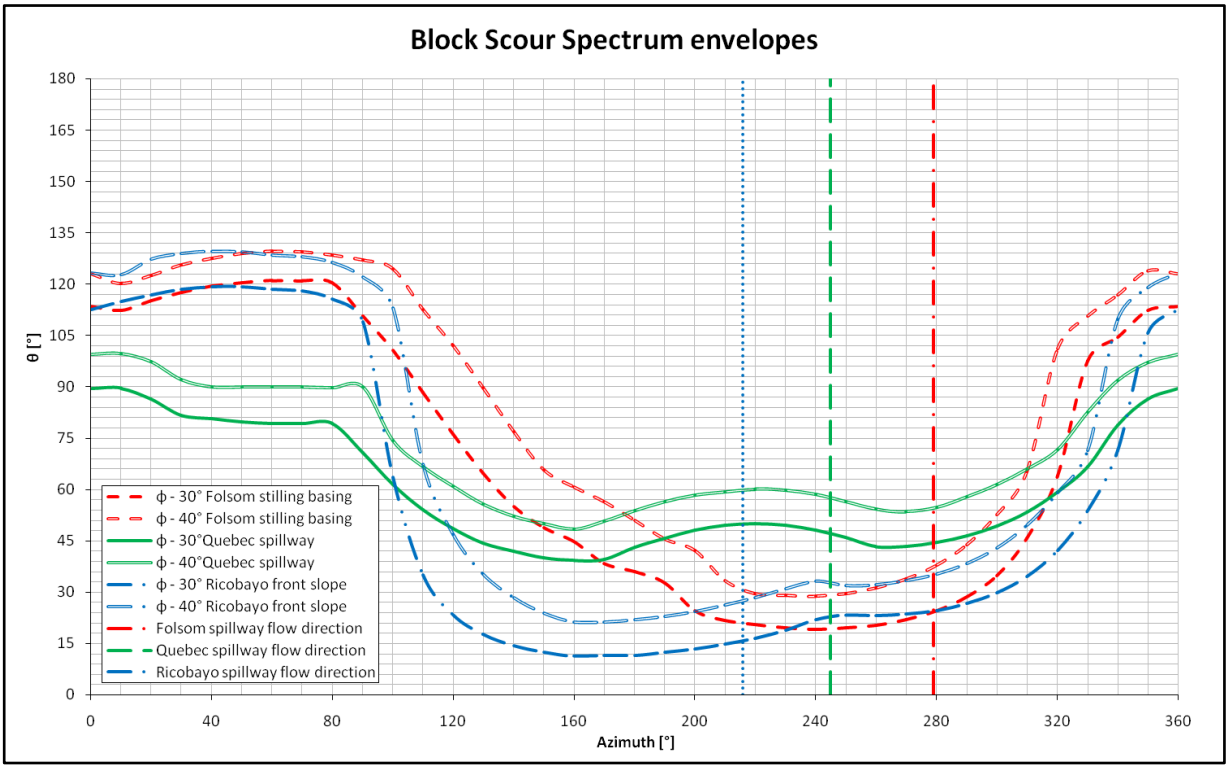

Fig. 6-2: 30° and 40° envelopes of the Folsom dam auxiliary spillway when approaching the stilling basin, the Quebec spillway and the Ricobayo spillway at the front slope. The vertical lines mark the orientation of the different spillways.

Immediately the differences between the three example spillways can be seen. It is important to keep in mind that all three sites are built on nearly the same granitic basement showing complex fracturing. Through using information based on joint orientations, orientations of the spillways itself and the inclination of the channels the BSS shows a consistency in its results. The spillway of the Ricobayo dam is known for its scour problems, and the result of the minimum envelope reflects this topic very well. While Figure 6-1 gives a slight indication of the hazard potential of the Ricobayo spillway, Figure 6-2 shows clearer results.

Figure 6-2 shows very well that the angle of vector rotation for the Ricobayo spillway front slope (blue lines) is at its minimum for its orientation. Compared to the spillway situated in Quebec, which shows the highest values (green lines). The results for the Folsom dam auxiliary spillway are seen to be slightly more favorable than the Ricobayo spillway in Figure 6-2. Today the spillway is lined and secured with anchors and other stabilization methods. Especially for the channel part when it approaches the stilling basin the BSS shows a high risk for failure. A certain hazard is evident that at some point Folsom dam auxiliary spillway can act like the Ricobayo channel. The angle of rotation drops to very

low values in the alignment of the spillway (figure 6-2) and clearly marks a hazard potential.

The Canadian spillway is an example for a channel that did not need any lining for safety until now. Even though the canal has been excavated in a similar material it appears to be stable. This is indicated through the Block Scour Spectrum (Kieffer & Goodman, 2012), by virtue of higher minimum stability envelopes as compared to Folsom dam auxiliary spillway and the Ricobayo dam spillway.

The comparison of the minimum stability envelopes of the example spillways indicates that the Block Scour Spectrum is a powerful three dimensional tool for giving an indicator of potential block scour occurrences.

7 Summary and conclusion

The result of this thesis indicates that the recently introduced Block Scour Spectrum Analysis (Kieffer & Goodman, 2012) can be used as a powerful three dimensional tool to give an indicator of potential failure occurrences and failure modes. The analysis has been used to compare three spillway sites. All three sites are situated in granitic bedrock with complex fracturing, applying the straight forward method Block Theory (Goodman & Shi, 1985) in combination with the Block Scour Spectrum (Kieffer & Goodman, 2012) a certain regularity can be achieved.

Considering the results of the three sites one can gain insight to the extreme scour events that happened at the Ricobayo spillway site. The Block Scour Spectrum shows that the alignment of the spillway was highly unfavorable in terms of scour potential, as the inherent rock mass resistance to block scour was very low in this direction. Mobilization of blocks is especially possible in the area of the front slope.

The spillway of the dam located in Quebec shows a higher inherent scour resistance as shown by the Block Scour spectrum analysis. Results from the Folsom dam auxiliary spillway when approaching the stilling basin are generally intermediate between the Spanish spillway and the one in Quebec. If left unprotected the Folsom dam spillway would behave increasingly susceptible to block scour erosion where it steepens near its terminus.

The BSS is a useful tool for developing an index of scour potential. It is very fast to use and the input parameters are not difficult to obtain. Through using the orientation of the main joints and the orientation of the spillway itself it is possible to quantify the relative scour susceptibility in 3D.

8 Reference cited

Annandale, G.W., Melville, B. & Chiew, Y.-M. (2002): Scour case studies. - Mitteilungsblatt der Bundesanstalt für Wasserbau Nr. 85, 16 p.

Annandale, G.W. (1995): Erodibility. – Journal of Hydraulic Research 33(4), 471-494.

Annandale, G.W. & Smith, S. (2001): Calculation of Bridge Pier Scour using the Erodibility Index Method. - DOT Department of Transportation Research, final report, Colorado, 48 p.

Bagheri, M. (2009): Model Uncertainty of Design Tools to Analyse Block Stability. – Licentiate Thesis, Royal Institute of Technology Stockholm, 180 p.

Barton, N.R., Lien, R. & Lunde, J. (1974): Engineering classification of rock masses for the design of tunnel support. – Rock mechanics 6 (4), 189-239.

Barton, N.R. (1973): Review of a new shear strength criterion for rock joints. – Engineering Geology Elsevier 7, 287-322.

Barton, N.R. (1987): Rock mass classification and tunnel reinforcement selection using the Q-System. – Proc. ASTM Symposium on Rock Classification Systems for Engineering Purposes, Cincinnati Ohio

Bollaert, E.F.R. (2010): The Comprehensive Scour Model: Theory and Feedback from Practice. –5th International Conference on Scour and Erosion, San Francisco.

Bollaert, E.F.R. & Hofland, B. (2004): The Influence of Flow Turbulence on Particle Movement due to Jet Impingmement. – 2nd Scour and Erosion Conference, Singapore.

Bollaert, E.F.R. & Schleiss, A. (2005): Physically Based Model for Evaluation of Rock Scour due to High-Velocity Jet Impact. – Journal of Hydraulic Engineering Vol. 131/3, 153-165.

Bollaert, E.F.R. (2004, 1): A comprehensive model to evaluate scour formation in plunge pools. – International Journal of Hydropower & Dams, 94-101.

Bollaert, E.F.R. (2004): A new procedure to evaluate dynamic uplift of concrete linings or rock blocks in plunge pools. – International Conference Hydraulics of Dams and River structures, Iran, 125-132.

Bollaert, E.F.R. (2010): A Prototype-Scaled Rock Scour Prediction Model. – USSD conference, Sacramento

Bollaert, E.F.R., Munodawafa, M.C. & Mazvidza, D.Z. (2012): Kariba Dam Plunge Pool Scour: quasi-3D Numerical Predictions. – ICSE6, Paris

Bollaert, E.F.R. (2002): Transient water pressure in joints and formation of rock scour due to high velocity jet impact. Communication of the laboratory of hydraulic construction (LHC), No. 13 EPFL, Lausanne, ISSN 1661-1179

Bureau of Reclamation & US Army Corps of Engineers (2012): Erosion or rock and soil (chapter 5). – retrieved from http://www.usbr.gov (4th of August, 2013), last modified 11/15/2012.

Canadian Shield Foundation (2013): Understanding the Canadian Shield. - retrieved from http://canadianshieldfoundation.ca/?page_id=39 (4th of August, 2013).

Cox, D. (1999): Great Lakes Origin by Diastrophic Processes. – retrieved from http://www.sentex.net/~tcc/gtl-shield.html (25th of August, 2013)

Cramer, C.H., Toppozada, T. R. & Parke, D.L. (1978): Seismicity of the Foothills Fault System between Folsom and Oroville, California. – Bulletin of the Seismological Society of America, 245-249.

Deere, D.U. (1963): Technical description of rock cores for engineering purposes. - Rock mechanics and engineering geology 1(1): 18. Vienna: Springer.

Deere, D.U. & Deere, D.W. (1988): The rock quality designation (RQD) index in practice. In Rock classification systems for engineering purposes, (ed. L. Kirkaldie). – ASTM special publication 984, 91-101, Philadelphia: Am. Soc. Test. Mat.

Diego Martín, Y. (2007) in Nec. otium, XIX, XX, XXI: comercio e industria en Zamora, Museo Etnográfico de Castilla y León (Zamora, Espagne), ISBN 849357810X, 9788493578107, 371 p.

Encyclopaedia Britannica (2013): Encyclopaedia Britannica. Editiors of Encyclopaedia Britannica. (last update 1st of June, 2014): Canadian Shield. – retrieved from http://www.britannica.com/EBchecked/topic/91992 (26th of August, 2013)

George, M.F. & Sitar, N. (2012): Block Theory application to scour assessment of unlined rock spillways. – Geotechnical Engineering, department of civil and environmental engineering, University of California, Berkeley, Report No. UCB GT 12-02.

Goodman, R.E. & Shi, G. (1985): Block Theory and its Application to Rock Engineering. - Prentice- Hall International, ISBN 0-13-078189-4,338 p.

Goodman, R.E. & Shi, G. (1989): Block Theory Software package, University of California, Berkeley.

Goodman, R.E. (1989): Introduction to Rock Mechanics 2nd Edition. – ISBN 0-471-81200-5.

Goodman, R.E. (1976): Methods of Geological Engineering in Discontinuous Rocks. – St. Paul: West Publishing Company.

Goodman, R.E. (2013): personal communication,University of Berkeley.

Google maps (2013): www.maps.google.at.

Guia Tecnica de Securidad de Presas (1997) – Aliviaderos y Desagües – AMI Ricobayo.

Hall, P.E & Dressel, W. (n. d.): Folsom Dam Safety of Dams Modification – Auxiliary Spillway Phase I and Phase II.

Hydro Quebec (2013)

Hydro Quebec (2003): Environmental Monitoring at the La Grande Complex.

Hydrofoundation (2013) – information retrieved from www.hydrofoundation.org.

Hydro Quebec (2004): The La Grande Complex visitor booklet. – ISBN 2-550-41276-1.

Iberduero, S.A. (n. d.): Salto de Ricobayo – Aliviadero, 7 p.

Iberduero, S.A. (1937): Planta del aliviatero: modificaciones. Scale 1:500, Plan Nr. 3365.

Iberduero S.A. (1986). Salto de Ricobayo II, Geotechnical report.

IGME (Instituto Geológico y Minero España). (1978). Mapa Geológico de España (Hoja número 368, Carbajales de Alba), Scale 1:50.000.

Kaspar, M. (2012): Geological Conditions Favoring Extreme Scour of an Unlined Spillway at Ricobayo Dam, Zamora, Spain – Master Thesis, University of Technology, Graz, 156 p.

Kieffer, D.S. & Goodman, R.E. (2012): The Block Erodibility Spectrum Analysis.

Kieffer, D.S. & Goodman, R.E. (2012): Assessing scour potential of unlined rock spillways with the Block Scour Spectrum. – Geomechanics and Tunneling 5, Volume 5.

Kirsten, H.A.D. (1982): A Classification System for Excavation in Natural Minerals. – The civil Engineer in South Africa, 292-308.

Kirsten, H.A.D. (1988): Case histories of groundmass characterization for excavatability in Rock Classification Systems for Engineering Purposes. – ASTM STP-984, American Society for Testin and Materials, Philadelphia.

Mehdi, B. (2009): Model Uncertainty of Design Tools to analyse Block Stability.

Meirelles Coelho Rocha, L.F. (2012): Response of Ricobayo Dam spillway walls to extensive rock scour. – Master Thesis, University of Technology, Graz.

Nzakimuena, T.-J. & Zulfiquar, A.P. (2009): Rock Erosion Downstream of the Spillways at Hydro-Quebec Installations, Quebec, Canada – Some Case Histories. – ICOLD Committee on Hydraulics for dams, 11 p.

Price, D.G. & De Freitas, M. (2009): Engineering Geology: Principles and practice. – Springer, ISBN: 978-3-540-29249-4, 450 p.

Quebec Biodiversity (n.d.): Natural History of Quebec. – retrieved from http://redpath-museum.mcgill.ca/Qbp/Natural%20History/nat_hist.html (4th of August, 2013).

Roc Science Inc. (2013): Dips 6.0, Graphical and statistical analysis of orientation data, Toronto, Ontario.

Sawadago, O. (2010): Scour of unlined dam spillways. – Master thesis, University of Stellenbosch.

State of California, Department of conservation (2007): Geological map. - retrieved from www.quake.ca.gov/gmaps/GMC/stategeologicmap.html (26th of August, 2013).

Steinbauer, C. (2012): Kolkbildung im Bereich des Ottenstein Staudammes, Niederösterreich. – Master Thesis, University of Technology, Graz.

U.S. Army Corps of Engineers (2012): Folsom Dam Auxiliary Spillway Project, Phase IV. – 95% Design Documentation Report, Chapter 6, Sacramento District.

U.S. Department of Agriculture (2001): Field Procedures Guide for the eadcut Erodibility Index. – National Engineering Handbook, Chapter 52, Part 628 Dams.

U.S. Department of the Interior Bureau of Reclamation (2013): information retrieved from www.usbr.gov.

U.S. society on dams (USSD) (2013): information retrieved from www.ussdams.com.

Whipple, K.X., Hancock, G.S. & Anderson, R.S. (2000): River incision into bedrock: Mechanics and relative efficacy of plucking, abrasion and cavitation. – Geological Society of America Bulletin.

Wittler, R.J., Mefford, B.W., Abt, S.R., Ruff, J.F. & Annandale, G.W. (1995): Spillway and Dam Foundation Erosion: Predicting Progressive Erosion Extents.

Wyllie, D.C. & Mah, C.W. (2004): Rock Slope Engineering. – Civil and Mining 4th Edition, Spon Press ISBN 0-203-49908-5, New York.

9 Appendix

A1 Stability plot of the removable JP's for the three analyzed dam spillways

A1.1 Folsom dam auxiliary spillway

JP 0010 30°

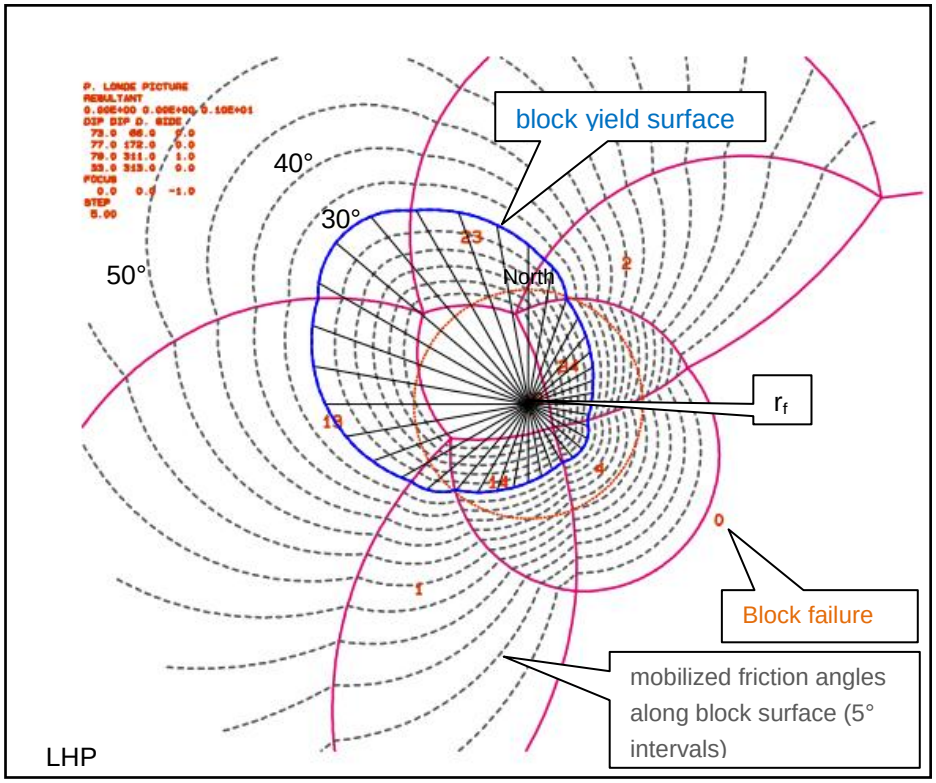

A1. 1: Stability plot for JP 0010 (30°). The dashed lines represent the mobilized friction angles along the block surface in 5° intervals. The radial lines show the azimuth dependent rotations of the original weight vector which is required to intercept the 30° block yield surface. The red number show the different occurring failure modes, one digit numbers mean plane sliding; two digit numbers wedge sliding. r_f is the resultant force.

JP 0010 40°

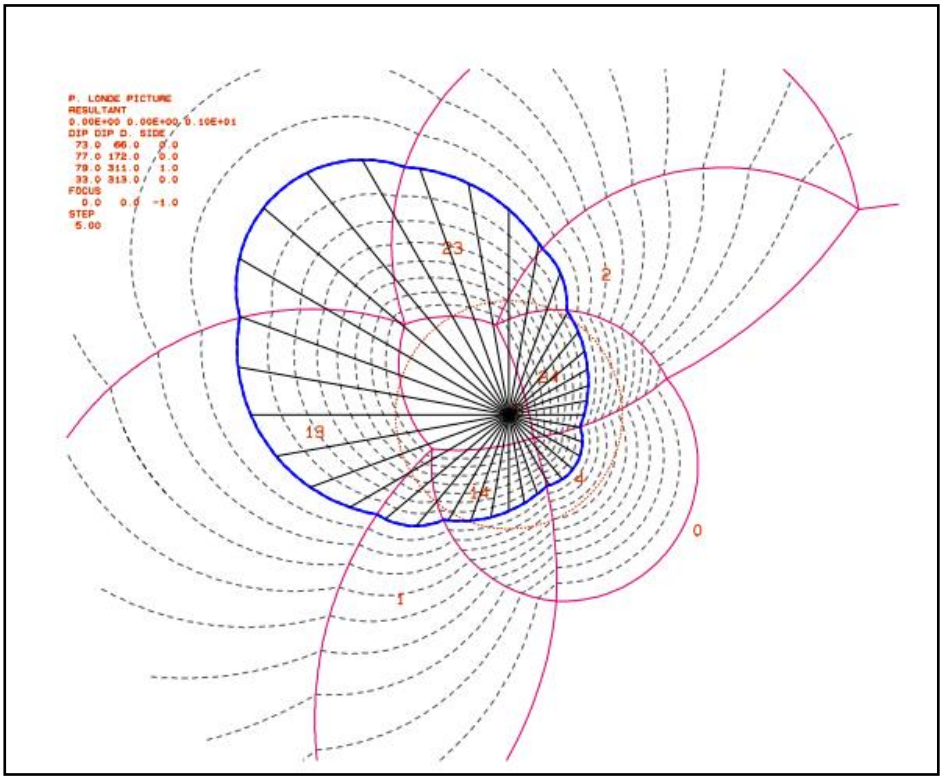

A1. 2: Stability plot for JP 0010 (40°)

JP 0000 (30°)

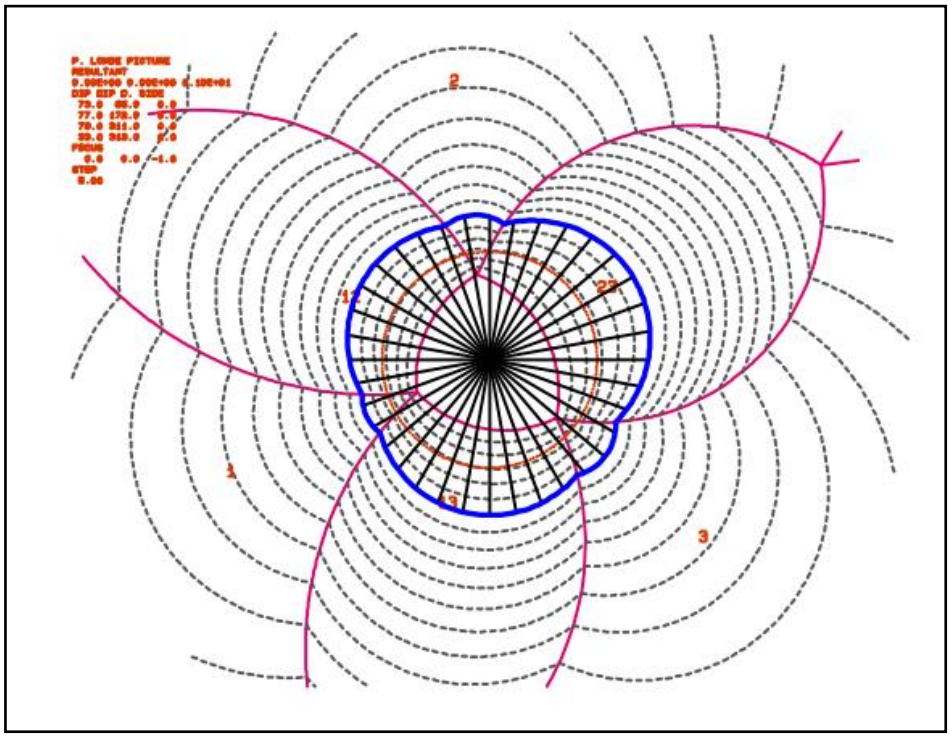

A1. 3: Stability plot for JP 0000 (30°)

JP 0000 (40°)

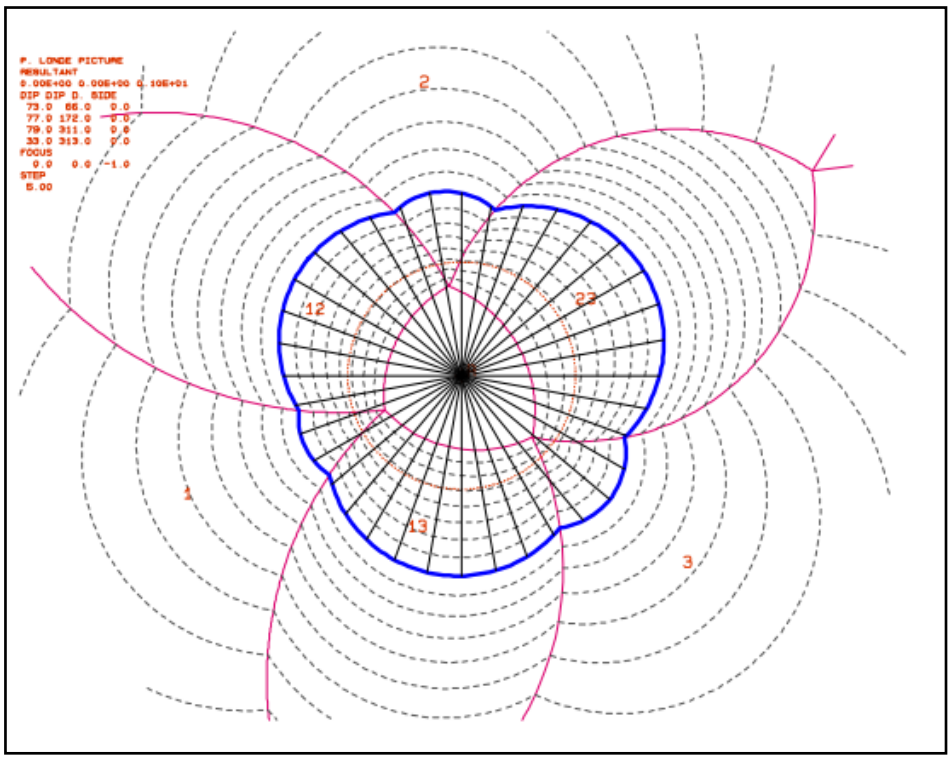

A1. 4: Stability plot for JP 0000 (40°)

JP 1000 (30°)

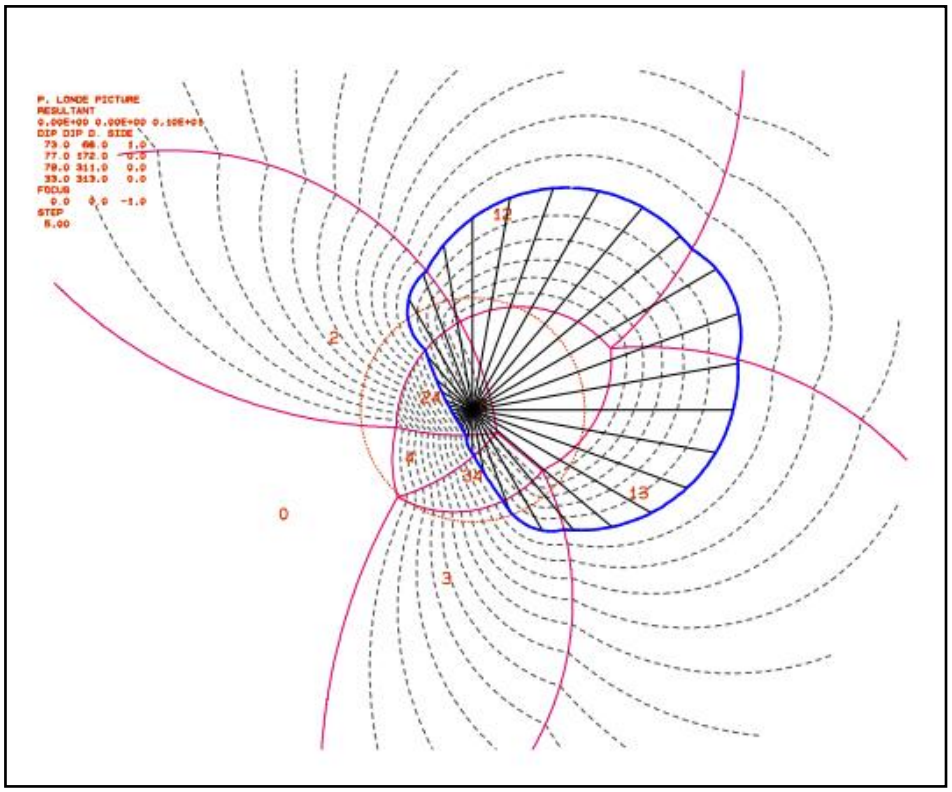

A1. 5: Stability plot for JP 1000 (30°)

JP 1000 (40°)

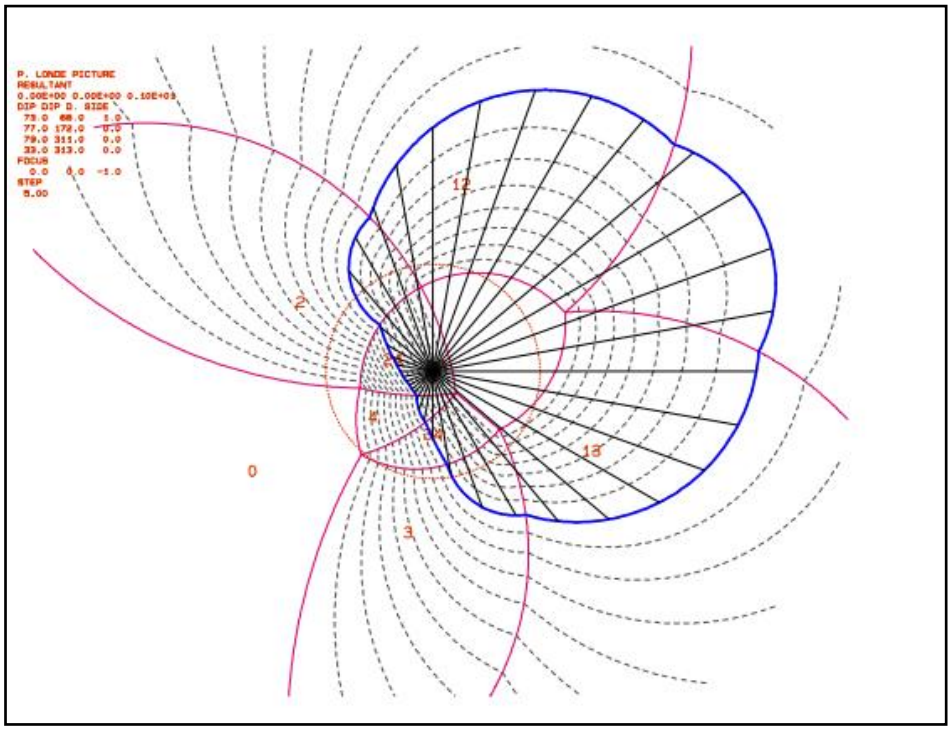

A1. 6: Stability plot for JP 1000 (40°)

JP 1010 (30°)

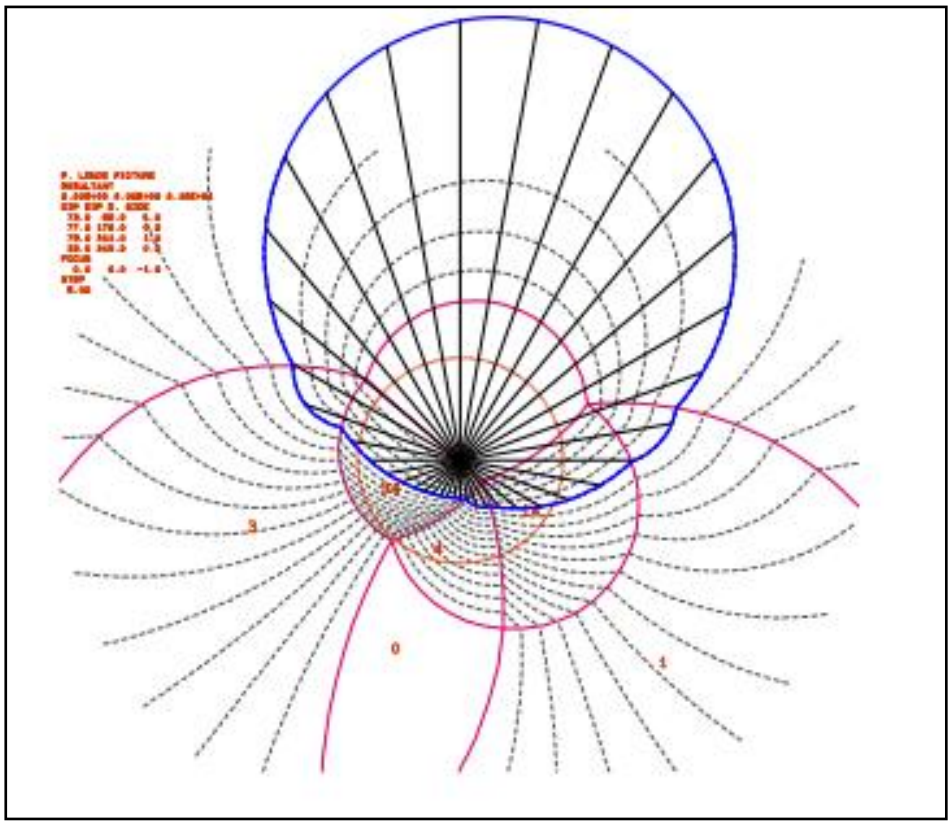

A1. 7: Stability plot for JP 1010 (30°)

JP 1010 (40°)

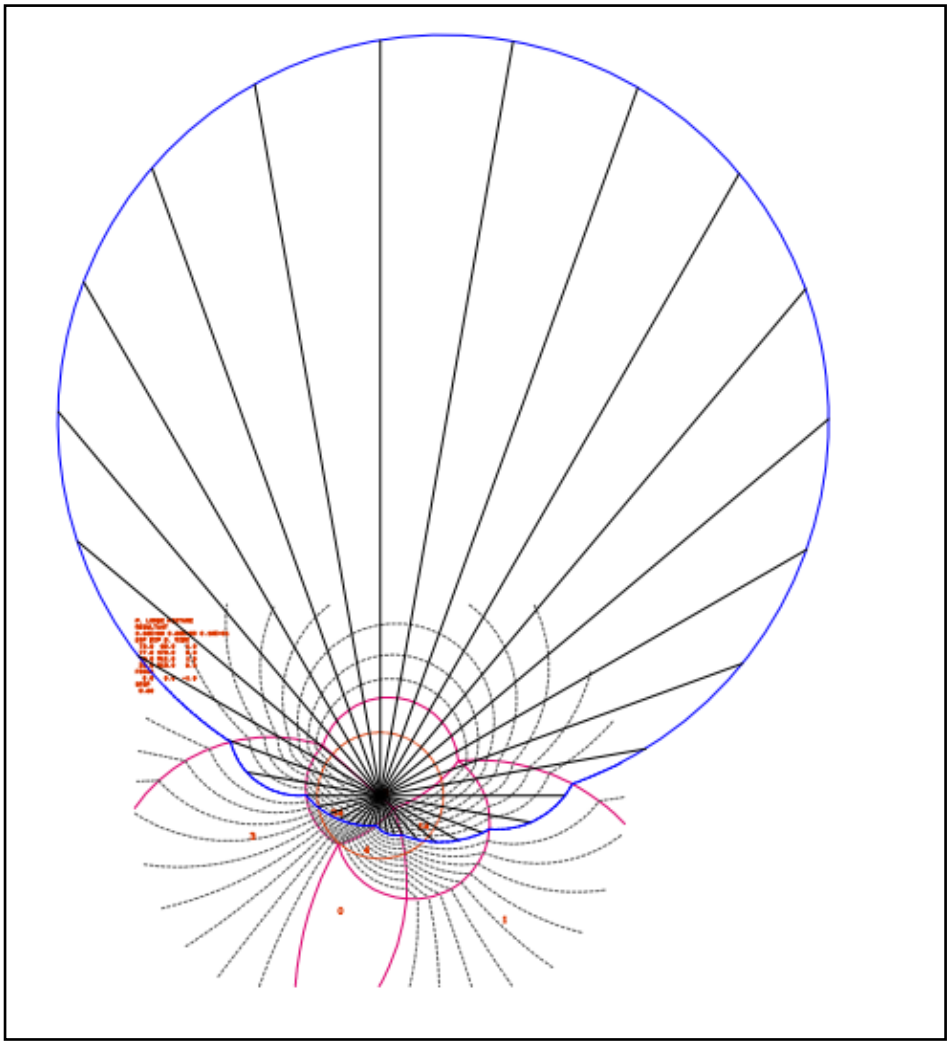

A1. 8: Stability plot for JP 1010 (40°)

A1.2 Quebec dam spillway

JP 0001 (30°)

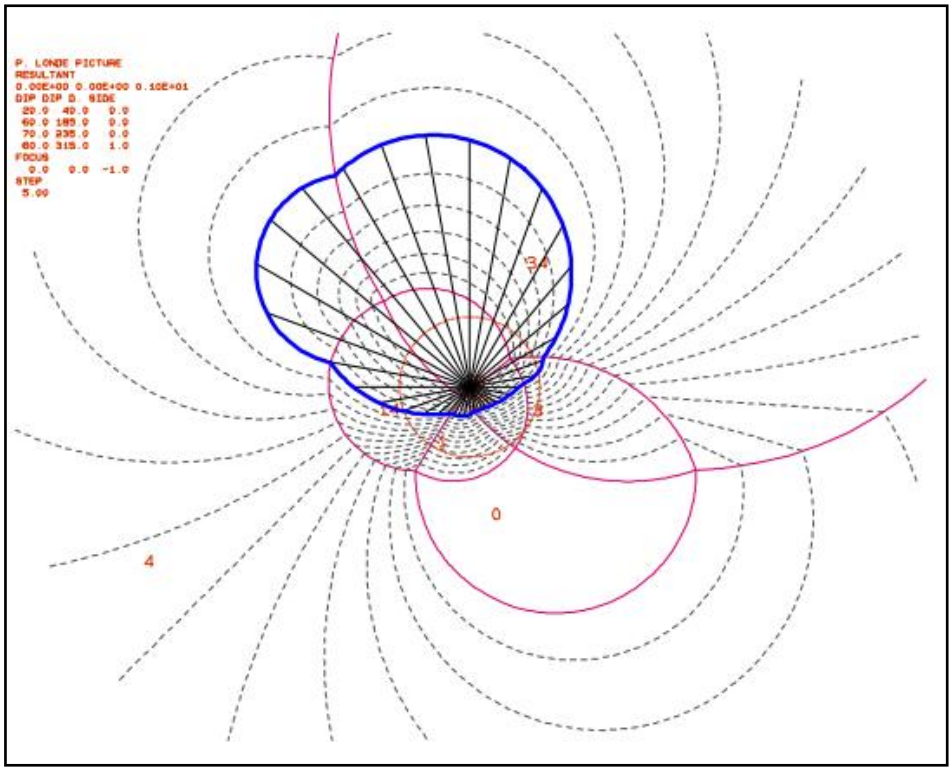

A1. 9: Stability plot for JP 0001 (30°)

JP 0001 (40°)

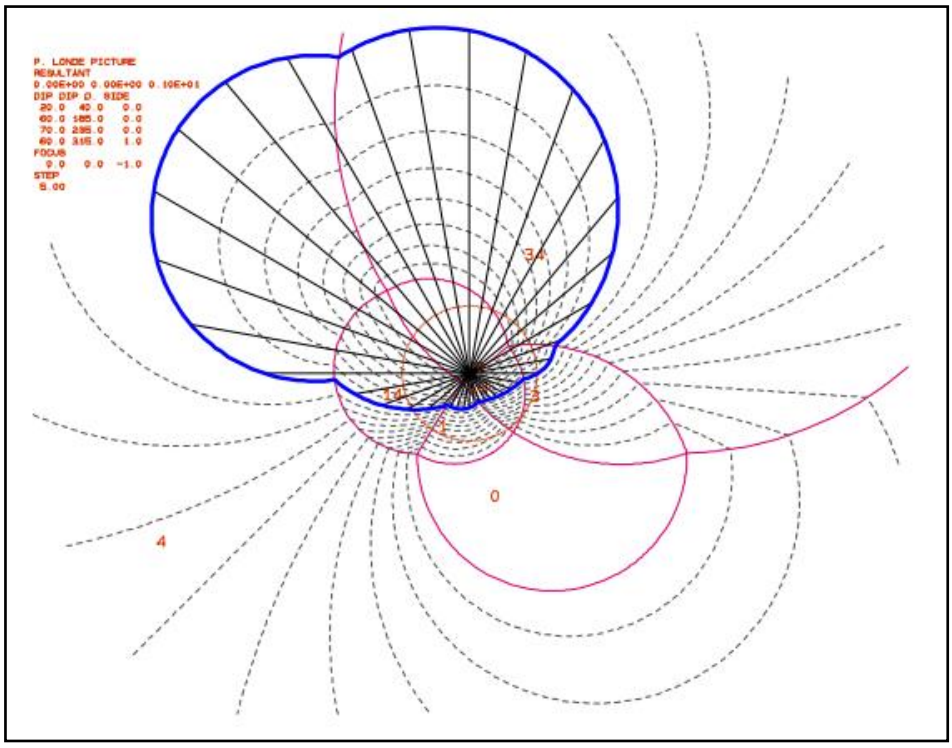

A1. 10: Stability plot for JP 0001 (40°)

JP 0010 (30°)

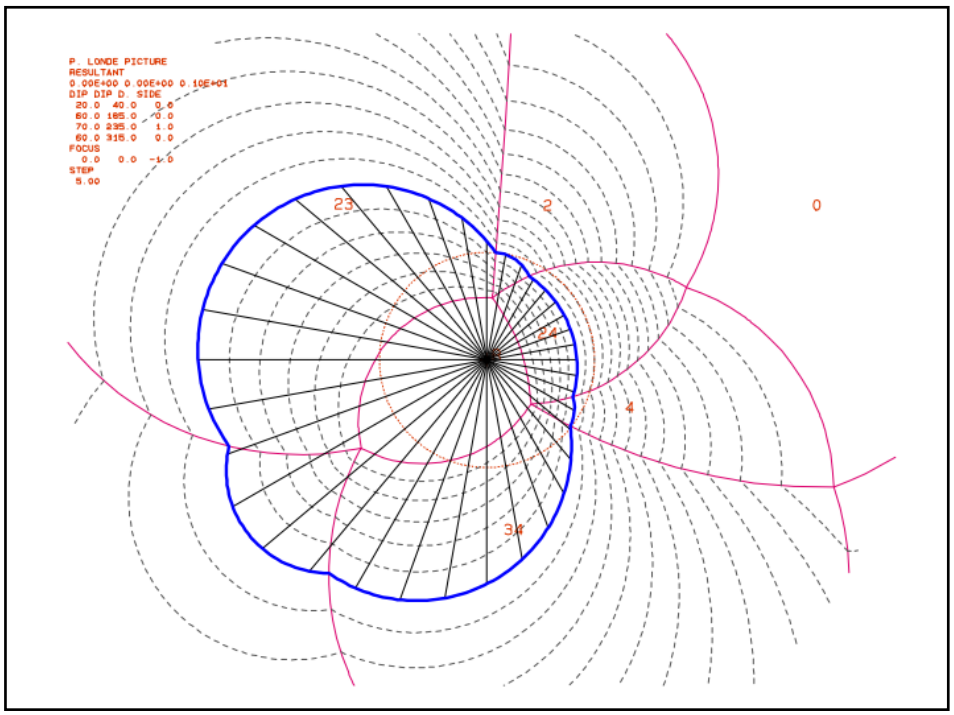

A1. 11: Stability plot for JP 0010 (30°)

JP 0010 (40°)

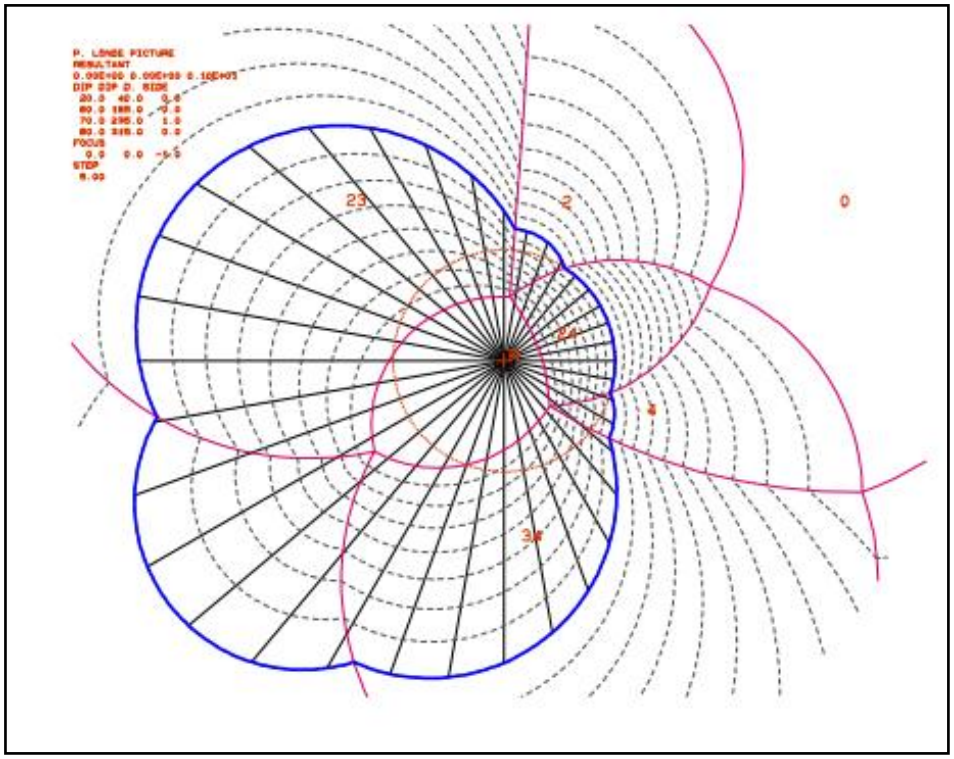

A1. 12: Stability plot for JP 0010 (40°)

JP 0000 (30°)

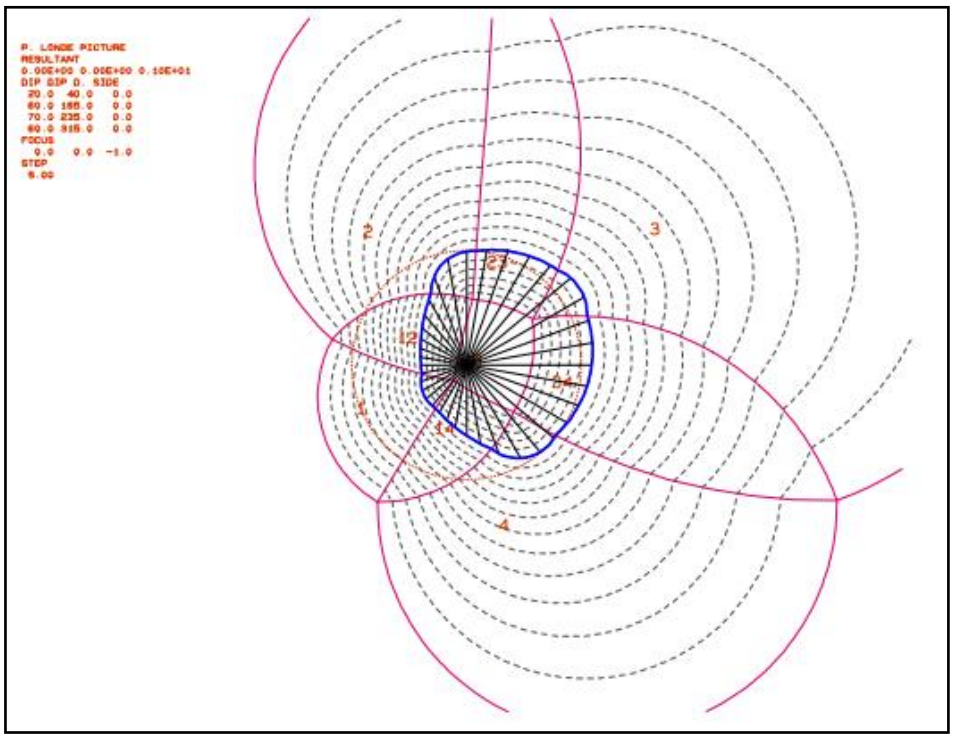

A1. 13: Stability plot for JP 0000 (30°)

JP 0000 (40°)

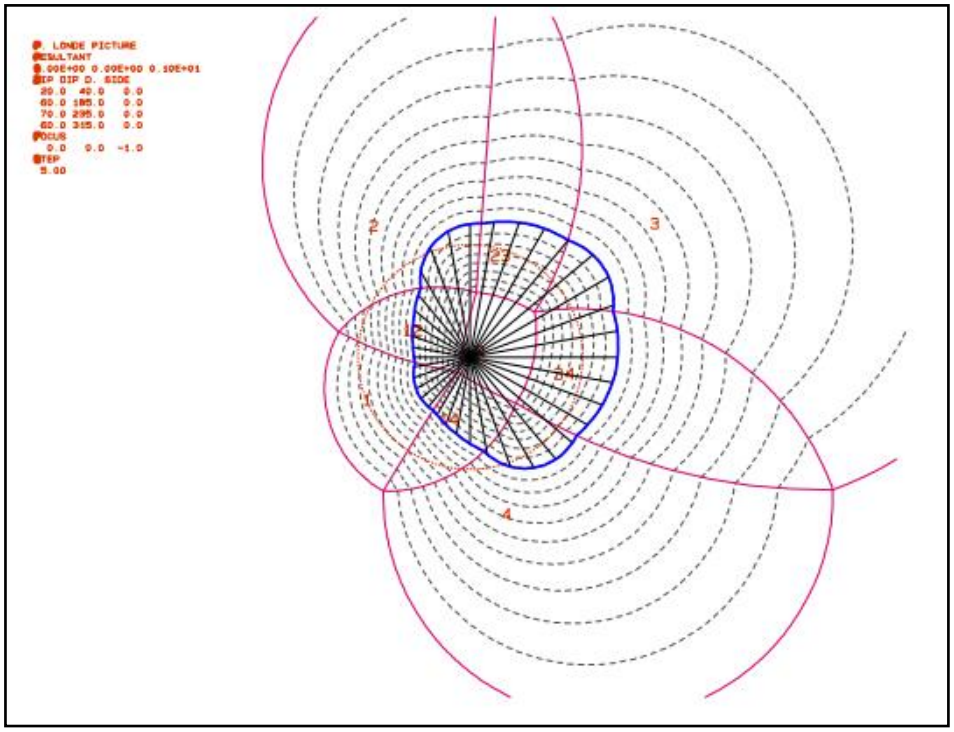

A1. 14: Stability plot for JP 0000 (40°)

A1.3 Ricobayo dam spillway

JP 01001 (30°)

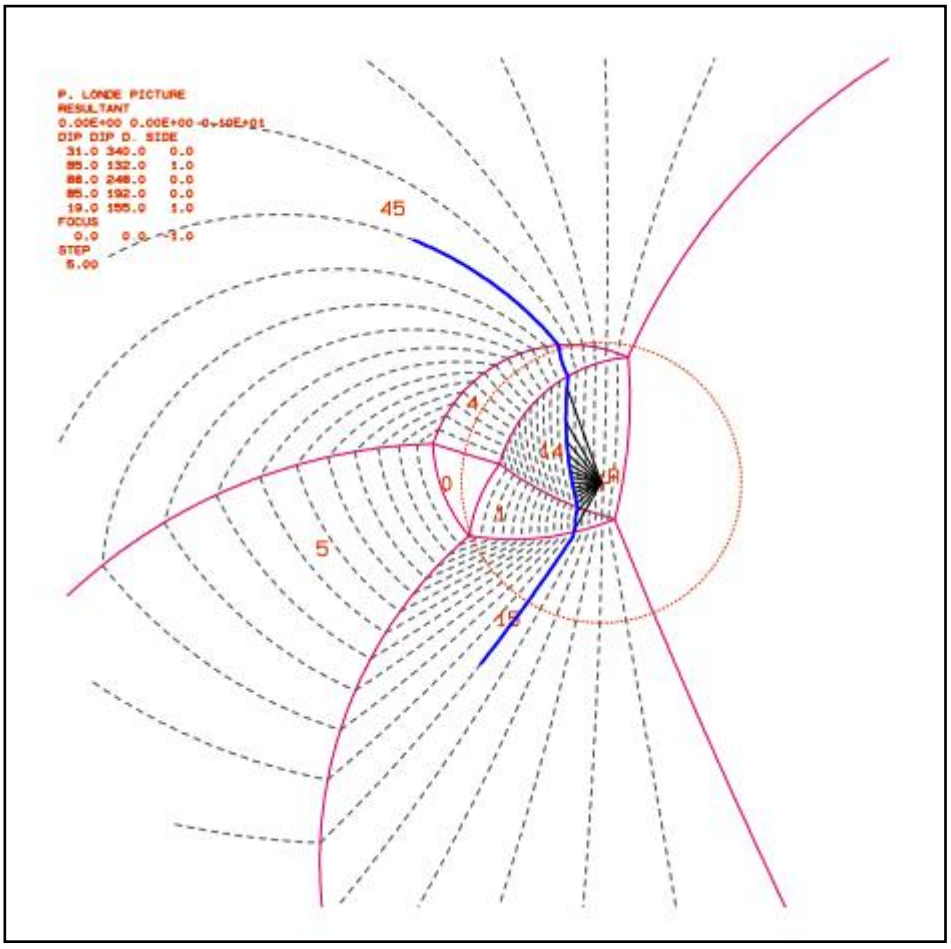

A1. 15: Stability plot of JP 01001 (30°)

JP 01001 (40°)

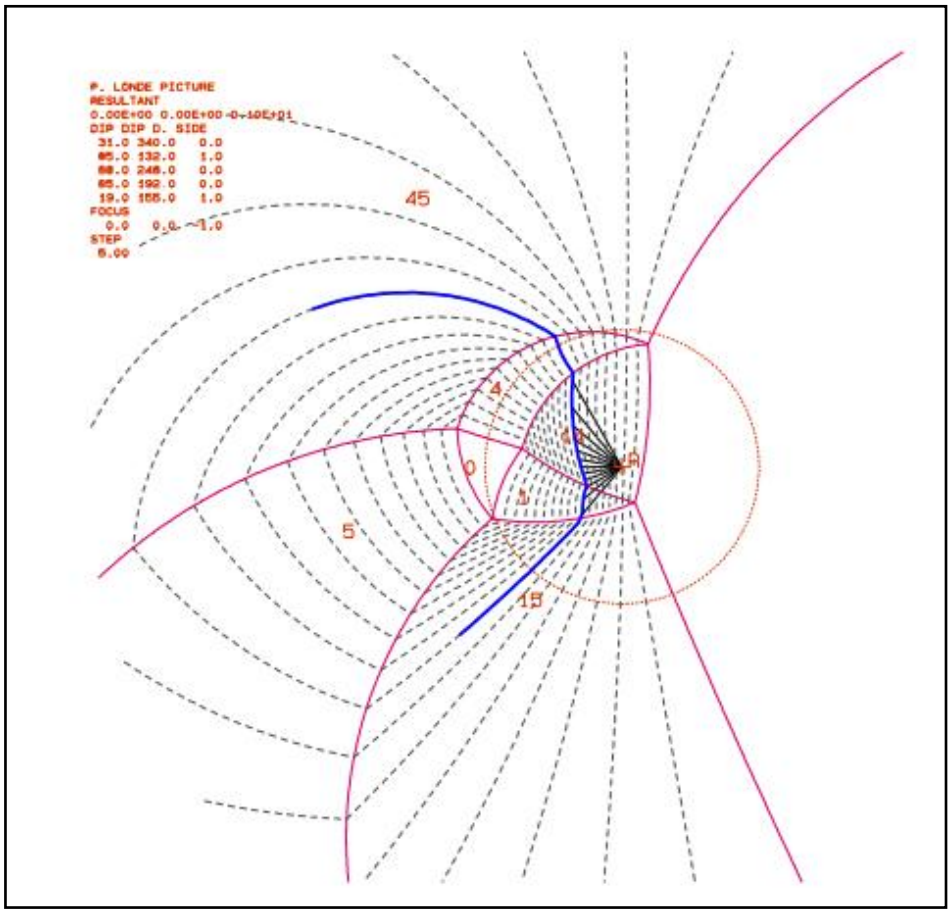

A1. 16: Stability plot of JP 01001 (40°)

JP 10000 (30°)

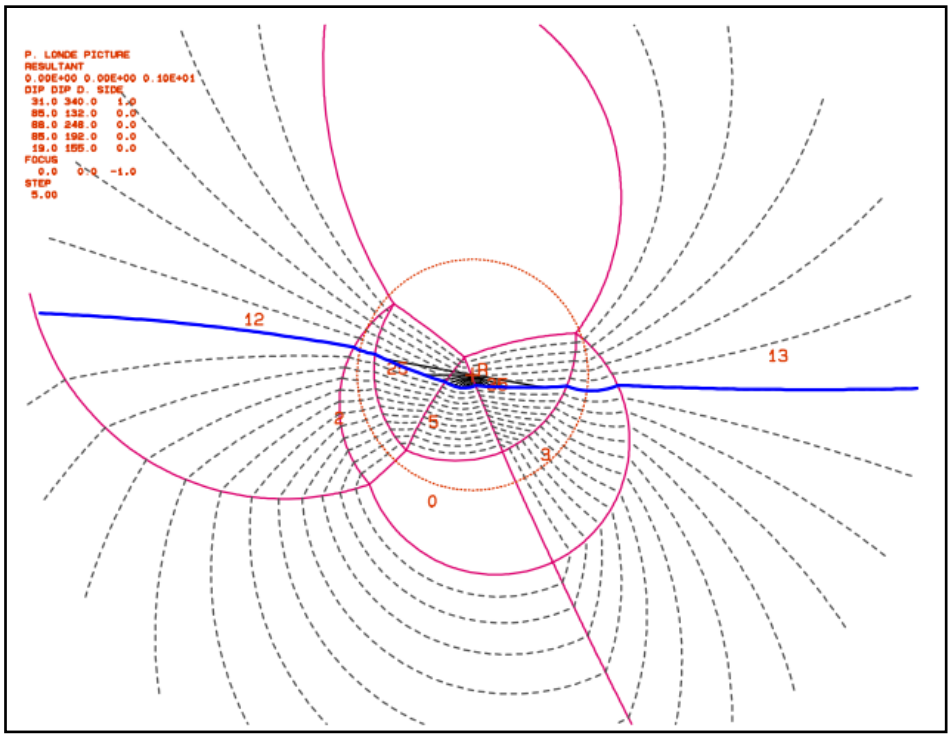

A1. 17: Stability plot for JP 10000 (30°)

JP 10000 (40°)

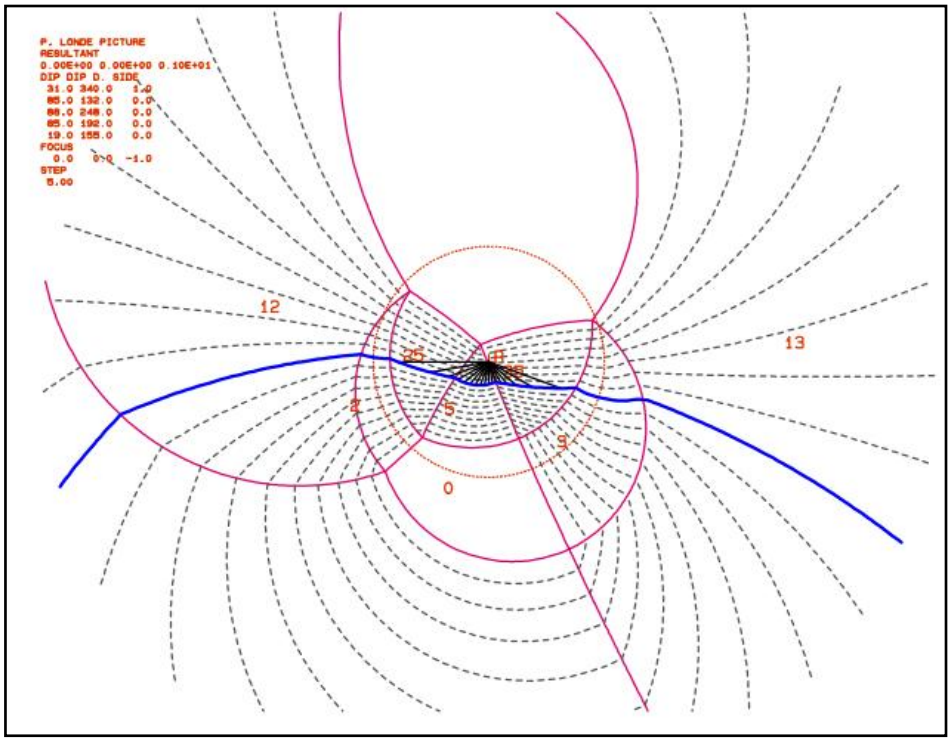

A1. 18: Stability plot for JP 10000 (40°)

JP 11000 (30°)

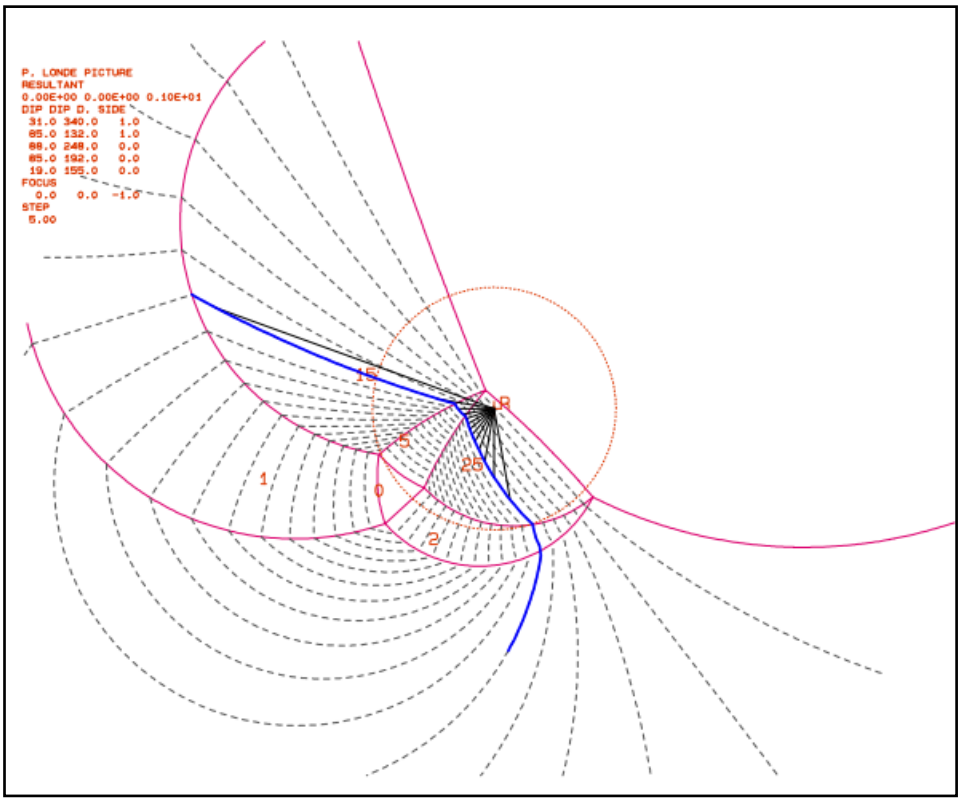

A1. 19: Stability plot for JP 11000 (30°)

JP 11000 (40°)

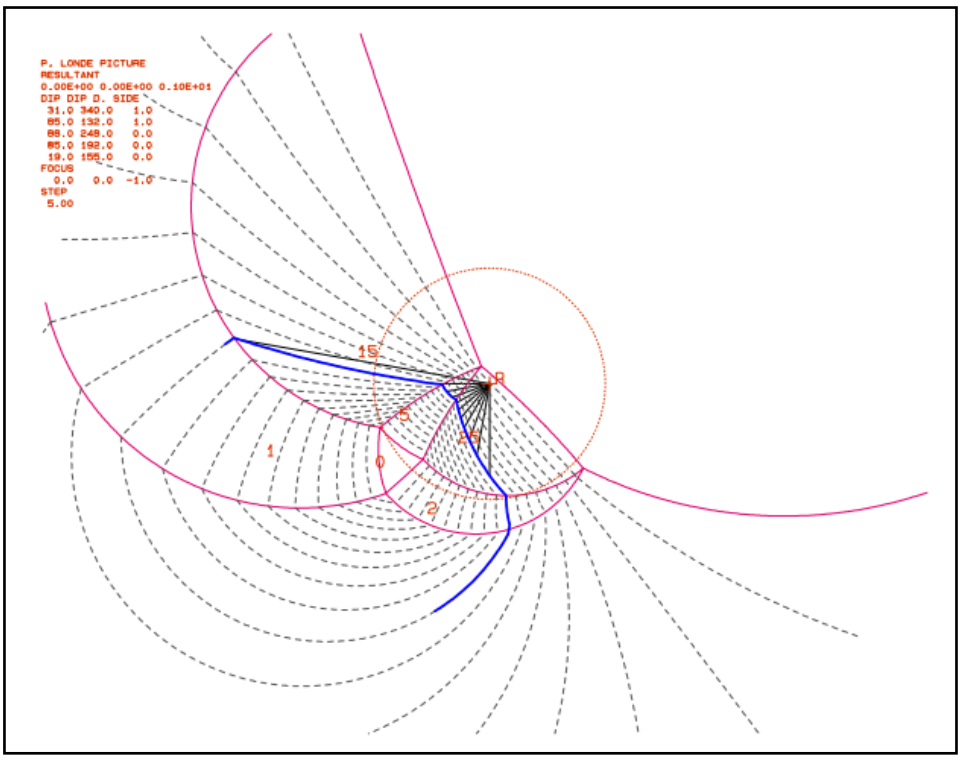

A1. 20: Stability plot for JP 11000 (40°)

JP 00000 (30°)

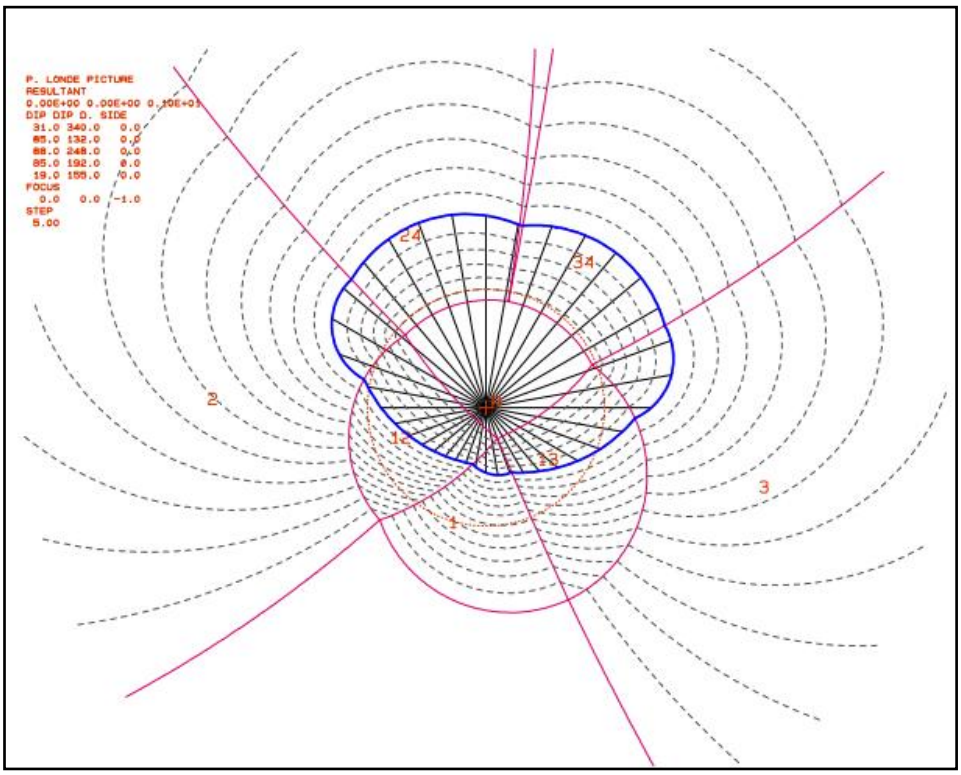

A1. 21: Stability plot for JP 00000 (30°)

JP 00000 (40°)

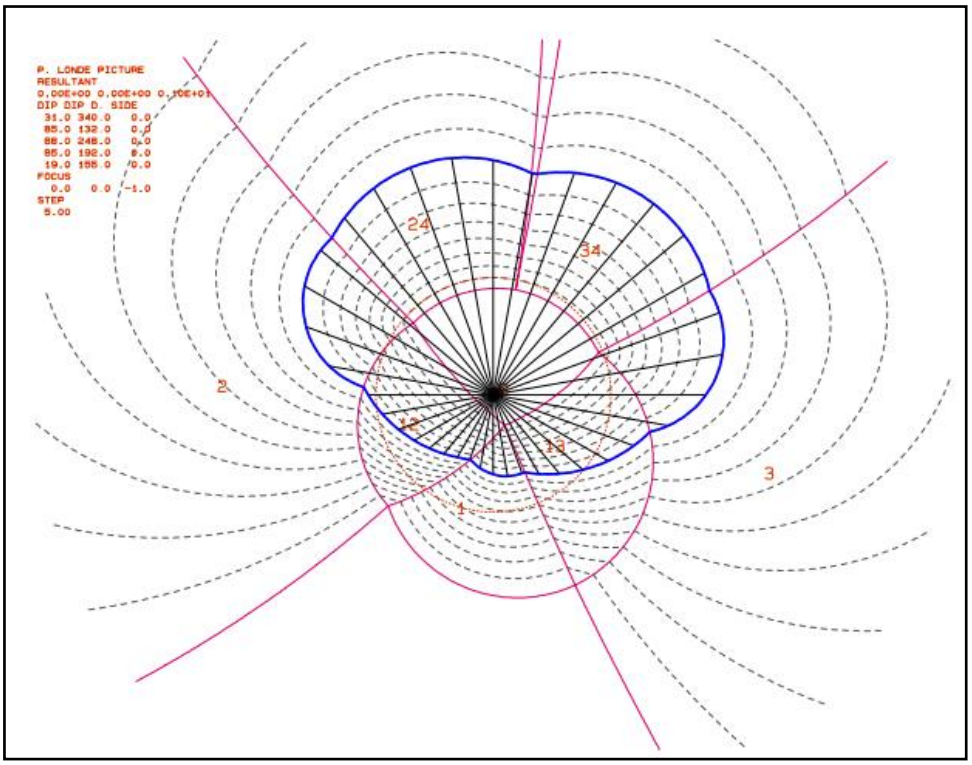

A1. 22: Stability plot for JP 00000 (40°)

JP 00010 (30°)

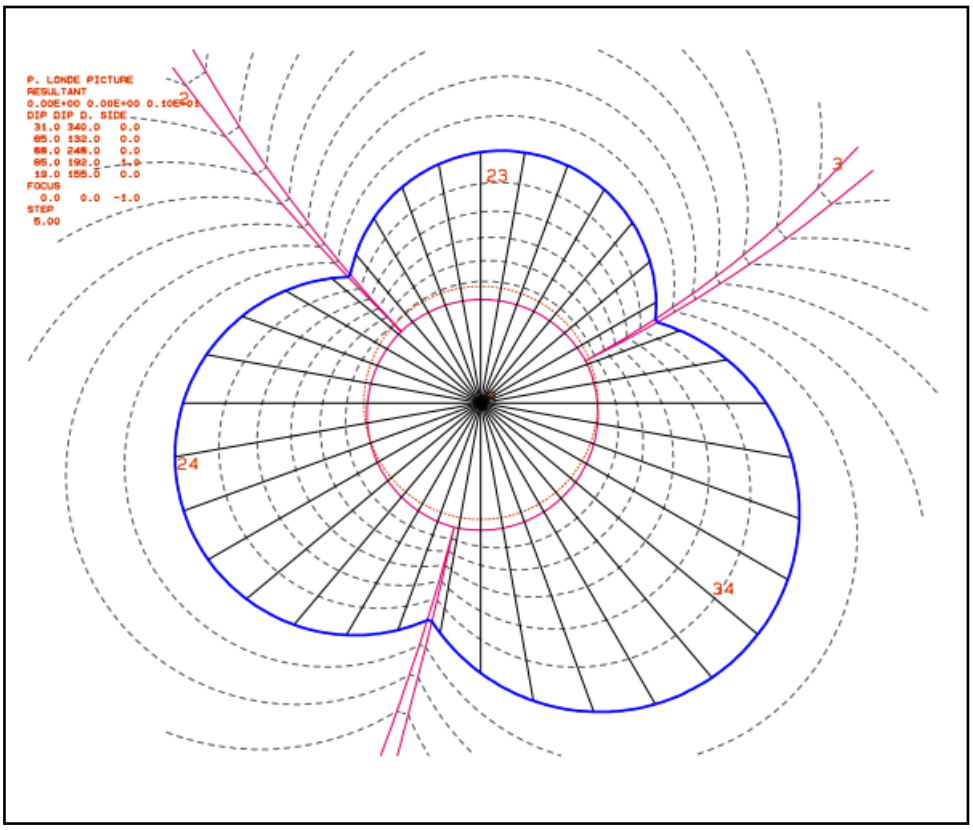

A1. 23: Stability plot for JP 00010 (30°)

JP 00010 (40°)

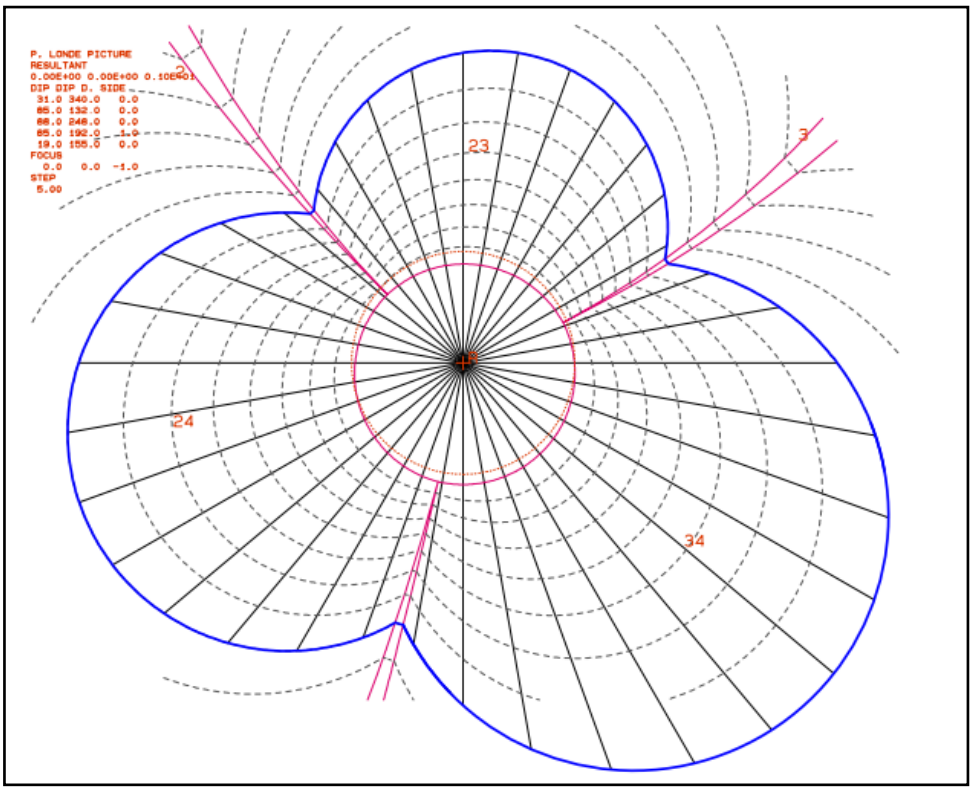

A1. 24: Stability plot for JP 00010 (40°)

JP 01000 (30°)

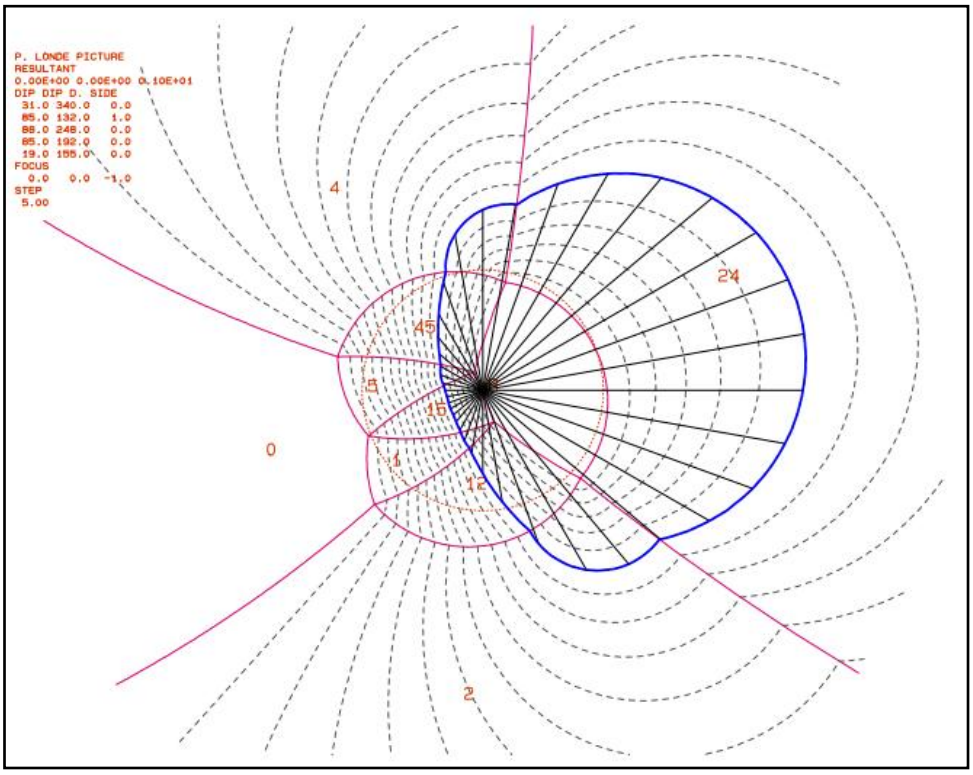

A1. 25: Stability plot for JP 01000 (30°)

JP 01000 (40°)

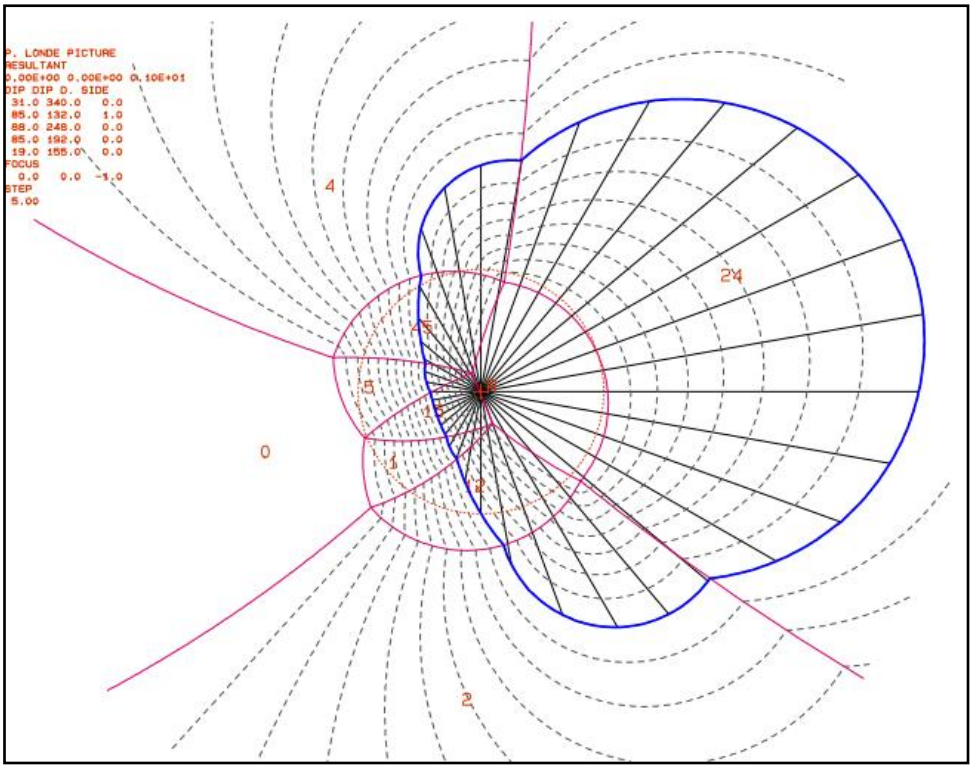

A1. 26: Stability plot for JP 01000 (40°)

JP 01010 (30°)

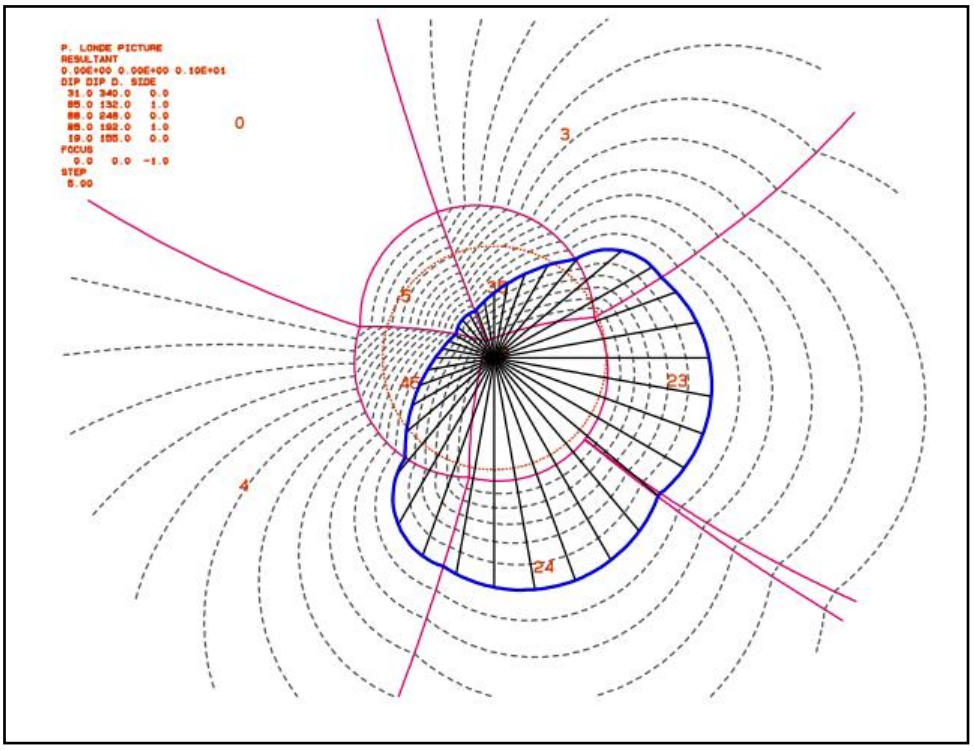

A1. 27: Stability plot for JP 01010 (30°)

JP 01010 (40°)

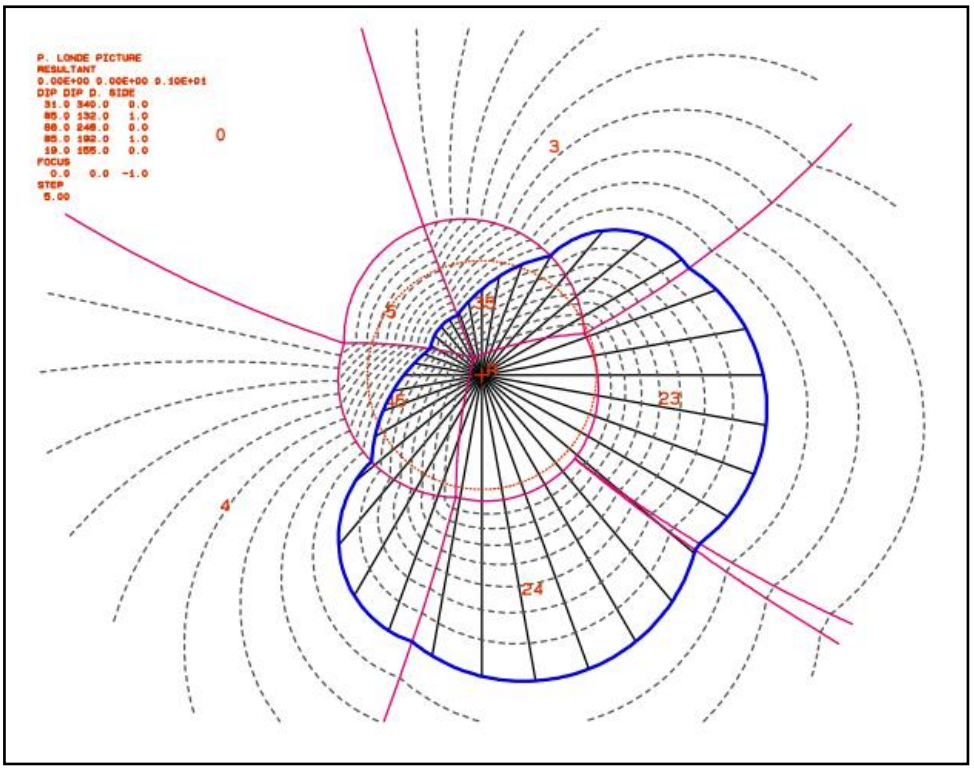

A1. 28: Stability plot for JP 01010 (40°)

JP 00100 (30°)

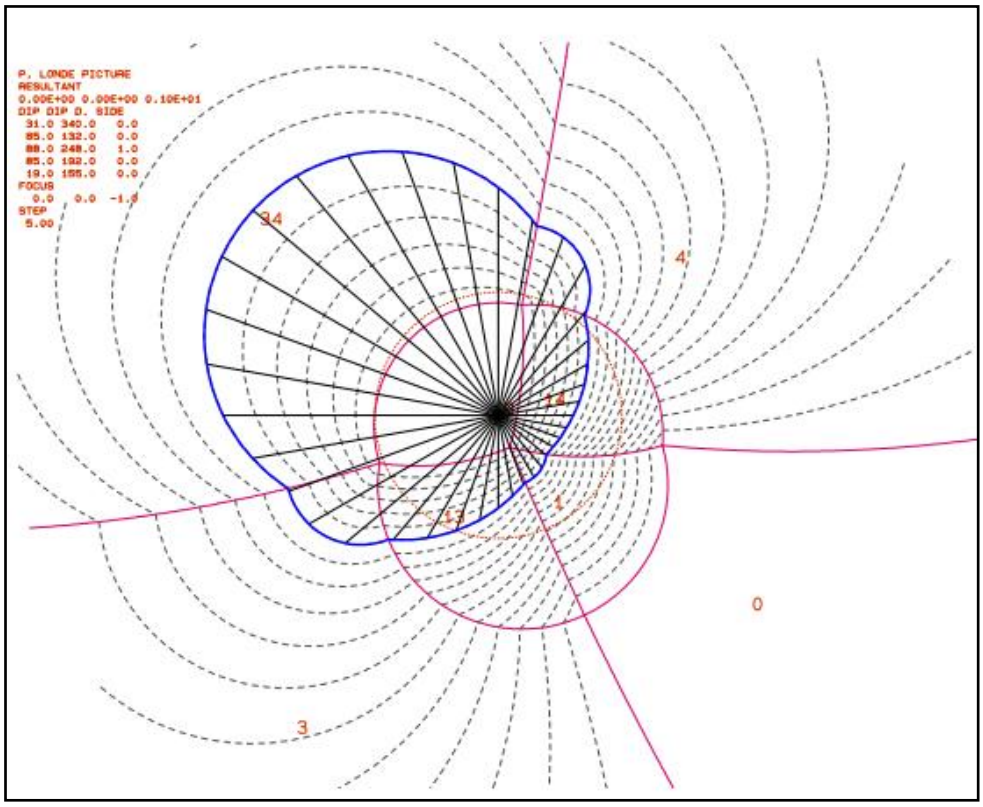

A1. 29: Stability plot for JP 00100 (30°)

JP 00100 (40°)

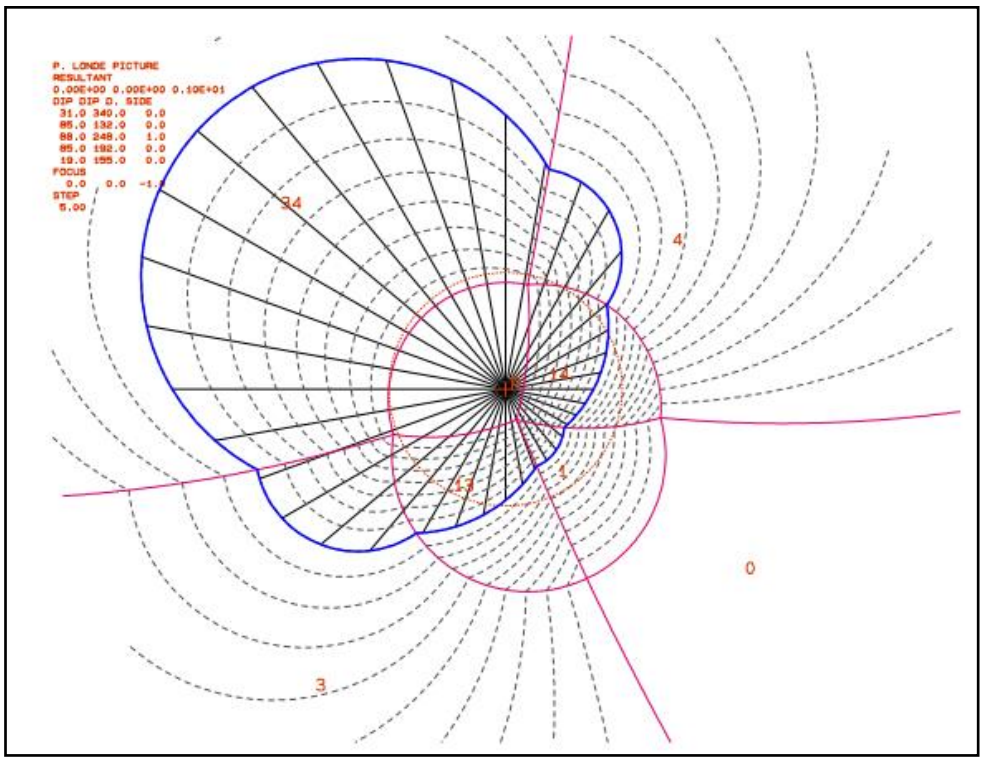

A1. 30: Stability plot for JP 00100 (40°)

JP 01110 (30°)

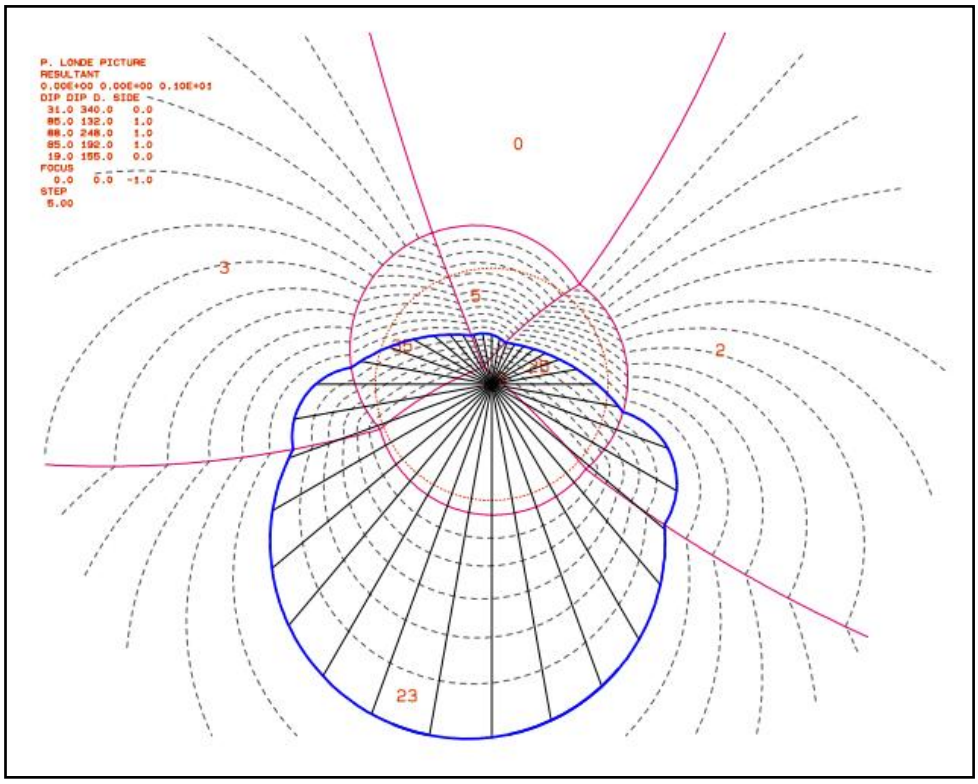

A1. 31: Stability plot for JP 01110 (30°)

JP 01110 (40°)

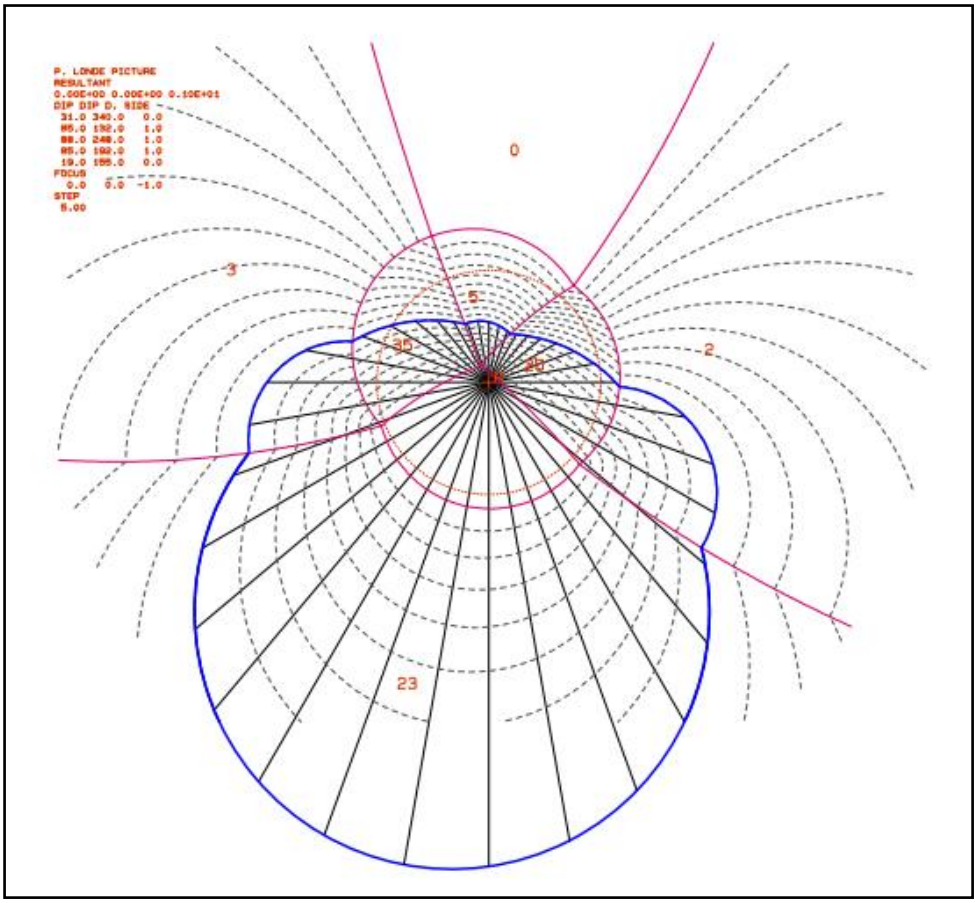

A1. 32: Stability plot for JP 01110 (40°)